

**The Molecular Characterisation of
Dimethylarginine Dimethylaminohydrolase-1 and
Determination of its Role in Portal Hypertension**

**Thesis submitted for the degree of
Doctor of Philosophy at UCL**

by

Gautam Mehta

August 2015

I, Gautam Mehta, confirm that the work presented in this thesis is my own. Where information has been derived from other sources, I confirm that this has been indicated in the thesis, and the section 'Experimental Acknowledgements' on page 9.

Acknowledgements

I would like to thank my supervisors, Dr Raj Mookerjee and Professor Rajiv Jalan, for giving me the opportunity to undertake this PhD in cirrhosis and vascular biology. Their advice, guidance and mentorship throughout the duration of this project has been greatly appreciated. I am particularly grateful for the scientific freedom I was given, which allowed me to develop my own ideas. I am also grateful to Dr Shanie Budhram-Mahadeo for the lab supervision and encouragement she provided at the Rayne Institute.

I would also like to thank all the members of staff and students of the Liver Failure Group at the Royal Free Campus and the Medical Molecular Biology Unit at the Rayne Institute. Specific thanks go to Nathan Davies, Abe Habtesion, Vikram Sharma, Katie Poulton, Samir Ounzain and James McCormick.

I would like to thank the Wellcome Trust for funding my PhD studentship.

Finally, special thanks go to my parents and to Alex to whom I owe so much, in particular their never-ending support, faith and inspiration.

Table of Contents

Acknowledgements	3
Table of Contents	4
Abstract	8
Experimental Acknowledgements	9
Chapter 1 – General Introduction	10
1.1 Natural history and clinical significance of portal hypertension in cirrhosis	11
1.2 Pathobiology of portal hypertension in cirrhosis	13
1.2.1 Intrahepatic resistance.....	13
1.2.2 The role of nitric oxide	14
1.3 Nitric oxide synthases	15
1.3.1 Regulation of nitric oxide synthases	15
1.3.2 Functions of nNOS, iNOS and eNOS	17
1.4 Vascular alterations in cirrhosis	21
1.4.1 The sinusoidal circulation	21
1.4.2 The systemic and splanchnic circulations.....	24
1.5 Inflammation and portal hypertension	25
1.5.1 The role of inflammation in modifying portal pressure	25
1.5.2 Mechanisms of intrahepatic resistance in hepatic inflammation.....	26
1.6 The role of the DDAH-ADMA system	30
1.7 Aims	34
Chapter 2 – Generic Materials and Methods	36
2.1 General Materials	36
2.1.1 Plasmids and reagents for molecular biology	36
2.1.2 Reagents for Cell Culture	36
2.2 DNA Manipulation	37
2.2.1 Standard Polymerase Chain Reaction (PCR)	37
2.2.2 Agarose gel electrophoresis	37
2.2.3 DNA extraction and purification from agarose gel	38
2.2.4 DNA determination	38
2.2.5 Ligation of isolated DNA into vector	38
2.2.6 Transformation of bacteria with plasmid DNA	39
2.2.7 Restriction enzyme digest	39
2.2.8 Plasmid modification by annealed oligonucleotide cloning.....	40
2.3 Cell Culture	40
2.3.1 Maintenance of cell lines and primary cells	40
2.3.2 Storage of cells	41
2.4 RNA manipulation	42
2.4.1 RNA isolation from cells and tissues	42
2.4.2 RNA determination	42
2.4.3 Deoxyribonuclease (DNaseI) treatment of RNA.....	42
2.4.4 cDNA synthesis	42
2.4.5 Quantitative real-time PCR.....	43
2.5 Transient transfection analyses	44

2.5.1 Transient transfection of cell lines	44
2.5.2 Luciferase reporter gene assay	45
2.6 Polyacrylamide gel electrophoresis (PAGE)	45
2.6.1 Resolving gel	45
2.6.2 Stacking gel	46
2.6.3 Protein extraction	47
2.6.4 Protein concentration measurement	47
2.6.5 Western blotting	47
2.7 Histology and immunohistochemistry	49
2.8 <i>In vivo</i> studies	50
2.8.1 Bile duct ligation surgery	50
2.8.2 Haemodynamic measurements	52
Chapter 3 – Characterisation of Hepatic DDAH-1 in Cirrhosis: Rats and Humans	53
3.1 Introduction	53
3.1.1 The bile duct-ligated rat model of cirrhosis	54
3.1.2 Gene therapy	56
3.2 Results	63
3.2.1 Optimization of immunohistochemical staining of DDAH-1	63
3.2.2 Localization of hepatic DDAH-1 expression in healthy human liver and in cirrhotic liver	63
3.2.3 Localisation of hepatic DDAH-1 in healthy rodent liver	65
3.2.4 Histological characterization of the bile duct-ligation rat model of cirrhosis	65
3.2.5 Quantification of DDAH-1 expression in healthy and cirrhotic rodent liver	66
3.2.6 Effect of ADMA on endothelial NO production	67
3.3 Effect of DDAH augmentation on portal pressure – gene therapy approaches...69	
3.3.1 Adeno-associated virus (AAV) cloning	70
3.3.2 Adeno-associated virus particle manufacture	72
3.3.3 Adeno-associated virus delivery of DDAH-1 to cirrhotic rodents	74
3.3.4 Hydrodynamic gene delivery of DDAH-1 in a rat model of cirrhosis	75
3.4 Discussion	79
Chapter 4 – Hepatic DDAH-1 Expression is Post-Transcriptionally Regulated by MicroRNAs in Cirrhosis	87
4.1 Introduction	87
4.1.1 MicroRNAs and post-transcriptional regulation	87
4.2 Results	93
4.2.1 mRNA expression in rats and humans with cirrhosis	93
4.2.2 miRNA expression in BDL cirrhotic rats	95
4.2.3 Bioinformatic analysis of DDAH-1 3'UTR	98
4.2.4 Luciferase reporter assays of the DDAH-1 3'UTR	103
4.2.5 Effect of hydrogen peroxide on hepatocyte DDAH-1 expression	107
4.2.6 Transfection of miRNA mimics and effects on DDAH-1 expression	108
4.2.7 <i>In situ</i> hybridisation for DDAH-1 and miR-128 in liver tissue	109
4.3 Discussion	113
Chapter 5 – DDAH-1 is Differentially Expressed as an Alternative Truncated mRNA Transcript in Human Placenta	119

5.1 Introduction	119
5.2 Results	121
5.2.1 Bioinformatic analysis of an alternative DDAH-1 transcript	121
5.2.2 Determination of human tissue expression of alternate DDAH-1 transcript	125
5.2.3 <i>In vitro</i> translation of the predicted protein of the alternate DDAH-1 transcript ...	133
5.3 Discussion	135
Chapter 6 – Discussion and Future Work	140
7.0 References:	148
8.0 Supplemental methods	159

List of Common Abbreviations

AAV	Adeno-associated virus	miR	MicroRNA
ACLF	Acute-on-chronic liver failure	mRNA	Messenger RNA
ADMA	Asymmetric dimethylarginine	NADPH	Nicotinamide adenine dinucleotide phosphate
ADP	Adenosine diphosphate	ncRNA	Non-coding RNA
ALT	Alanine aminotransferase	nNOS	Neuronal nitric oxide synthase
APS	Ammonium persulphate	NO	Nitric oxide
AST	Aspartate aminotransferase	NOSIP	Nitric oxide synthase interacting protein
BAEC	Bovine aortic endothelial cell	NOSTRIN	eNOS traffic inducer
BCA	Bicinchoninic acid	OCA	Obeticholic acid
BDL	Bile duct ligation	PAGE	Polyacrylamide gel electrophoresis
BH4	Tetrahydrobiopterin	PAMP	Pathogen-associated molecular pattern
CaM	Calmodulin	PBS	Phosphate-buffered saline
CCL4	Carbon tetrachloride	PCR	Polymerase chain reaction
cGMP	Cyclic guanosine monophosphate	PE	Pre-eclampsia
DAMP	Damage-associated molecular pattern	PPIA	Peptidylprolyl isomerase A
DDAH-1	Dimethylarginine dimethylaminohydrolase-1	PPVL	Partial portal vein ligation
DEPC	Diethylpyrocarbonate	PRMT	Protein arginine methyltransferase
DMEM	Dulbecco's modified Eagle's medium	qPCR	Quantitative PCR
DMSO	Dimethyl sulfoxide	RIPA	Radioimmunoprecipitation assay
DNA	Deoxyribonucleic acid	RNA	Ribonucleic acid
dNTP	Deoxyribose nucleoside triphosphate	ROS	Reactive oxygen species
DTT	Dithiothreitol	RT	Reverse transcriptase
ECL	Enhanced chemiluminescence	SDMA	Symmetric dimethylarginine
EDTA	Ethylenediaminetetraacetic acid	SDS	Sodium dodecyl sulphate
eNOS	Endothelial nitric oxide synthase	SEC	Sinusoidal endothelial cell
FAD	Flavin adenine dinucleotide	SEM	Standard error of the mean
FMN	Flavin mononucleotide	Ser	Serine
FXR	Farnesoid X receptor	SOC	Super optimal broth
HRP	Horseradish peroxidase	TAE	Tris-acetate-EDTA
HSC	Hepatic stellate cell	TE	Tris-EDTA
HVPG	Hepatic venous pressure gradient	TEMED	Tetramethylethylenediamine
IL	Interleukin	Thr	Threonine
iNOS	Inducible nitric oxide synthase	TLR	Toll-like receptor
ITR	Inverted terminal repeat	TNF	Tumour necrosis factor
L-NMMA	L-NG-monomethyl arginine citrate	TSS	Transcription start site
LB	Luria-Bertani	Tyr	Tyrosine
LPS	Lipopolysaccharide	UTR	Untranslated region
MAP	Mean arterial pressure	VEGF	Vascular endothelial growth factor

Abstract

Portal hypertension is a grave step in the progression of cirrhosis, associated with complications and mortality. The pathobiology of portal hypertension involves fibrosis as well as increased intrahepatic vascular tone. Nitric oxide (NO), synthesized by endothelial nitric oxide synthase (eNOS), is a key regulator of intrahepatic vascular tone. Asymmetric dimethylarginine (ADMA) is a competitive inhibitor of eNOS, which has been implicated in the pathobiology of portal hypertension – ADMA levels are elevated in cirrhosis and correlate with portal pressure. The major pathway of elimination of ADMA is the enzyme dimethylarginine dimethylaminohydrolase-1 (DDAH-1). The main aims of this thesis are: (i) delineate the expression and regulation of hepatic DDAH-1 in cirrhosis and portal hypertension, and (ii) determine a causal relationship between hepatic DDAH-1 and portal hypertension in cirrhosis.

In initial experiments, hepatic DDAH-1 protein expression was significantly decreased in patients with cirrhosis and bile duct-ligated (BDL) rats. Immunohistochemistry demonstrated that DDAH-1 expression was restricted to the hepatocyte. *In vitro* work with endothelial cells demonstrated that exogenous ADMA is an inhibitor of NO generation at pathophysiological levels.

Subsequent experiments demonstrated that DDAH-1 expression was decreased by exposure to hydrogen peroxide (H₂O₂), and this mechanism was related to the DDAH-1 3'UTR. Further studies demonstrated the presence of predicted microRNA (miR) binding sites in the DDAH-1 3'UTR, and miR-128 was found to be elevated in BDL rat liver compared with sham controls, as well as being a regulator of DDAH-1 protein expression through gain-of-function and loss-of-function experiments.

Finally, a novel truncated transcript of DDAH-1 was demonstrated in human placenta. This transcript was found to be protein-encoding, with bioinformatic evidence of a proximal promoter. Thus, a switch in transcript may play a role in placental vascular disorders such as pre-eclampsia.

In summary, hepatic DDAH-1 is reduced in cirrhosis, and is causally related to the development of portal hypertension. DDAH-1 undergoes post-transcriptional regulation through microRNA regulation and alternative transcription.

Experimental Acknowledgements

In Chapter 4;

Dr Fatma Mohamed supervised and assisted with histological staining, including immunohistochemistry.

Dr Takis Athanasopoulos supervised and assisted with the manufacture of adeno-associated viral particles.

Dr Nathan Davies carried out rodent surgery, including bile duct ligation, administration of viral vectors and plasmid DNA, and physiological measurements.

In Chapter 5;

Dr Helen Jones assisted with the Affymetrix *in situ* hybridization and staining.

In Chapter 6;

Dr Katie Poulton assisted with the collection and processing of human placental tissue.

Chapter 1 – General Introduction

Portal hypertension is a milestone in the progression of cirrhosis and heralds the onset of the most fatal complications of liver disease. This vascular dysfunction within the hepatic circulation leads to several feared consequences of cirrhosis, including the development of varices, porto-systemic encephalopathy and ascites. Indeed, the measurement of portal pressure, through the technique of hepatic venous pressure gradient (HVPG) measurement, is the single best predictor of complications and death amongst patients with liver disease¹.

Portal hypertension in cirrhosis results from increased resistance to portal blood flow within the liver, as well as increased portal inflow to the liver from splanchnic dilatation. These vascular changes develop on the background of complex alterations to cardiac and systemic haemodynamics, as well as altered immune function and increased inflammatory stress.

The major current pharmacological therapy for portal hypertension, non-selective β -adrenoceptor blockers, acts by reducing cardiac output and thereby decreasing splanchnic inflow into the liver. However, this therapy is inadequate in a significant number of patients, and moreover does not take into account recent insights into the inflammatory effects and molecular mechanisms of portal hypertension in cirrhosis.

The following section of this thesis will outline current perspectives on the epidemiology, pathobiology and current treatment of portal hypertension in cirrhosis.

1.1 Natural history and clinical significance of portal hypertension in cirrhosis

According to the Office for National Statistics, liver-related deaths are the 5th commonest cause of death in the United Kingdom². Moreover, deaths from liver disease have continued to rise over the last three decades, unlike the other four leading causes of death in the United Kingdom. The natural history of cirrhosis has traditionally been viewed as a progressive process, characterised by the development of portal hypertension and the subsequent onset of the complications of cirrhosis.

D'Amico and colleagues proposed a classification of the natural history of cirrhosis based on the presence or absence of portal hypertension, in four stages³. Stage 1 is defined by the absence of ascites or varices. Stage 2 is characterized by the absence of ascites and the presence of varices that have never bled. Stages 1 and 2 represent compensated cirrhosis. Stage 3 is defined by the presence of ascites with or without varices that have never bled. Stage 4 is characterized by the presence of variceal bleeding in patients with or without the presence of ascites. Using this classification, in a systematic review of over a hundred studies, the median 1-year survival is 99 %, 97 %, 80 %, and 43 %, respectively³. The prognostic value of portal hypertension in determining the natural history of cirrhosis has been validated in large prospective cohorts, demonstrating that portal pressure, as measured by the hepatic venous pressure gradient, is the strongest predictor of complications and death in cirrhosis^{1, 4}.

More recently, the role of infection and renal failure in the natural history of cirrhosis has been highlighted. The presence of any infection on the background of cirrhosis leads to a four-fold increase in mortality (odds ratio 3.8, 95% confidence interval 2.1-

4.2), as compared with uninfected patients. Renal dysfunction in cirrhosis is associated with an almost eight-fold increase in risk of death (odds ratio 7.6, 95% confidence interval 5.4-10.8)⁵. These observations have led to the proposal of a fifth stage in the natural history of cirrhosis, which is characterized by either the presence of refractory symptoms (e.g. ascites) or the presence of infection or renal failure in patients with cirrhosis (figure 1.1).

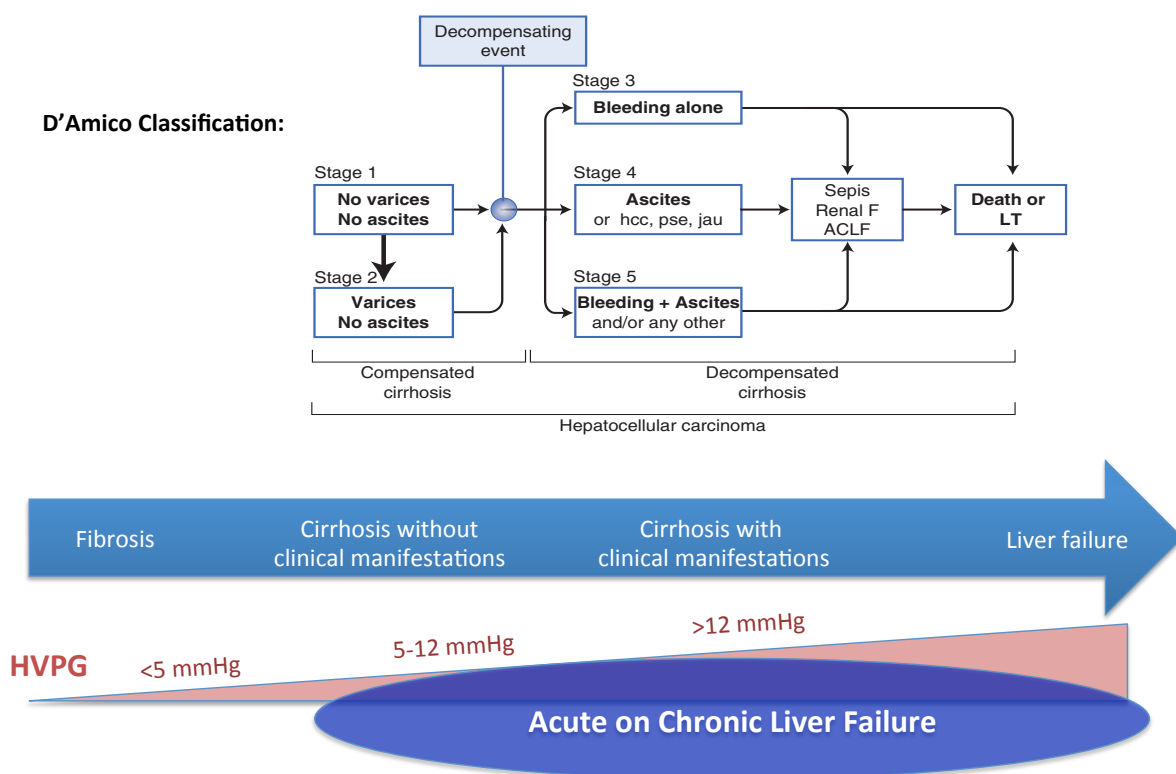


Figure 1.1: This figure represents the proposed step-wise progression of compensated cirrhosis to decompensation, which is manifest by ascites and hepatic encephalopathy, through to infection and renal failure. This progression is accompanied by a progressive rise in hepatic venous pressure gradient (HVPG). Additionally, multiorgan failure can ensue either from compensated cirrhosis or decompensated cirrhosis following a defined or undefined insult, a condition referred to as acute on chronic liver failure (ACLF – *vide infra*).

Therefore, the pivotal role of portal hypertension in the pathogenesis of these complications is illustrated by the progressive rise in portal pressure being the only pathophysiological event, independent of aetiology of liver disease, to predict complications and outcome.

1.2 Pathobiology of portal hypertension in cirrhosis

As mentioned above, the pathobiology of portal hypertension in cirrhosis is complex, and involves changes in the architecture of the liver, but also occurs as a consequence of endothelial dysfunction within the liver and in the systemic circulation.

1.2.1 Intrahepatic resistance

The hallmark of cirrhosis is the development of architectural distortion in the form of nodular fibrosis and scarring, which leads to portal hypertension through obstruction of sinusoidal blood flow. However, a recent body of work has demonstrated that upward of one-third of this intrahepatic vascular resistance is due to a reversible, modifiable component. Molecular mechanisms of this increase in vascular tone include an imbalance of vasodilator and vasoconstrictor compounds, dysfunction of sinusoidal endothelium, and activation of contractile elements in vascular smooth muscle and myofibroblastic-phenotype hepatic stellate cells (HSCs).

1.2.2 The role of nitric oxide

Advances in vascular biology over the last two decades have highlighted the role of nitric oxide (NO) in endothelial function. Indeed, Furchgott, Ignarro and Murad received the Nobel Prize in Medicine in 1998 for the discovery of endothelium derived relaxing factor, and its subsequent characterisation as NO⁶⁻⁸. The realisation that endothelial dysfunction plays a key role in the pathobiology of portal hypertension in the context of cirrhosis was a further major advance. Groszmann and colleagues first demonstrated that NO is a key regulator of vascular tone in normal rodent liver, and went on to show that cirrhotic rodent liver demonstrated intrahepatic endothelial dysfunction characterised by impaired responsiveness to acetylcholine, and decreased production of NO⁹.

The nature of this intrahepatic endothelial dysfunction was further characterised by Rockey and colleagues in their study of rodents with cirrhosis, induced by bile duct ligation (BDL) and by carbon tetrachloride (CCl₄) treatment¹⁰. In both these models of chronic liver injury, hepatic nitric oxide synthase activity and production of cyclic guanosine monophosphate (cGMP), which is produced by guanylyl cyclase after stimulation by NO, were reduced. However endothelial nitric oxide synthase (eNOS) messenger RNA (mRNA) and protein levels were unchanged, suggesting that the defect in endothelial NO production is due to post-translational modification of the eNOS enzyme, or due to the presence of endogenous eNOS inhibitors.

1.3 Nitric oxide synthases

1.3.1 Regulation of nitric oxide synthases

The variety of roles of NO as a messenger molecule have only been described over the last decade. As well as acting as endothelium-derived relaxing factor, NO serves regulatory functions in neurotransmission, gene transcription, mRNA translation (eg. by binding to iron-responsive elements), and post-translational modification of proteins (eg. by ADP ribosylation)¹¹⁻¹⁵.

There are three isoforms of NO synthase in mammals: neuronal NOS (nNOS), inducible NOS (iNOS) and endothelial NOS (eNOS). All three isoforms utilise L-arginine as substrate, and molecular oxygen and nicotinamide adenine dinucleotide phosphate (NADPH) as co-substrates. Flavin adenine dinucleotide (FAD), flavine mononucleotide (FMN) and tetrahydropterin (BH4) are co-factors. All isoforms act as homodimers (figure 1.2).

The enzymatic synthesis of NO occurs through electron transfer from NADPH, via the flavins FAD and FMN, in the C-terminal reductase domain of eNOS to the haem in the N-terminal oxygenase domain of eNOS¹⁶. The oxygenase domain also binds BH4, molecular oxygen and the substrate L-arginine. At the haem site, electrons are used to reduce and activate O₂ to oxidise L-arginine to L-citrulline and NO. Sequences near the cysteine ligand of haem are also involved in L-arginine and BH4 binding. Thus, enzymatic synthesis of NO is a two-stage process; the first step is the hydroxylation of L-arginine to *N*-hydroxy-L-arginine, and the subsequent step is oxidation of *N*-hydroxy-L-arginine to citrulline and NO.

1.3.2 Functions of nNOS, iNOS and eNOS

nNOS

Neuronal NOS, or nNOS, is important in synaptic signalling during processes such as learning, memory and neurogenesis. In the central nervous system, nNOS mediates long-term potentiation, and blood pressure regulation^{11, 17}. In the peripheral nervous system, nNOS containing nitrenergic nerves are responsible for penile erection. The NO released induces smooth muscle relaxation mediated by cGMP, which is in turn degraded by phosphodiesterases¹⁸. This is the basis for the action of phosphodiesterase inhibitors (eg Sildenafil) in the treatment of erectile dysfunction.

iNOS

Inducible NOS is not constitutively expressed in cells, but its expression is induced by bacterial lipopolysaccharides, cytokines and other agents¹⁹. Although primarily identified in macrophages, iNOS can be detected in several types if the appropriate inducing agent is present¹⁹. When induced, iNOS produces large amounts of NO in a calcium-independent fashion. This high concentration of NO is cytotoxic locally, due to the production of reactive oxygen species and reactive nitrogen species forming adducts to protein-bound iron, inhibiting key enzymes that contain iron in their catalytic centres²⁰. Moreover, NO also forms adducts with genomic DNA causing strand breaks and fragmentation²¹.

eNOS

Endothelial NOS is generally expressed in endothelial cells, although the enzyme has been detected in cardiac myocytes, platelets, neurons, placenta and kidney tubular epithelium. In the liver, McNaughton et al have demonstrated eNOS expression in healthy hepatocytes and endothelial cells, although in cirrhotic liver hepatocyte eNOS expression is increased whilst endothelial eNOS expression remains unchanged^{16, 22}.

In a similar manner to nNOS, eNOS binds calmodulin in a calcium-dependent manner. Several other proteins also interact with eNOS and regulate its activity as part of a multiprotein complex. For example, heat shock protein 90 (Hsp90), caveolin-1, activating kinase Akt1, and the trafficking proteins eNOS traffic inducer (NOSTRIN) and eNOS-interacting protein (NOSIP) all interact with eNOS¹⁶.

Additionally, the enzyme is also regulated by post-translational modifications, such as myristoylation, palmitoylation and phosphorylation, which regulate membrane binding and activity²³. The myristoyl group is covalently attached to the N-terminus of the protein, and localises eNOS to the cell membrane. Mutation studies of the myristoyl group have shown that it is necessary for membrane localisation and maximal enzyme activity – loss of N-myristoylation confers cytosolic localisation and reduced activity, but in isolated activity assays the enzyme is fully functional²⁴. Similarly, palmitoylation in the oxygenase domain of the enzyme occurs following myristoylation, and is thought to stabilise eNOS to the membrane²³. Again, palmitoyl-deficient eNOS has an altered subcellular distribution in that it is virtually absent from the plasma membrane, although the palmitoyl-deficient enzyme is not catalytically inferior to the wild-type enzyme²⁵.

These modifications regulating subcellular location of eNOS represent one level of post-translational regulation - eNOS has been demonstrated to localize to the plasma membrane and the golgi apparatus in most cell types. The predominant location of eNOS in the cell membrane is within flask-shaped invaginations of the plasma membrane, termed caveolae¹⁶. These areas are enriched in cholesterol and sphingolipids, creating a distinct area that facilitates protein-protein interactions.

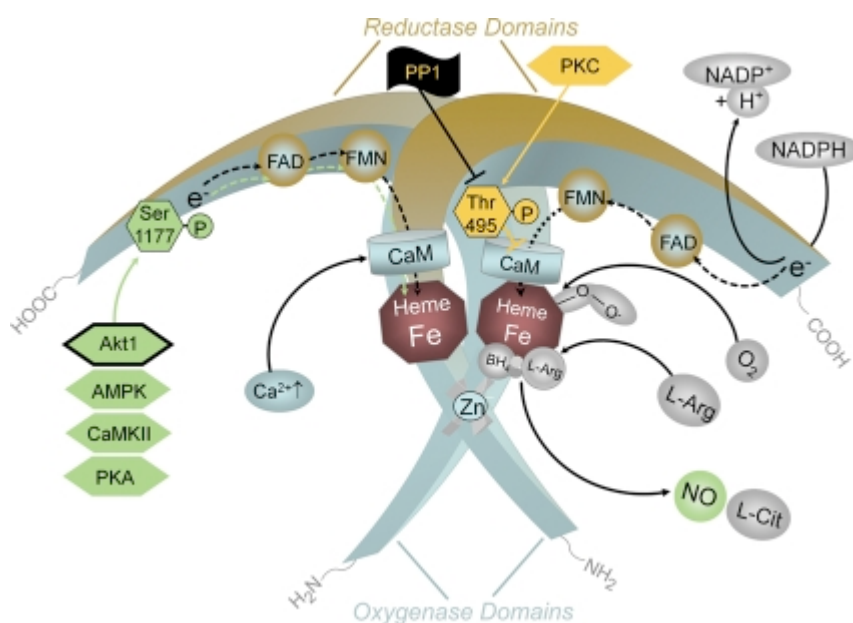


Figure 1.2b – adapted from Forstermann and Sessa¹⁶. An increase in intracellular Ca^{2+} leads to enhanced binding of calmodulin (CaM) to the enzyme, which in turn facilitates the flow of electrons from NADPH in the reductase domain to the haem in the oxygenase domain. In resting endothelial cells, Ser1177 is usually not phosphorylated. Phosphorylation is induced in response to shear stress, as well as other stimuli such as exposed to oestrogens, vascular endothelial growth factor (VEGF), insulin, bradykinin or fluid shear stress. The kinases responsible for phosphorylation (green hexagons) depend on the primary stimulus. Oestrogen and vascular endothelial growth factor elicit phosphorylation of Ser1177 by activating serine/threonine kinase Akt. Phosphorylation of the Ser1177 residue increases the flux of electrons through the reductase domain and thus enzyme activity. The Thr495 residue of human endothelial NOS tends to be constitutively phosphorylated in endothelial cells. Thr495 is a negative regulatory site, and its phosphorylation is associated with a decreased electron flux and enzyme activity.

Caveolin-1 is a protein which resides in caveolae, and acts as a tonic inhibitor of eNOS²⁶. The localization of eNOS within the caveolae renders the enzyme inactive due to the interaction of eNOS with caveolin-1. This interaction requires that eNOS be both myristoylated and palmitoylated.

Thus, at a cellular level, the recruitment of calmodulin (in response to increased intracellular calcium) and hsp90 to eNOS displaces caveolin-1 from the enzyme, leading to eNOS activation¹⁶. Caveolin-free eNOS is then translocated from the caveolae to the cytoplasm. Its enzymatic function there is greatly upregulated, including also Ca²⁺-independent steps. As a result, the electron flow from the reductase to the oxygenase domain is initiated, and NO is produced. In addition, in the caveolae the substrate l-arginine is recycled from l-citrulline, ensuring a sufficient pool for eNOS.

In addition, eNOS activity is influenced by posttranslational phosphorylation. The eNOS protein can be phosphorylated on several serine (Ser), threonine (Thr), and tyrosine (Tyr) residues. Phosphorylation of Ser1177 occurs in response to shear stress, by the kinase Akt1, and occurs independent of changes in intracellular calcium²⁷. Akt1 also mediates eNOS phosphorylation as a result of oestrogen, vascular endothelial growth factor (VEGF) and insulin signaling, thus Akt1 is important for both agonist and shear-stress activation of eNOS²⁸. Indeed, endothelial cells from Akt1 deficient mice have defects in eNOS phosphorylation, NO production and angiogenesis, which are reversed by Akt1 gene transfer²⁹.

The Thr495 residue of eNOS is constitutively phosphorylated in endothelial cells, and is thus a negative regulatory site. Phosphorylation of Thr495 is associated with decreased electron flux and enzyme activity. The constitutively active kinase that

phosphorylates eNOS Thr495 is suggested to be protein kinase C, and dephosphorylation of Thr495 occurs through the action of protein phosphatase1.

1.4 Vascular alterations in cirrhosis

1.4.1 The sinusoidal circulation

The sinusoidal circulation represents the capillary bed of the liver, and is highly specialised to facilitate metabolic exchange³⁰. The sinusoidal endothelial cells (SECs) are uniquely separated by small fenestrae, which are arranged in clusters of pores. Moreover these membrane-bound pores lack a specialised basement membrane, thus contrasting with the fenestrated endothelium found in the kidney, pancreas and brain. These fenestrae are dynamic structures that contract and dilate in response to alterations in sinusoidal blood flow and pressure³¹. Furthermore, the fenestrae control exchange of metabolic products between the circulation and hepatocytes, and also perform scavenger functions through endocytic capacity. Additionally, the SECs appear to have immune regulatory functions and antigen presenting capability³².

Several morphological abnormalities affect the sinusoidal circulation in cirrhosis. Anatomical changes such as fibrotic scar and regenerative nodule formation, which result in mechanical compression of the hepatic vasculature, have been traditionally implicated as the major cause for increased intrahepatic resistance. However, early changes in the sinusoidal vasculature include the loss of fenestrae and deposition of matrix within the space of Disse – processes that result in sinusoidal capillarisation and impede the exchange of solutes between the sinusoidal circulation and the liver parenchyma³³.

Shah and colleagues demonstrated in the isolated, perfused rat liver that eNOS is present in SECs, and that the production of NO is a regulator of hepatic vascular tone³⁴.

In cirrhosis, several investigators have demonstrated that intrahepatic NO is deficient. In both cholestatic and CCl₄ models of cirrhosis, Rockey et al demonstrated lower cGMP levels and lower eNOS activity¹⁰. In humans with cirrhosis, Mookerjee and colleagues have demonstrated increased eNOS protein expression, but lower eNOS activity in patients with alcoholic liver disease³⁵. Goh et al also found increased eNOS protein expression in patients with biliary cirrhosis although did not assay NOS activity³⁶. Sarela et al. also demonstrated decreased constitutive NOS activity in group of patients with primarily alcohol-related cirrhosis³⁷.

Following its generation in SECs, NO modulates vascular tone through a vasodilator effect on adjacent vascular smooth muscle. However, intrahepatic vascular tone is also regulated by HSCs, which adopt a myofibroblastic phenotype when activated³⁸. These activated HSCs have extensive coverage of the sinusoidal network through cellular extensions and can modulate intrahepatic resistance through contractility. In studies from humans and rodents, activated HSCs show increased responsiveness to endogenous vasoconstrictors (eg. endothelins, norepinephrine, angiotensin II, leukotrienes, thromboxane A₂) leading to increased contractility and intrahepatic resistance³⁹⁻⁴². The intrahepatic vasculature displays increased sensitivity to these vasoconstrictors in cirrhosis. Additionally, the activated HSCs play a key role in angiogenesis, leading to intrahepatic shunting and vascular collateral formation^{43, 44}.

On the other hand, iNOS is virtually absent in the normal liver, but highly upregulated in response to a variety of inflammatory or oxidative stresses. However, the role of

NO produced by iNOS in the regulation of the sinusoidal circulation has been an issue of debate. The treatment of rats with nonspecific NOS or primarily eNOS inhibitors results in a rapid exacerbation of liver injury following stresses such as endotoxin injection^{45, 46}. At the same time, in spite of marked upregulation of iNOS under these conditions, specific iNOS antagonists have little effect on liver perfusion^{47, 48}. These results suggest that NO is necessary to maintain the sinusoidal perfusion, but that eNOS is the key regulator of intrahepatic vasoactive NO. The specific localization of eNOS in endothelial cells is also significant, in that NO generated by endothelial cells is capable of diffusing to local sites of action to control sinusoidal resistance. In diseased liver, the translocation of eNOS away from the cell membrane may render it inactive²². Moreover, the expression of eNOS or iNOS in parenchymal cells or kupffer cells may have roles other than regulating sinusoidal blood flow.

Therefore, although other vascular mediators, e.g. thromboxane A₂, endothelins, hydrogen sulphide, carbon monoxide, are altered in cirrhosis, increasing constitutive NOS activity in the sinusoidal circulation is a rational goal for therapy of portal hypertension³⁰. Indeed, adenoviral mediated gene transfer of eNOS and nNOS to the liver results in lowered portal pressure in rodent models of cirrhosis^{49, 50}. Statins also augment eNOS activity and NO production, through increasing the phosphorylation of eNOS by Akt, and statins have been found to moderately decrease portal pressure in rodents and humans with chronic liver disease^{51, 52}.

1.4.2 The systemic and splanchnic circulations

The decreased bioavailability of intrahepatic NO in cirrhosis contrasts with the observed increase in whole body NO and splanchnic vasodilation. Several investigators have demonstrated increased NO breakdown products in the peripheral circulation in patients with cirrhosis. Vallance and Moncada initially suggested that splanchnic vasodilatation in cirrhosis may be due to low-level endotoxaemia and iNOS induction⁵³. Indeed, Jalan and colleagues recently demonstrated increased systemic NO production associated with endotoxemia in critically ill patients with advanced cirrhosis and placement of transjugular intrahepatic porto-systemic shunt⁵⁴. Plasma from these patients, when incubated with HUVEC cells, decreased eNOS activity but increased iNOS activity, leading to the hypothesis that increased systemic NO production in advanced cirrhosis is due to iNOS induction.

Data from rodent studies seem to vary depending on whether a pre-sinusoidal model of portal hypertension has been used, such as partial portal vein ligation (PPVL), or a model of cirrhosis. In the PPVL model, which is a model of portal hypertension but not of cirrhosis, it is clear from studies using knockout mice that eNOS is responsible for the major part of the observed vasodilatation rather than iNOS^{55, 56}. However, these animals are less representative of the pathophysiology of advanced cirrhosis, with less systemic inflammation and immune dysfunction. In rodents with biliary cirrhosis and portal hypertension, aortic iNOS expression is induced by the administration of bacterial LPS⁵⁷. Moreover, the role of iNOS expression in perivascular cells in cirrhosis has recently been investigated. Kajita et al. demonstrated that the adventitial layer of mesenteric vessels contain resident macrophages under control conditions, and in rats with biliary cirrhosis these cells increased in number and adopted an activated phenotype expressing iNOS⁵⁸. The

authors further showed cultured vessels from these animals that cirrhotic mesenteric vessels show increased NO generation in response to LPS, and reduced contractility to alpha-adrenoceptor agonists. Therefore, there is emerging evidence that paracrine effects of iNOS activation in inflammatory cells may increase mesenteric flow in advanced cirrhosis, and thereby augment portal hypertension. This is in direct contrast to the situation in the intrahepatic circulation (*vide supra*), where despite upregulation of hepatic iNOS expression following LPS administration, specific iNOS antagonists have little effect on liver blood flow.

1.5 Inflammation and portal hypertension

1.5.1 The role of inflammation in modifying portal pressure

These concepts of vascular dysfunction in cirrhosis are complimented by the recent description of the syndrome of acute-on-chronic liver failure (ACLF), an increasingly recognised entity describing an acute deterioration of liver function, regardless of underlying stage of cirrhosis, either secondary to superimposed liver injury or due to precipitating factors such as infection⁵⁹. In the recent prospective CANONIC study, patients with ACLF could be distinguished from those with acute decompensation of cirrhosis on the basis of hepatic and/or extrahepatic organ failure, the presence of a marked systemic inflammatory response, and high short-term mortality⁶⁰. Conceptually, the development of ACLF marks a departure from the traditional stepwise view of progression of cirrhosis and portal hypertension (figure 1.1). In the CANONIC study, patients with previously well-compensated cirrhosis had a significantly higher mortality following the development of ACLF than those with decompensated cirrhosis, marking a sharp contrast to the dogma of progressive liver disease. From a pathophysiological perspective it is likely that inappropriate pro-

inflammatory responses and systemic inflammation are key processes in the development of ACLF. Indeed, in CANONIC, mortality progressively increased with increasing severity of inflammation, as measured by leukocyte count and C-reactive protein.

Several investigators have found associations between systemic inflammation and severe portal hypertension. Rincon and colleagues demonstrated markedly elevated portal pressures in patients with alcoholic hepatitis and cirrhosis⁶¹. Similarly, Mookerjee et al demonstrated severe portal hypertension amongst patients with acute decompensation of alcoholic-related cirrhosis and histological evidence of steatohepatitis⁶².

1.5.2 Mechanisms of intrahepatic resistance in hepatic inflammation

It has been suggested that hepatic innate immune signalling contributes to portal hypertension through effects on fibrosis and intrahepatic vascular tone. The role of pathogen-associated molecular patterns (PAMPs) in the progression of fibrosis, in particular through TLR4 signalling, has been extensively studied. TLR4 is expressed on both parenchymal and non-parenchymal cell types in the liver, and its signaling is involved in the progression injury induced by viral hepatitis, alcoholic and non-alcoholic steatohepatitis, and cholestatic and drug-induced liver diseases⁶³. Several rodent studies support the importance of TLR4 in liver fibrosis. In response to liver injury induced by BDL or CCl₄ exposure, knockout mice that are deficient in TLR4, or in other signaling molecules of the TLR4 pathway such as CD14, LBP, MyD88, and TRIF, develop less fibrosis than wild type⁶⁴⁻⁶⁶. Selective decontamination of gut flora also suppresses the increase in plasma LPS and attenuates liver fibrosis in

these rodent models⁶⁵.

Although the TLR4 signaling pathway is involved in fibrosis, the elegant experiments by Seki et al demonstrate that this is a Kupffer cell (KC)-independent process⁶⁵. By contrast, in more advanced cirrhosis, KCs play a more prominent role in the development of hepatic inflammation and oxidative stress, leading to increased intrahepatic resistance. In alcoholic-related cirrhosis, TLR signaling on KCs leads to the production of pro-inflammatory cytokines such as TNF- α , IL-6, and IL-8, initiating both hepatic and systemic inflammation⁶⁷. A further downstream effect of TLR activation on KCs is the production of reactive oxygen species (ROS)⁶⁸. KCs also produce vasoactive mediators, predominantly from the cyclooxygenase-thromboxane A2 pathway, in response to PAMPs. LPS administration to cirrhotic rats leads to production of thromboxane A2 and cysteinyl leukotrienes, and augmented portal hypertension. Moreover, both KC depletion and treatment with the leukotriene antagonist Montelukast abrogate portal hypertension in this model^{69, 70}. There is also evidence of KC activation in humans - in cirrhotic patients a serum marker of KC activation, sCD163, has been shown to closely correlate with HVPG, severity of liver disease and risk of variceal haemorrhage⁷¹.

Thus, as discussed above, molecular mechanisms of increased intrahepatic resistance in cirrhosis include an imbalance of vasodilator and vasoconstrictor compounds, dysfunction of sinusoidal endothelium, and activation of contractile elements in vascular smooth muscle, portal myofibroblasts and HSCs. A further downstream effect of innate immune signaling and local oxidative stress is on SEC function. As noted above, local intrahepatic NO production is decreased in cirrhosis, although expression of the enzyme eNOS in SECs remains normal or increased, suggesting that NO production reduced due to either post-translational modification

of eNOS enzyme, such as decreased eNOS phosphorylation, or altered levels of endogenous eNOS cofactors/inhibitors. Several of these have been described in cirrhosis, including elevated levels of eNOS inhibitors asymmetric dimethylarginine (ADMA) and caveolin-1, and decreased levels of the eNOS co-factor tetrahydrobiopterin⁷²⁻⁷⁴

ROS generation in cirrhosis is due to both increased production from KCs, as well as decreased activity of elimination systems such as superoxide dismutase⁷⁵. Indeed, gene transfer of superoxide dismutase has been shown to lower portal pressure in rodent models of cirrhosis⁷⁶. Oxidative stress leads to decreased NO bioavailability through a number of mechanisms – ROS directly interact with NO leading to the formation of peroxynitrite and other reactive nitrogen species⁷⁷. Additionally ROS lead directly to eNOS dysfunction through eNOS ‘uncoupling’ and decreased eNOS phosphorylation, as well as increasing the formation of eNOS inhibitors⁷⁷. In this context, the role of the NOS inhibitor asymmetric dimethylarginine (ADMA) in regulating intrahepatic eNOS activity is of significant interest (figure 1.3).

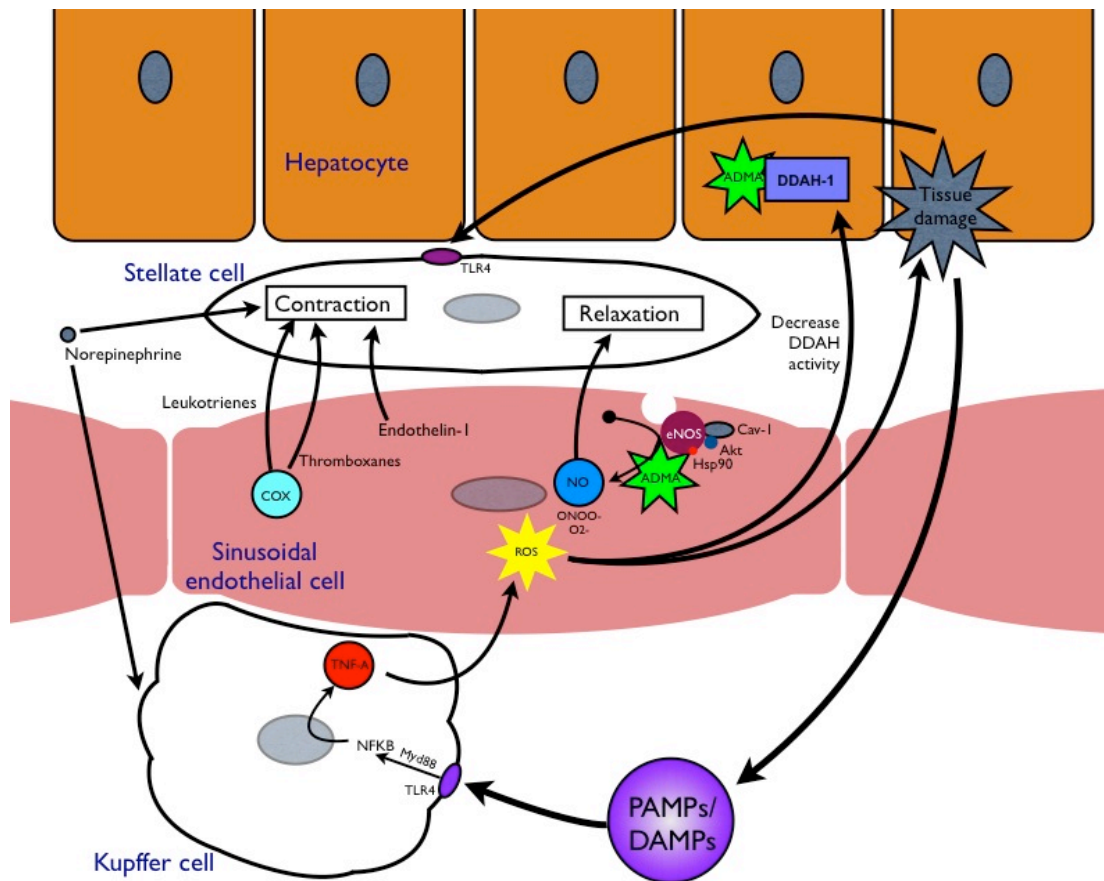


Figure 1.3 – adapted from Mehta et al⁷⁸. Nitric oxide (NO) regulates intrahepatic vascular tone, through maintaining HSCs in a quiescent phenotype and promoting vasodilatation through cGMP signaling. Asymmetric dimethylarginine (ADMA) is a paracrine, competitive inhibitor of NO synthesis by endothelial nitric oxide synthase (eNOS), and is metabolized in the hepatocyte by dimethylarginine dimethylaminohydrolase-1 (DDAH-1). Inflammation leads to ROS generation by KCs, which inhibits DDAH-1 activity thereby leading to eNOS inhibition and decreased local NO production. ROS also interact with free NO generating further reactive nitrogen species (RNS) contributing to local tissue damage and propagating innate immune signaling through DAMPs. The activated SEC also produces further vasoactive mediators such as endothelin-1 and thromboxanes/leukotrienes which increase HSC contractility thereby increasing intrahepatic resistance. Noradrenaline, which is elevated in ACLF, also increases HSC contractility and augments local innate immune signaling.

1.6 The role of the DDAH-ADMA system

Asymmetric dimethylarginine (ADMA) is a product of the post-translational methylation of arginine residues within proteins, and the subsequent proteolysis of these arginine methylated proteins. These methylated arginine residues are competitive inhibitors of all nitric oxide synthases, competing with L-arginine to bind the active site of NOS. To date, they are the only known by-products of post-translational protein modification to have biological effects.

Protein arginine methylation is a common post-translational modification, and has been shown to coordinate cellular functions such as signal transduction, transcriptional regulation and protein-protein interactions⁷⁹. ADMA is synthesized following the methylation of arginine residues in proteins by a group of methyltransferases that are termed protein arginine methyl-transferases (PRMTs)⁸⁰. To date, 11 mammalian PRMTs have been identified. The three methylated arginine products are N-monomethyl-L-arginine (L-NMMA), NN-symmetric dimethylarginine (SDMA) and ADMA. Only L-NMMA and ADMA are inhibitors of NOS and circulating levels of ADMA are considerably higher than L-NMMA, hence ADMA is considered the principal methylarginine inhibitor of NOS activity.

Methylarginines only appear in the cytosol as a result of protein degradation, and no direct synthetic route for the production of ADMA, SDMA and L-NMMA from free arginine has yet been identified. Furthermore, the synthesis and degradation of methylated argenines are closely coupled with the synthesis and degradation of methylated proteins⁸¹. Thus, intracellular ADMA levels are governed by PRMT activity, protein turnover and clearance.

Intracellular levels of ADMA are in the low micromolar range, whereas intracellular arginine levels are 10-100 fold greater. However, despite this vast excess of arginine, supplementation of arginine can enhance endothelial function through increased NO generation⁸². This has been termed the 'arginine paradox'. However, recent work in human endothelial cells has demonstrated that not all intracellular arginine is available for metabolism by membrane bound eNOS⁸³. Moreover, enzyme kinetic studies have demonstrated that even with physiological concentrations of L-arginine, dose-dependent inhibition of NO formation in endothelial cells was observed with extracellular ADMA concentrations as low 5uM⁸⁴. Therefore, ADMA is likely to be a critical regulator of endothelial function at pathophysiological levels.

ADMA is removed from the body through predominantly by metabolism by the dimethylarginine dimethylaminohydrolase (DDAH) enzymes, although renal excretion and metabolism by the alternative AGX-2 pathway also occurs (figure 1.4)^{85, 86}. There are 2 DDAH enzymes, DDAH-1 and DDAH-2, although DDAH-1 has far greater hydrolase activity than DDAH-2 and hence is the principal pathway of ADMA elimination⁸⁷. Heterozygous deletion of DDAH-1 results in a 40-45% decrease in total DDAH activity in vivo, and also causes a phenotype of systemic hypertension and endothelial dysfunction⁸⁸.

It follows, therefore, that pharmacological modulation of methylarginine levels is an attractive therapeutic strategy in conditions characterised by decreased NO bioavailability and endothelial dysfunction, and further that this could be achieved through targeting methylarginine synthesis by PRMTs or by targeting degradation through DDAHs. However, PRMTs may not be suitable targets for pharmacological manipulation since they are essential for many fundamental biological processes.

For example PRMT1 plays an important role in the regulation of histone function, and deletion of PRMT1 is lethal in utero⁸⁹. Additionally, targeting PRMT activity is complicated by the presence of numerous PRMT isoforms that share substantial sequence homology⁹⁰.

By contrast, hepatic DDAH-1 is an attractive target for therapy in cirrhosis and portal hypertension. The liver is a major site of DDAH-1 expression and DDAH activity⁹¹. Plasma levels of ADMA are elevated in cirrhosis, and are elevated further in ACLF precipitated by alcoholic hepatitis⁷². Hepatic levels of ADMA correlate with HVPG in patients with ACLF, associated with decreased hepatic expression of DDAH-1. Moreover, DDAH-1 is sensitive to oxidative stress⁹², hence ROS production by activated KCs is hypothesized to decrease DDAH-1 expression and activity, and thereby increase levels of the eNOS inhibitor ADMA, thus decreasing local NO generation (figure 1.3).

A further evolving area of interest is ADMA-independent actions of DDAH-1, possibly mediated through direct protein-protein interaction. DDAH-1 has been shown to directly interact and regulate the phosphorylation of neurofibromin⁹³. Additionally, DDAH-1 is thought to phosphorylate Akt independent of ADMA metabolizing activity⁹⁴, as well as play a role in cell cycle regulation⁹⁵. These observations, which require further study, have important implications for any off-target effects of therapeutic strategies to augment DDAH-1.

Unlike DDAH-1, DDAH-2 is expressed in immune cells and has been suggested to play a role in the regulation of iNOS-mediated NO generation in conditions of inflammation and infection⁹⁶. The genetic location of DDAH-2 in the major histocompatibility complex III region of chromosome 6 lends support to this

hypothesis⁹⁶, as does data demonstrating an association between human DDAH-2 promoter polymorphisms and outcome in sepsis⁹⁷. Recently, Lambden et al characterized the phenotype of *Ddah2*^{-/-} mice, which display unchanged basal blood pressure, unlike the *Ddah1*^{+/-} mouse which displays systemic hypertension⁹⁸. Moreover, the *Ddah2*^{-/-} mouse displays increased sensitivity and mortality to polymicrobial sepsis compared to wild type, consistent with a role in immune regulation and function.

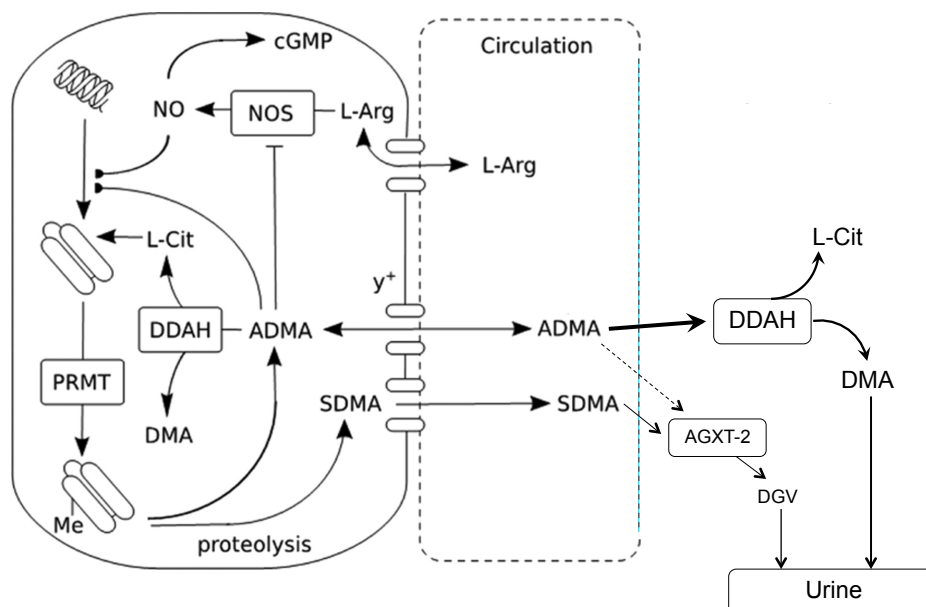


Figure 1.4: The DDAH-ADMA pathway - adapted from Leiper and Caplin⁹⁹. L-arginine (L-Arg) is present in the circulation at >100 times the concentrations of the free endogenous methylarginines: ADMA and symmetric dimethylarginine (SDMA). ADMA but not SDMA inhibits all 3 isoforms of nitric oxide synthase (NOS), decreasing the production of nitric oxide. L-arginine and the free methylarginines are thought to enter the cell (shown on the left) through the y⁺ transporter. ADMA and SDMA are generated intracellularly following the methylation, by protein-arginine methyltransferases (PRMT), and subsequent proteolysis, of constituent protein arginine residues. ADMA but not SDMA is hydrolyzed by DDAH to form dimethylamine (DMA) and L-citrulline (L-Cit), which can be reincorporated into proteins. The major pathway of ADMA elimination is metabolism by DDAH-1 with the product DMA excreted in the urine. Both SDMA and ADMA are also substrates for alanine-glyoxylate aminotransferase-2 (AGXT2), leading to the formation of symmetrical and asymmetrical α-keto-δ-dimethylguanidino valeric acid (DGV) that is also excreted in the urine.

1.7 Aims

The aims of this thesis are: (i) to delineate the expression and regulation of hepatic DDAH-1 in cirrhosis and portal hypertension, in both rodent models and humans, and (ii) to determine if there is a causal relationship between hepatic DDAH-1 and portal hypertension in cirrhosis.

Therefore, the specific questions addressed by this study are:

- *What is the cellular location of DDAH-1 within the liver in humans and rodents?*
- *Is hepatic DDAH-1 expression altered in cirrhosis and portal hypertension, in humans and rodents?*
- *Does gene therapy to reconstitute hepatic DDAH-1 lower portal pressure in a rodent model of portal hypertension?*
- *What is the mechanism of altered hepatic DDAH-1 expression in cirrhosis and portal hypertension, in humans and rodents?*
- *Are alternative transcripts of DDAH-1 of biological or pathobiological significance?*

These aims are important, since extending current understanding of the regulation of DDAH-1 in conditions of oxidative stress has implications for portal hypertension as well as other conditions characterized by endothelial dysfunction, and will also allow

potential translation of mechanisms to augment hepatic DDAH-1 as a therapeutic strategy in in portal hypertension.

Chapter 2 – Generic Materials and Methods

2.1 General Materials

2.1.1 Plasmids and reagents for molecular biology

All general chemicals and reagents were of analytical grade and purchased from Sigma-Aldrich (Gillingham, UK). All solutions used for RNA extraction were prepared using sterile DEPC treated water purchased from Life Technologies Ltd (Paisley,UK). The pGEM-T Easy vector, and Dual Luciferase Reporter (DLR) Assay System were purchased from Promega UK (Southampton, UK). ABI real time PCR reagents were purchased from Life Technologies Ltd (Paisley,UK), including TaqMan gene expression master mix, and TaqMan gene expression probes. General real-time components (optical seals, 96 well plates) were also purchased from Life Technologies Ltd (Paisley,UK).

FuGene 6 transfection reagent was obtained from Roche Products Ltd (Welwyn Garden City, UK). The QIAquick gel extraction kit and plasmid Mini/Midi Prep kits were purchased from Qiagen Ltd (Manchester, UK). The Superscript II RT-PCR kit, T4 DNA ligase, RNase-free DNase, synthesised oligonucleotides and deoxynucleotide (dNTPs) were purchased from Life Technologies Ltd (Paisley,UK). Restriction enzymes and buffers were obtained from New England Biolabs (UK) Ltd (Hitchin, UK). Other reagents not outlined here were from suppliers indicated throughout this chapter.

2.1.2 Reagents for Cell Culture

HEK293T embryonic kidney cells and HepG2 hepatocytes were purchased from European Collection of Cell Cultures (Public Health England, Salisbury, UK). Cell culture media, L-glutamine, penicillin/streptomycin, fetal bovine serum and fetal horse serum were all purchased from Life Technologies Ltd (Paisley,UK). Bovine aortic endothelial cells (BAECs),

and BAEC cell culture media, were purchased from Cell Applications Inc (UK distributor: ECACC, Public Health England, Salisbury, UK)

Cells were grown in sterile six-well plates, 6mm and 10mm petri dishes, 25cm³ and 75cm³ flasks (Nunc, Fisher Scientific UK Ltd, Loughborough, UK).

2.2 DNA Manipulation

2.2.1 Standard Polymerase Chain Reaction (PCR)

Standard PCR was used to amplify DNA fragments for cloning, diagnostic or semi-quantitative analysis (for example, diagnostic PCR of recombinant plasmids during cloning process) PCR reactions were set up using 100-500ng DNA sample, 1X Abgene buffer, 1.5mM MgCl₂, 0.2mM dNTP, 500nM forward primer, 500nM reverse primer and 1.25 Units of GoTaq (Promega UK) Taq polymerase, in a final volume of 50µl. Typical thermocycling parameters were 1 cycle for 94°C; 25-30 cycles 94° C for 45 seconds, 59°C for 45 seconds; 72°C for 45 seconds; and a final extension step of 72°C for 5 minutes.

2.2.2 Agarose gel electrophoresis

1X loading buffer [40% (^{v/v}) glycerol, 60% (^{v/v}) TE Buffer (Tris Ethylene diamine tetra-acetic acid (EDTA), 10 mM Tris-HCL, 1mM EDTA, pH 8.0)] and 1X bromophenol blue were added to the DNA samples of interest. Samples were then pulse-spun in a centrifuge (Eppendorf Minifuge, 20 seconds, 12,000 rpm) and loaded onto the appropriate percentage agarose gel in 1X Tris-Acetate EDTA (TAE) buffer (400mM Tris-HCL, 20mM glacial acetic acid, 0.1mM EDTA, pH8.0) and run alongside an appropriate sized marker (Promega UK, 100bp and 1kbp). The gel contained ethidium bromide added at a concentration of 0.035µg/ml. The gel was typically electrophoresed in 1X TAE buffer for 1 hour at 80 V. The gel and associated

migrated bands were then visualised on ultraviolet light using a gel documentation and imaging system (Bio-Rad Laboratories Ltd, Hemel Hempstead, UK).

2.2.3 DNA extraction and purification from agarose gel

The required electrophoresed DNA fragments were extracted with a scalpel from the agarose gel and purified using the QIAquick gel extraction kit (Qiagen Ltd), as described in the suppliers handbook. Purified DNA was typically quantified and stored at -20°C.

2.2.4 DNA determination

DNA concentration was determined using the NanaDrop™ (ND-1000, Fisher Scientific UK Ltd, Loughborough, UK) spectrophotometer, with absorbance measured at wavelengths of 260nm and 280nm. The DNA purity was determined by the ratio of the absorbance at 260nm/ 280nm.

2.2.5 Ligation of isolated DNA into vector

The appropriate amount of insert DNA was placed into the ligation reaction with 100ng of the vector (pGEM-T Easy, Promega UK). Typically the appropriate amount of insert is calculated so that there was a 3x insert:1x vector ration; $(\text{vector, ng} \times \text{insert size, kb}) \div (\text{size of vector, kb} \times \text{insert:vector ration}) = \text{ng of insert}$. The reaction also contained 3U of T4 DNA Ligase (Life Technologies Ltd), 1X TD DNA ligase buffer and H₂O, to make final volume 10µl. A control reaction is also established where the insert DNA fragment is omitted, thereby allowing one to determine the presence of re-circularised vector plasmid. Both reactions were incubated overnight at 4°C.

2.2.6 Transformation of bacteria with plasmid DNA

Typically 5µl of the ligation reaction was added to 100µl DH5α chemically competent cells (Life Technologies Ltd), mixed gently and incubated on ice (or at 4°C) for 30 minutes. Heat shock treatment at 37°C for 45 seconds was executed using a pre-calibrated water bath. The reaction was then allowed to recover on ice for 2 minutes prior to the addition of 400µl pre-warmed SOC, a high nutrient broth media. The reaction was then incubated for exactly 1 hour at 37°C in a rotating incubator at 225 rpm. Following this 1-hour incubation step, half of the reaction volume was extracted and spread onto a Luria broth (LB) agar plates containing the appropriate selection antibiotic for transformed cell selection (eg. Ampicillin 100µg/ml). Where blue/white selection of transformants was necessary, 40µl X-Gal (20mg/ml) was added to the LB agar plates. Plates were inverted and incubated for 16 hours at 37°C.

Subsequently, single isolated transformant colonies were picked and grown in 10ml of LB (containing the appropriate selection antibiotic) for 16 hours in a rotating incubator at 37°C, at 225 rpm. Using the QIAprep Spin Miniprep kit (Qiagen Ltd) according to the manufacturers instructions, plasmid DNA for diagnostic digest was extracted from 6ml of the 16 hour growth culture. For positive clones, their remaining 4ml of culture was used to make a 20%(v/v) glycerol stock for long-term storage at -80° C, and the remaining 10-15ml was used to establish a secondary culture to extract plasmid DNA for the purpose of further cloning, sequencing or transfection. The plasmid DNA was extracted using the Qiagen Plasmid Mini Kit, following the manufacturer's instructions.

2.2.7 Restriction enzyme digest

Plasmid DNA was digested using 10U of the required restriction endonuclease (New England Biolabs (UK) Ltd) in a final volume of 20µl, which also contained 1X appropriate restriction endonuclease buffer (Life Technologies Ltd). The digests were incubated for 2

hours at 37°C therefore ensuring complete digestion. Double digests were set up in compatible buffers where appropriate.

2.2.8 Plasmid modification by annealed oligonucleotide cloning

Mutations were introduced into plasmid sequences (for example, to determine functionality of predicted regulatory DNA sequences) through cloning of complementary annealed oligonucleotides. Oligonucleotide sequences were designed using Primer3 primer design software (<http://primer3.ut.ee/>), to predict the formation of hairpins and loops that would prevent successful annealing. Complementary oligonucleotides, with overhangs to allow subsequent directional cloning, were purchased from Life Technologies Ltd.

Oligonucleotides (1ug of each, in equimolar concentrations) were then resuspended in 50uL annealing buffer (10mM Tris, pH7.5-8.0, 50mM NaCL, 1mM EDTA). After heating to 90-95°C for 3-5 minutes, the samples were allowed to slowly cool to room temperature (~45 minutes). Annealing was confirmed by agarose gel electrophoresis as in section 2.2.2, although the gel was visualised using methylene blue staining rather than UV irradiation to eliminate the possibility of DNA damage for subsequent experiments. Methylene blue staining was performed in 0.002% methylene blue (^{w/v}, Sigma-Aldrich M-4159) solution in 0.1X TAE (0.004M Tris 0.0001 M EDTA) for 1 hour at room temp. DNA extraction and ligation was subsequently performed as in 2.2.3-2.2.5.

2.3 Cell Culture

2.3.1 Maintenance of cell lines and primary cells

Both cell lines (HEK293T and HepG2) were routinely cultured as monolayers in Dulbecco's modified Eagles medium (DMEM) containing glutamax-1, which was supplemented with 100

units/ml streptomycin, 100 units/ml penicillin and 10% (v/v) foetal bovine serum, in a humidified atmosphere at 37°C composed of 5% CO₂. HEK293T and HepG2 cells were typically passaged upon reaching 70-80% confluence thereby ensuring the preservation of myoblast cellular phenotype. To passage, cells were washed once with pre-warmed phosphate-buffered saline (PBS) and incubated with a trypsin-EDTA solution (0.2% trypsin, 1mM EDTA) for 2-4 minutes. The flasks were then gently agitated to disrupt cell adhesion, before re-suspending at a 1:4 dilution in fresh pre-warmed media.

Primary BAECs were purchased from Cell Applications Inc. at passage 3, and were cultured as monolayers in Bovine Endothelial Cell Growth Medium (Cell Applications Inc.), in similar conditions as above. All experiments were carried out in BAECs between passages 4 and 8. Cells were passaged with trypsin-EDTA as above.

2.3.2 Storage of cells

In the short-term cells were stored at -80°C, whereas for long-term storage cells were frozen in liquid nitrogen. For long-term freezing, cells were washed once with pre-warmed PBS and incubated with a trypsin-EDTA solution (0.2% trypsin, 1mM EDTA) for 2-4 minutes. The flasks were then gently agitated to disrupt cell adhesion. Before re-suspending in 1 ml cell culture media, an equal amount of cell culture media for storage was prepared and mixed with 20% (v/v) DMSO. Cells re-suspended in this DMSO containing culture media were then aliquoted and frozen slowly at -80°C by placing in an isopropanol containing insulated box. After 24 hours, these cell aliquots were transferred to a liquid nitrogen cell bank for long-term storage.

2.4 RNA manipulation

2.4.1 RNA isolation from cells and tissues

Total RNA was extracted from rat tissues using the RNeasy Maxi kit (Qiagen Ltd) or the miRNeasy Maxi kit (Qiagen Ltd) following the manufacturer's protocol. Total RNA was isolated from cell lines using the RNeasy Mini kit (Qiagen Ltd) or the miRNeasy Mini kit (Qiagen Ltd) according to the manufacturer's protocol. Briefly, media was removed and cells were washed twice in pre-warmed PBS. 350µl of RNeasy RLT lysis buffer is then added to the cells. Lysate was collected and RNA extraction was executed as described in the RNeasy or miRNeasy kit handbook (Qiagen Ltd).

2.4.2 RNA determination

RNA concentration was determined using the NanaDrop™ (ND-1000, Fisher Scientific UK Ltd) spectrophotometer, with absorbance measured at wavelengths of 260nm and 280nm. The RNA purity was determined by the ratio of the absorbance at 260nm/ 280nm.

2.4.3 Deoxyribonuclease (DNaseI) treatment of RNA

1µg of total RNA was incubated with DNaseI (Sigma-Aldrich) according the manufacturer's instructions (on column digestion). The DNaseI treated RNA was then reverse transcribed as described in section 2.4.3.

2.4.4 cDNA synthesis

1 µg of DNaseI treated total RNA was incubated with 0.5µg oligo dT, and 0.5mM dNTP mix for 10 minutes at 70°C in a Perkin Elmer Cetus DNA thermal cycler. The reaction was then placed on ice for 2 minutes and briefly centrifuged to remove condensation. This reaction was then supplemented with 1X First strand buffer (Invitrogen), 10mM DTT and 200 U Superscript II reverse transcriptase (RT) enzyme (Invitrogen) giving a total reaction volume

of 20µl. Control reactions (minus RT) were also established that contained equal volume of H₂O instead of Superscript II RT enzyme. The reactions were then incubated in the thermal cycler at 42°C for 55 minutes; 70°C for 10 minutes and then finally back on ice for recovery. The subsequent cDNA was typically diluted 1:5 with DEPC treated H₂O, with 1µl used for down-stream PCR amplification.

2.4.5 Quantitative real-time PCR

Multiple reactions were set up as a master mix and a typical 20µl reaction would contain: 1µl template cDNA (1:5 dilution from RT reaction), 1µl 20X pre-formulated assay mix (Applied Biosystems – containing 0.9mM forward and reverse primers coupled to 250nM FAMTM-dye labelled TaqMan MGB probe), 10µl 2X TaqMan Universal PCR master mix (Applied Biosystems), ddH₂O to a final volume of 20µl.

Typically a “no template” control was also included using ddH₂O instead of cDNA template. For TaqMan gene expression analysis, Cyclophilin A (PPIA) was used as a reference gene to normalise mRNA abundance between different samples. The amplification reaction was executed in a ABI Prism® 7900HT sequence detection system (Life Technologies Ltd). The cycling conditions were 50°C for 2 minutes (holding step), 95°C for 10 minutes (holding step) and then 40 cycles of 95°C (denaturation) and 60° C for 1 minute (annealing and extension step). The data were automatically sorted and analysed using the comparative $\Delta\Delta CT$ method¹⁰⁰. This method allows the quantitative determination of fold induction of gene of interest between different samples using the following formula:

$$\text{Fold induction} = 2^{-\Delta\Delta CT}$$

$$\Delta CT = \text{mean CT}(\text{gene of interest}) - \text{mean CT}(\text{reference gene})$$

$$\Delta\Delta CT = \Delta CT(\text{calibrator}) - \Delta CT(\text{unknown})$$

The calibrator sample, which is typically represented by the non-treated or basal control sample, allows for corrections to be made for inter-assay variation. It is important to note that the above formula is based on the assumption that the efficiency of the PCR reaction for both the reference internal control gene, and the gene of interest is identical with a doubling of product being achieved with every cycle.

2.5 Transient transfection analyses

2.5.1 Transient transfection of cell lines

Approximately 40,000 HEK293T or Hep2G2 cells/well were seeded and incubated for 24 hours prior to transfection. Transfections were carried out using the non-liposomal transfection reagent Fugene6 (Roche Products Ltd), according to the manufacturer's instructions. In some experiments, cells were co-transfected with 0.5µg of pMirReport Firefly luciferase construct and 0.1µg of pTK-Renilla luciferase expressing plasmid to act as a control of transfection efficiency.

Firefly and Renilla luciferase activities were measured 48 hours post- transfection using the Dual-Glo luciferase assay system (Promega UK) as described in section 2.5.2.

All transfections within each experiment were performed in triplicate, with each experiment typically performed on a minimum of at least three separate occasions. Data from transfections are expressed as mean \pm 1 standard error of mean (SEM) relative to promoter construct specified, and differences between samples were detected using a one-way ANOVA, with $p < 0.05$ considered to be statistically significant.

For non-luciferase reporter transfections, six-well plates were seeded as before and transfected with a maximum of 1.5µg over-expression plasmid. 48 hours post transfection total RNA was isolated from cell as described in section 2.4.1.

2.5.2 Luciferase reporter gene assay

Firefly and Renilla luciferase activities were measured 48 hours post transfection using the Dual-Glo™ luciferase assay system (Promega UK) and a Luminat LB9507 luminometer (Berthold Technologies). The assay was undertaken as described in the users' handbook (Dual-luciferase assay handbook, Promega UK). Briefly, cells in the six well plates were lysed using the luciferase cell lysis buffer (CLB, Promega UK). The first luminescence from the firefly luciferase, representing promoter reporter activity, was measured by adding 100µl of LARII substrate into 40µl of cell lysate in a fresh luminometer tube. The second luminescence for Renilla luciferase (representing the internal control activity) was quantified by the addition of 50µl of Stop and Glo substrate to quench the first reaction and simultaneously initiate Renilla luciferase reaction. Data were then extrapolated as relative luciferase activity, the ratio of the first Firefly luminescence over the second Renilla luminescence.

2.6 Polyacrylamide gel electrophoresis (PAGE)

2.6.1 Resolving gel

Proteins were separated according to molecular weight devised by Laemmli¹⁰¹, with minor modifications, using mini-protean or protean XL vertical slab gel apparatus (Bio-Rad Laboratories Ltd). Prior to casting resolving gels, all solutions were de-gassed. N, N, N', N'-tetramethylethylenediamine (TEMED) and ammonium persulphate (APS) were added to the polyacrylamide solution with stirring immediately prior to casting of the gels (Table 2.1). Gels were over-layered with water saturated butan-2-ol, covered with aluminium foil and

allowed to polymerise for 2 hours.

Table 2.1: Constituents of resolving gels for SDS-PAGE

	Volumes (ml)			
	8% Gel	10% Gel	12% Gel	Stacking Gel (5%)
30% (^{w/v}) Acrylamide mix	2.7	3.3	4.0	1.7
1.5M Tris-HCl (pH 8.8)	2.5	2.5	2.5	
1M Tris HCl (pH 6.8)				1.25
10% (^{w/v}) SDS	0.1	0.1	0.1	0.1
10% (^{w/v}) APS	0.1	0.1	0.1	0.1
TEMED	0.004	0.004	0.004	0.01
dH ₂ O	4.6	4.0	3.3	6.8

2.6.2 Stacking gel

A stacking gel (5%, table 2.2) was used to concentrate the proteins into tight bands prior to entering the resolving gel. Prior to casting the stacking gel, the butan-2-ol over-layer was removed from the surface of the resolving gel and the gel surface washed with water to remove all traces of butan-2-ol. After pouring the stacking gel on top of the resolving gel, a 15 well comb was placed into the stacking gel and it was allowed to polymerise for 1 hour.

2.6.3 Protein extraction

Cells were lysed in RIPA buffer (750 mM NaCl, 5% (v/v) NP40, 2.5% (w/v) DOC, 0.5% (w/v) SDS, 250 mM Tris-HCl pH 8.0) centrifuged at 13 000 x g for two minutes and the supernatant transferred to a clean eppendorf tube. Subsequently the protein concentration was determined using the BCA method (*vide infra*).

Rat liver tissue samples were processed in 100mg blocks. Tissue was ground to a fine powder using a pestle and mortar and lysed in 1ml of RIPA buffer (RIPA, 0.75 M NaCl, 5% (v/v) NP40, 2.5% (w/v) deoxycholate, 0.5% (w/v) SDS, 0.25 M Tris-HCl pH 8.0, 10 mM Dithio-L-threitol (DTT) containing protease inhibitors) and incubated on ice for 15 minutes. The lysate was centrifuged at 13 000 x g for 5 minutes at 4°C and the clarified supernatant transferred to a clean siliconised eppendorf and the protein concentration determined using the BCA method.

2.6.4 Protein concentration measurement

Protein concentration for SDS-PAGE was determined using the Pierce bicinchononic acid (BCA) protein assay kit (Life Technologies Ltd). BCA solution was made by combining 50 parts of reagent A with 1 part reagent B. 200 µl of BCA mix was added to 2 µl of protein sample and incubated at 37°C for 30 minutes and the absorbance measured using a Genios microplate reader (Tecan UK Ltd, Reading, UK) at $\lambda = 560$ nm. Protein concentration was determined by comparing the O.D. of the sample solution to a BSA standard curve.

2.6.5 Western blotting

Typically 40 µg of protein sample was used for both cell culture lysate and tissue lysate

samples. The protein samples were mixed with PBS, NuPAGE LDS sample buffer (4×) and β-mercaptoethanol (50x) to a total volume of 20µl, and were boiled for three minutes prior to loading.

Samples were loaded onto 1D-PAGE gels and electrophoresed at 200 volts for one hour in protein running buffer (191.8 mM Glycine, 25 mM Tris, 1% (w/v) SDS). The stacking gel was removed and the resolving gel placed onto a sponge and two pieces of filter paper pre-soaked in transfer buffer (protein running buffer containing 25 % (v/v) methanol). A piece of Hybond-C membrane (GE Healthcare Life Sciences, Little Chalfont, UK) was cut to the same size as the gel and pre-soaked in transfer buffer. The membrane was placed on the surface of the gel and two-pieces of pre-soaked filter paper placed on top of the membrane followed by a second sponge. Proteins were transferred to the membrane at 100 volts for 1 hour. The membrane was then incubated in 4% (w/v) non-fat milk for 1 hour at room temperature to block non-specific proteins.

Antibodies were dissolved in 4% (w/v) non-fat milk, the membrane added and probed over night at 4°C. Membranes were washed in Tris-buffered saline containing 0.05% (v/v) Tween 20 (Sigma-Aldrich, UK) three times for 5 minutes each. The membranes were then added to 4% (w/v) non-fat milk containing horseradish peroxidase (HRP) conjugated secondary antibody (1:1000 dilution, Dako UK Ltd, Ely, UK), incubated for 1 hour at room temperature and washed three times for 5 minutes each.

Proteins were visualized using enhanced chemiluminescence (ECL, GE Healthcare Life Sciences). Excess TBS-T was removed by placing the membrane on to absorbent paper, the ECL reagent pipetted on to the membrane and incubated at room temperature for 1

minute. Excess ECL reagent was removed and the membranes exposed to photosensitive film to visualize the proteins.

Densitometry of protein bands was automatically measured using Image Lab software on the gel documentation and imaging system (Bio-Rad Laboratories Ltd). Data were calculated as the ratio of target protein band to loading control protein band density, and were expressed as mean \pm 1 SEM. Differences between samples were detected using a one-way ANOVA, with $p < 0.05$ considered to be statistically significant.

2.7 Histology and immunohistochemistry

Tissues were fixed in 10% formalin, embedded in paraffin and 4 μ m sections were cut on a rotary microtome. Paraffin embedded sections were dewaxed and rehydrated using serial alcohol and water immersion according to standard techniques. For some sections, antigen retrieval was carried out by microwaving the section in 10mM sodium citrate buffer, pH 6.0, for five minutes. Sections were incubated in 1% hydrogen peroxide to quench endogenous peroxidase activity and then incubated in 5% normal goat serum. Subsequently, individual sections were incubated overnight with antibodies specific for DDAH-1 (Abcam, Cambridge, UK). After washing, sections were incubated in biotin-conjugated secondary antibody (Vector Laboratories Ltd, Peterborough, UK) followed by streptavidin-biotin peroxidase complex solution (Dako UK Ltd). Colour reactions were developed by incubating sections in 3'3-diaminobenzidine (Sigma-Aldrich, UK) for 5 minutes and rehydrated through ethanol series into xylene. Rehydrated sections were mounted using DPX mounting media and images captured on a Zeiss Axioscope 2 plus microscope (Carl Zeiss Ltd, Cambridge, UK).

2.8 *In vivo* studies

All animal experiments were conducted according to the Home Office guidelines under the UK Animals in Scientific Procedures Act 1986. All experiments in this thesis were performed in male Sprague- Dawley (SD) rats, weighing 220–250g. All rats were housed in the Comparative Biology Unit, UCL, and given free access (*ad libitum*) to standard rodent chow and water until the night before their sacrifice, with a light/dark cycle of 12 hours (the dark phase extended from 1900–0700 hours), at a temperature of 22–23°C and humidity of approximately 50%.

2.8.1 Bile duct ligation surgery

Surgery was performed after induction anaesthesia with (1L/min oxygen with 5% isoflurane) and maintenance with 2% w isoflurane. All rats were given subcutaneous injection of Bupivacaine 5 mg/kg body weight perioperatively as analgesic as specified in the project licence. All rats underwent bile duct ligation to induce biliary cirrhosis or a sham operation. A midline abdominal incision was made. The common bile duct was isolated and three ligatures were tied with the highest one as proximal as to the porta hepatis and sectioned between the two distal sutures. Sham operated rats underwent laparotomy and isolation of the common bile duct without any ligature or section.

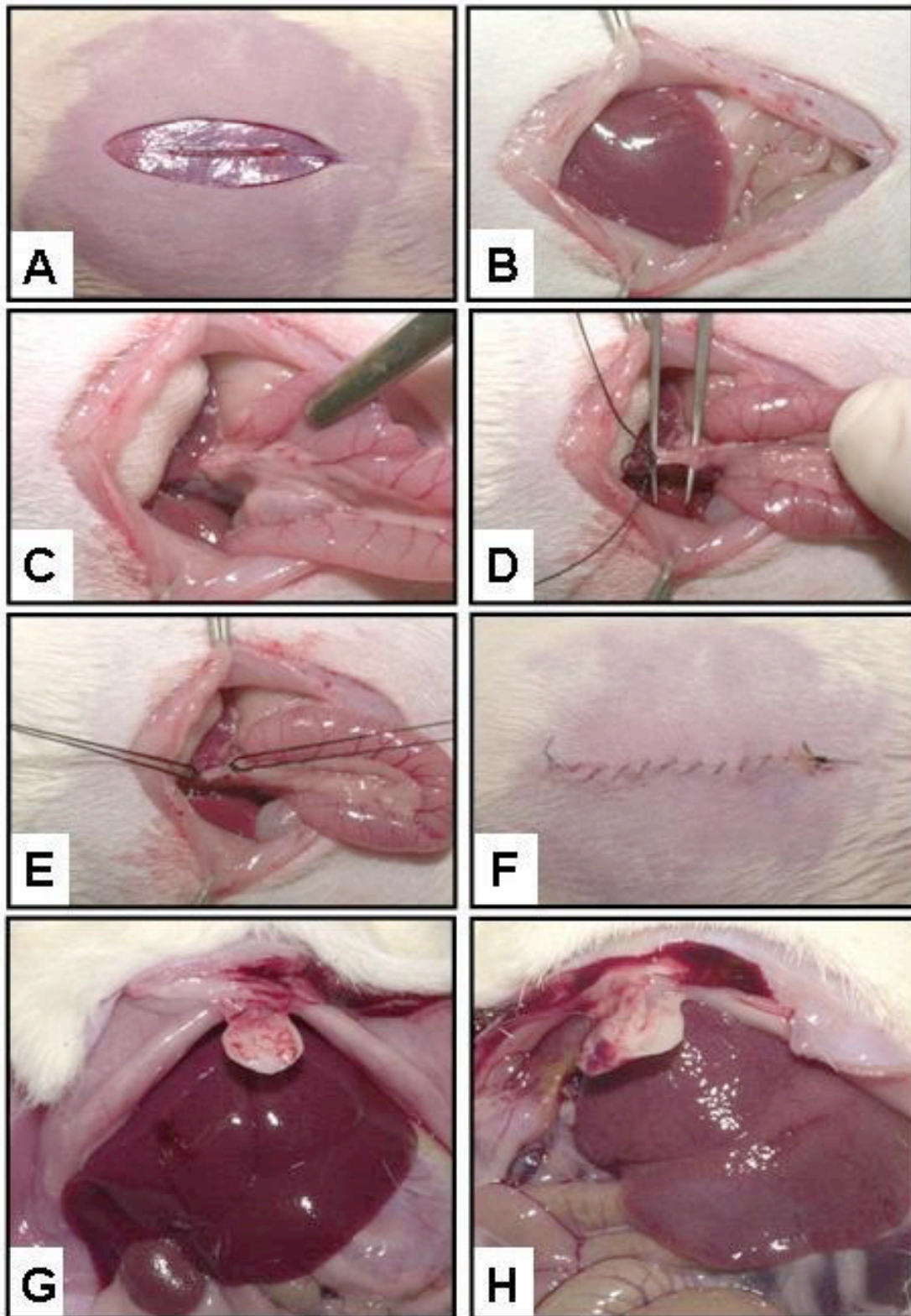


Figure 2.1: Common bile duct ligation in male Sprague-Dawley rats. (A) Under isoflurane anaesthesia the abdominal wall was shaved and a small incision with a scalpel was made. (B) The abdominal cavity was opened, and stretched and fixated with two sterile high-grade steel tweezers. (C) Liver lobules were turned down and intestines were carefully pulled out.

(D) The common bile duct was fixed with forceps and obstructed with a piece of string. (E) A second ligature was set in a distance of approximately 1 cm, and the common bile duct was severed between these ligatures. (F) Intestines were replaced in the abdominal cavity and the incision was closed in layers. (G) The livers of sham-operated animals show no sign of nodularity at day 28 after surgery. (H) By contrast, livers of animals following bile duct ligation demonstrate nodularity at 28 days.

2.8.2 Haemodynamic measurements

All haemodynamic measurements were performed on the day of sacrifice under anaesthesia, with temperature maintained at 36-37 ° C, with a rectal temperature probe and a temperature controlled mat. After induction of anaesthesia, a midline incision was made at the neck, and the left carotid artery was isolated. The cranial end was tied off with a ligature. The caudal end was clamped with a vessel clamp and an incision was made onto the vessel to insert a Polythethylene tube (Portex, Kent, UK) to monitor Mean Arterial Pressure continuously. Portal pressure was measured by direct cannulation of the portal vein under vision. Both mean arterial pressure and portal pressure were transduced independently to a Powerlab transducer linked to a computer running LabChart v5.0.1 software (AD Instruments Ltd, Oxford, UK). A measurement of MAP and portal pressure was taken after three minutes of stabilization, or after a stable trace was obtained on the monitor. The mean of three readings taken one minute apart was taken as the correct value for that measurement.

Following this 3-minute recording period, the animal was sacrificed by vena caval puncture and exanguination. Tissues were immediately dissected and snap frozen in liquid nitrogen. If at laparotomy it was apparent that BDL surgery had failed, if there was no biliary dilatation or alteration of liver parenchyma, then this animal was excluded from further analysis.

Haemodynamic data is expressed as mean \pm 1 SEM, and differences between groups were detected using a one-way ANOVA, with $p < 0.05$ considered to be statistically significant.

Chapter 3 – Characterisation of Hepatic DDAH-1 in Cirrhosis: Rats and Humans

3.1 Introduction

This chapter addresses the characterization of hepatic DDAH-1 expression in health and in disease. Some background data exists with regard to DDAH-1 expression in liver, although progress in this field has been limited by the poor specificity of commercially available antibodies to DDAH-1. Leiper et al initially used Northern blotting to demonstrate that DDAH-1 is expressed in healthy rodent liver⁸⁷. Nijveldt et al went on to show that the liver is an important site of plasma ADMA metabolism in healthy rats, and thus by inference an important site of DDAH activity⁹¹. Subsequent observations in humans demonstrated that plasma ADMA levels were elevated in cirrhosis¹⁰², following hepatic resection¹⁰³, and in acute liver failure¹⁰⁴. Moreover, high plasma levels of ADMA were cleared following orthotopic liver transplantation for acute liver failure¹⁰⁴. Additionally, organ flux studies in humans confirmed that the liver is a major site of ADMA clearance¹⁰⁵.

Hepatic tissue ADMA levels are also elevated in cirrhosis and, importantly, elevated further in alcoholic hepatitis and correlate with portal pressure⁷². Hepatic DDAH levels were also decreased in cirrhotic patients in this study, although the exact isoform of DDAH that was characterized by Western blotting in this study remains a matter of debate. In fact, antibody specificity for isoforms of DDAH remains a hindrance to study of the DDAH-ADMA pathway. Indeed, at the time of writing, no immunohistochemistry studies for hepatic DDAH-1, in any species, have been published in a peer-reviewed manuscript as a consequence of limited antibody specificity.

Hu et al used a LoxP/Cre approach to produce an endothelium-specific DDAH1 exon 4 deletion, leading to the absence of endothelial DDAH-1 enzyme expression¹⁰⁶. These authors then demonstrated markedly reduced protein expression of DDAH-1 by Western blot in several organs, including kidney, lung and liver, with an associated rise in tissue ADMA level. The authors proceeded to conclude that expression of DDAH-1 is predominantly endothelial in these tissues. However, this is at odds with the demonstration of tissue parenchymal expression of DDAH-1 in kidney and lung^{107, 108} hence further study is required to resolve this apparent contradiction.

In the experiments described in this chapter, human specimens were initially used to delineate the expression and cellular location in healthy liver and in cirrhosis. These results were then validated in the bile duct-ligated rat model of cirrhosis. Subsequently, a gene therapy approach was used to over-express hepatic DDAH-1 in BDL rats with portal hypertension, to assert a causal link between changes in hepatic DDAH-1 expression and portal haemodynamics in cirrhosis. This approach was chosen over the use of DDAH-1 over-expressing transgenic, and DDAH-1 heterozygote knockout, mice^{88, 109}, since they are not suitable for hepatic haemodynamic studies due to their small size. Additionally, bile duct-ligation in mice leads to a more heterogenous phenotype in mice than in rats (*vide infra*), because mice have a gallbladder which rats do not have, hence the degree of cholestatic liver injury following biliary obstruction is more variable.

3.1.1 The bile duct-ligated rat model of cirrhosis

Several animal models of cirrhosis exist, although each has flaws whereby they fail

to completely represent the human condition. The two most commonly used rodent models of cirrhosis are the carbon tetrachloride (CCl₄) treated rat, and the bile duct-ligated (BDL) rat.

Acute administration of CCl₄ to rats induces acute hepatitis, primarily in a perivenular distribution. Continuous administration induces chronic liver injury and fibrosis, leading to cirrhosis. Therefore, the CCl₄ model is an excellent model for evaluating the pathobiology of progressive liver fibrosis. However, the main drawbacks of the CCl₄ model relate to cost and duration of the model, variability in the degree of liver injury, and failure to adequately replicate the syndrome of ACLF. Several routes of administration of CCl₄ have been described, including oral ¹¹⁰, intraperitoneal ¹¹¹ and inhaled ¹¹², and the route favoured varies between laboratories. At least 12 weeks of CCl₄ administration is required to develop micronodular cirrhosis with portal hypertension, and up to 20 weeks for ascites to develop¹¹³. A further complexity is that rats vary in sensitivity to CCl₄, even within genetically homogenous litters, hence predicting the degree of injury is difficult. Moreover, as noted in chapter 1, portal hypertension in advanced cirrhosis may be a consequence of factors other than progressive fibrosis, hence the CCl₄ model may not fully represent the pathobiology in this context.

The BDL model induces secondary biliary cirrhosis. It has been mainly developed in rats¹¹⁴, which are especially appropriate due to the lack of a gallbladder. This model develops biliary fibrosis/cirrhosis in 4-6 weeks (figure 2.1). However, the histological appearance is not typical of human disease, as it is characterised by marked cholangiocyte proliferation and expanded portal tracts, and the architectural

disturbances typical of cirrhosis are seldom found¹¹⁵. At 2 weeks rats develop mild portal hypertension¹¹⁶ and at 4 weeks severe portal hypertension, a hyperdynamic circulation, and a degree of portal-systemic shunting and ascites^{114, 117, 118}. Although the BDL model has disadvantages with regard to the pattern of hepatic fibrosis that develops following injury, the model replicates additional features of advanced cirrhosis and the ACLF syndrome, and is therefore considered appropriate for the study of portal hypertension in this setting. In particular, the BDL animal develops brain swelling representative of hepatic encephalopathy in ACLF, and features of the hepatopulmonary syndrome^{119, 120}. Furthermore, in response to bacterial lipopolysaccharide, the BDL rat develops features of oxidant injury and elevated TNF levels as well as exacerbated portal hypertension⁶⁹. Therefore, the BDL rat model was used in the majority of *in vivo* experiments in this thesis.

3.1.2 Gene therapy

Virus-mediated gene delivery in rodent models of cirrhosis and portal hypertension has been demonstrated previously. Yu et al used an adenovirus to deliver neuronal NOS (nNOS) to hepatocytes, sinusoidal endothelial cells (SECs) and stellate cells in BDL and CCl₄-treated cirrhotic rats⁵⁰. This group demonstrated transduction of all these cell types in rodent models of cirrhosis although at decreased efficiency compared with non-cirrhotic animals. Moreover, this group found that transduction with nNOS led to increased intrahepatic NO generation and decreased intrahepatic resistance. Similarly, van de Casteele et al used adenovirus to deliver eNOS to CCl₄-treated rodents with cirrhosis, with a similar reduction in portal pressure, although the hepatic expression of the transgene was not fully described⁴⁹. However, from a broader therapeutic perspective, it has been demonstrated that hepatic NOS over-

expression has limited efficacy in portal pressure reduction due to 'spill-over' systemic deleterious effects of increased NO generation, and the presence of endogenous inhibitors of NOS¹²¹. From the point of view of virus-mediated gene transduction in cirrhosis, Lavina et al also demonstrated efficient transduction of CCl₄-treated rodents with cirrhosis with an adenovirus expressing superoxide dismutase (SOD)⁷⁶. However, recombinant adenoviral vectors have been associated with immunogenicity, with activation of both innate and adaptive immune responses¹²². Moreover, these responses have been associated with significant liver injury with leucocyte infiltration and elevation of liver enzymes. Therefore, alternative viral vectors for liver-specific delivery of DDAH-1 were sought, to avoid confounding effects of liver inflammation on DDAH dysfunction and portal pressure.

Adeno-associated virus (AAV) vectors are human parvoviruses that were first discovered as contaminants in adenovirus culture. These single-stranded DNA vectors have the best safety record amongst viral vectors, since no human disease has ever been associated with human infection. Unlike wildtype AAV (wtAAV), recombinant AAV particles rarely integrate into host genomes, but form extrachromosomal concatemers in the target cell, leading to long-term episomal persistence¹²³.

The wtAAV genome is 4.7kb, and is composed of two genes *rep* and *cap*, which encode four replication proteins and three capsid proteins respectively (figure 3.1). The AAV genome is flanked by two inverted terminal repeats (ITRs) which have a T-shaped hairpin structure containing a terminal resolution site and a *rep*-binding element (RBE) that play essential roles in replication and encapsidation. The ITR is

the only required cis-acting viral component necessary for genome replication, integration and packing. The *rep* and *cap* genes can therefore be provided in *trans* from a different plasmid, along with a helper construct providing the adenovirus-derived Ad early region genes, *E1A*, *E1B*, *E4*, and *E2A*, as well as Ad virus associated RNAs. These components are essential for transcription and protein synthesis¹²⁴.

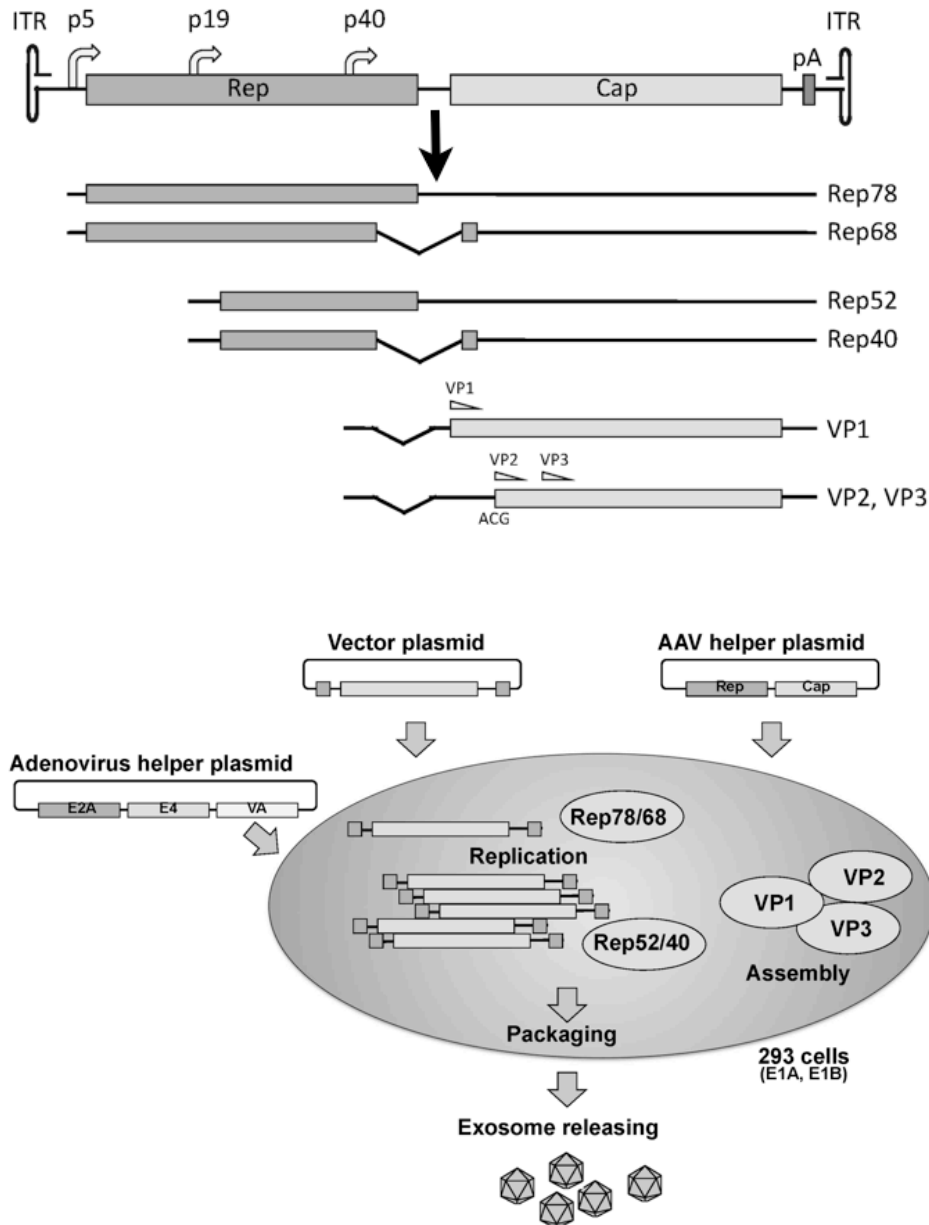


Figure 3.1. *Top panel:* The wild type AAV genome, with *rep* and *cap* genes flanked by ITRs. The genome encodes 4 replication proteins (Rep78, Rep68, Rep52, Rep40) and 3 capsid proteins (VP1, VP2, VP3). The large Rep proteins (Rep78 and Rep68) are produced from transcripts using p5 promoter, while small Rep (Rep52 and Rep40) are produced from p19 promoter. *Bottom panel:* The *rep* and *cap* genes can be provided in *trans* from a different plasmid, hence the vector can be replaced with a transgene expression cassette. Recombinant viral particle manufacture requires the *rep* and *cap* genes provided in *trans* along with a helper plasmid providing Adenovirus-derived Ad early region genes, E1A, E1B, E4, and E2A. This process is characterized by genome replication, assembly of the capsid proteins (VP1, VP2, and VP3), and packaging leading to virion production along with exosome release.

Unlike adenoviruses, little or no innate immune response occurs following AAV infection *in vivo*. An adaptive immune response does occur, which can eliminate the vector and transfected cells leading to loss of sustained transgene expression. However, this would not be expected to potentiate hepatic innate immune responses and thereby DDAH dysfunction in the same way as adenovirus-mediated innate immune activation. In this study, a hepatocyte-specific promoter 'LP1' was used for AAV mediated transgene delivery. The reasons for hepatocyte-restricted transduction of DDAH-1 were to mimic the physiological expression of DDAH-1 established in immunohistochemistry and cell separation studies (*vide infra*), and to minimize the immunogenicity of DDAH-1 expression hence prolonging the durability of transgene expression. The role of tissue-specific promoters in reducing or abrogating immune responses to the transgene product has been demonstrated in the setting of animal models of muscular dystrophy. The use of tissue-specific micro RNA elements to detarget transgene expression in dendritic cells, prevented cellular immune responses to a human sarcoglycan transgene following intramuscular injection in mice¹²⁵. The LP1 promoter was constructed by Nathwani and colleagues, using amplification of consecutive segments of the human apolipoprotein hepatic control region (HCR) and the human alpha-1-antitrypsin (hAAT) gene promoter including the 5'untranslated region¹²⁶.

Additionally, a further technical modification used in this study is a self-complementary (scAAV) AAV construct. A major limiting factor in the efficiency of single-stranded (ssAAV) vectors is their requirement for either host-cell mediated synthesis of the complementary-strand or annealing of the plus and minus strands from two separate viral particles co-infected into the same cell. McCarty et al.

developed a way to circumvent this problem by packaging both strands as a single DNA molecule. By utilising the knowledge that rAAV DNA of half or less than the wtAAV genome length can be packaged as a dimer¹²⁷ they have developed a self-complementary vector¹²⁸. In this construct the terminal resolution site (trs), from which replication initiates, is deleted from one of the ITR regions and the effect is that replication initiates from the wild-type ITR, proceeds through the mutant end without terminal resolution and continues back across the genome, using the opposite strand as a template to create the dimer. The result is a linear self-complementary genome with two wild-type ITRs at either end and a mutated ITR in the middle (Figure 3.2). After uncoating in the cell nucleus, the vector rapidly undergoes base pairing to form a double-stranded molecule without the help of the host, thus, bypassing the rate-limiting step. By contrast, following uncoating of the ssAAV vector genome, rearrangement into either circular or linear concatemers is an essential event for stable persistence of the transgene *in vivo*. If this rearrangement, through a double-stranded structural intermediate, does not occur then a rapid disintegration of linear single-stranded vector genome follows^{129, 130}. Recently, Nathwani et al. reported a 20-fold improvement in human FIX expression in mice, following transduction of the liver with an AAV8 pseudotyped scAAV vector¹²⁶.

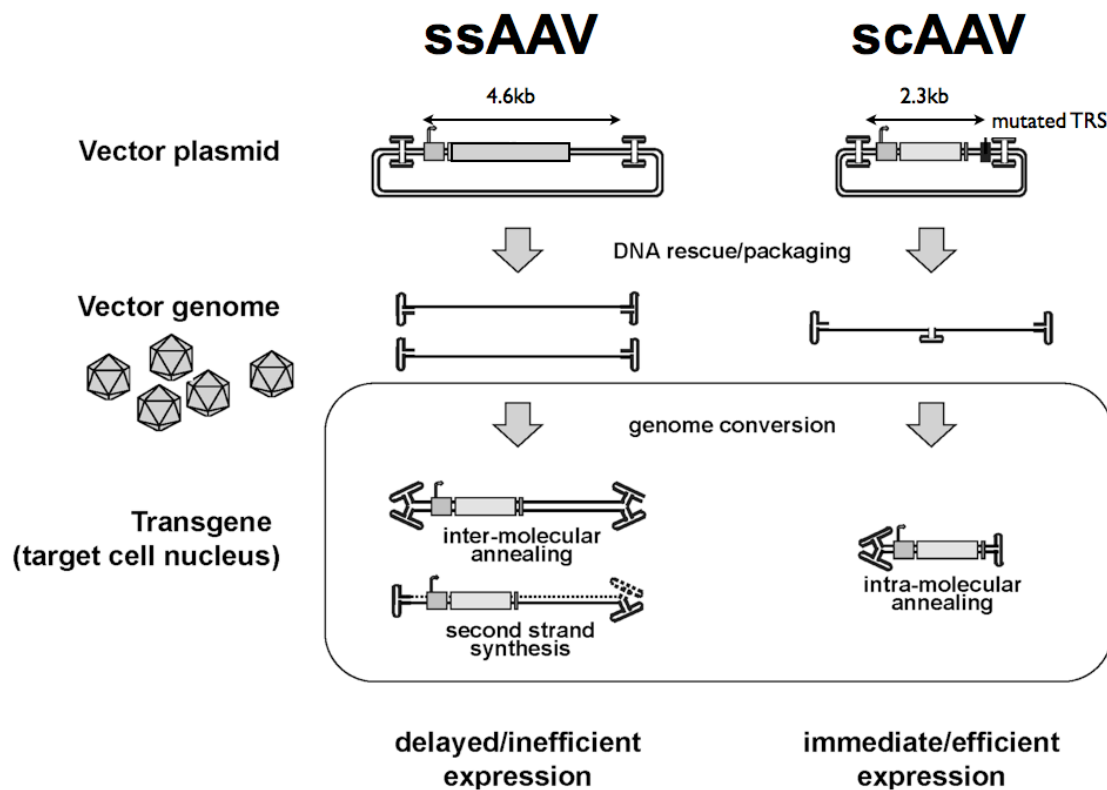


Figure 3.2: This diagram illustrates how single-stranded AAV (ssAAV) and self-complementary AAV (scAAV) vectors differ in the size of their transgene cassette, their replication and generation into viral particles. Both vectors are flanked by ITRs, however, the right-hand ITR of scAAV vectors is mutated by deleting the terminal resolution site (TRS). The effect is that replication initiates from the wild-type ITR, proceeds through the mutant end without terminal resolution and continues back across the genome, using the opposite strand as a template to create the dimer. The result is a linear self-complementary genome with two wild-type ITRs at either end and a mutated ITR in the middle. The scAAV transgene cassette, however, must be half the size of the conventional ssAAV vector, which is achieved by using truncated promoters and/or removing non-coding sequences. After uncoating in the cell nucleus, the vector genomes are converted into double-stranded transcriptionally active DNA. For ssAAV-mediated transduction, annealing of plus and minus genomes, and perhaps second-strand synthesis is required, both of which are considered rate limiting steps. For scAAV vectors, the complementary sequences rapidly hybridise to form stable DNA duplexes.

3.2 Results

3.2.1 Optimization of immunohistochemical staining of DDAH-1

Immunohistochemistry for DDAH-1 was performed on formalin-fixed paraffin-embedded human liver samples, according to the methods described previously. Samples were from a resection specimen from an individual with no history of heavy alcohol intake or of liver dysfunction, and from two patients with alcohol-related cirrhosis. Since no protocol for immunostaining for DDAH-1 in human liver has been published, optimization steps were performed using three different primary antibodies, varying antigen retrieval techniques, and staining conditions, on formalin-fixed paraffin-embedded sections of healthy human liver. The following strategy was adopted: three primary antibodies were used (Abcam Ab 2231 - Goat anti-DDAH1, Abcam Ab 82908 - Rabbit anti-DDAH1, Abcam Ab 180599 Rabbit anti-DDAH1), and systematically tested at three different concentrations (primary ab 1:50, 1:100 and 1:1000). Additionally, each of these primary antibody conditions was tried with and without prior microwave antigen retrieval techniques.

Following these optimization steps, the goat anti DDAH-1 antibody Ab 2231 with a microwave antigen retrieval technique demonstrated optimal staining for HRP-conjugated antibody with minimal background staining.

3.2.2 Localization of hepatic DDAH-1 expression in healthy human liver and in cirrhotic liver

Figure 3.2 demonstrates DDAH-1 protein expression in normal human liver tissue (left panel). DDAH-1 staining is evident primarily in parenchymal cells, predominantly in zone 3 hepatocytes. Tissue sections from patients with alcohol-related cirrhosis

(right panel) display typical architectural changes of cirrhosis, with nodule formation and the presence of fibrous bands. In these sections, DDAH-1 expression is still localized to hepatocytes, but from a non-quantitative perspective expression levels appear reduced.

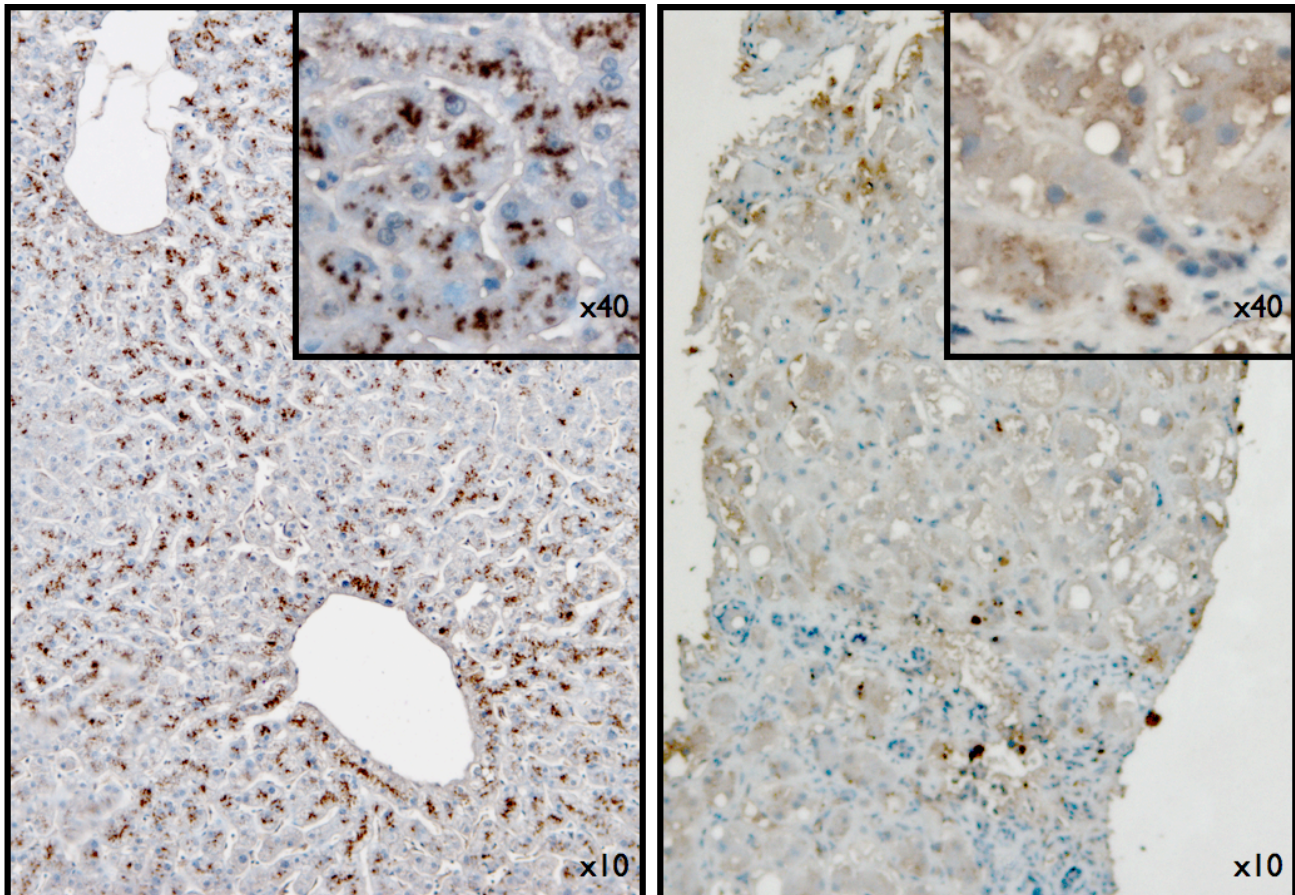


Figure 3.2: Representative sections of human liver (5 μ m thickness; x10 magnification, x40 magnification inset) from a control non-cirrhotic subject (left side image), and a patient with cirrhosis and portal hypertension (right side image). Hepatic DDAH-1 (horseradish peroxidase-conjugated dark brown staining) is located within the cytoplasm of hepatocytes of human liver. DDAH-1 levels appear decreased in cirrhotic liver (right side image) compared to healthy liver (left side image).

3.2.3 Localisation of hepatic DDAH-1 in healthy rodent liver

To confirm these findings in a rat model, samples were obtained from control Sprague-Dawley rats that had undergone hepatic cell separation by collagenase perfusion at the Yale Cell Isolation Core Facility (New Haven, Connecticut, USA – provided by Dr Yasuko Iwakiri) as previously described¹³¹. Cells were immediately stored in a lysis buffer until used for western blot, as previously described¹³². Subsequently, protein expression of DDAH-1 was assessed by western blot. In agreement with the human immunohistochemistry data, figure 3.3a demonstrates that DDAH-1 expression is predominantly restricted to the parenchymal cell fraction.

3.2.4 Histological characterization of the bile duct-ligation rat model of cirrhosis

Bile duct-ligated (BDL) rats were used for the majority of *in vivo* experiments presented in this thesis. As noted in section 3.1.1, the BDL model induces secondary biliary cirrhosis, although the histological appearance is not typical of human disease. Representative sections of sham-operated and BDL rat liver from the cohort of animals used in subsequent experiments are presented in figure 3.3. The sham liver demonstrates normal hepatic architecture, whereas the BDL liver has evidence of cross-linking of fibrous septa, representing bridging fibrosis.

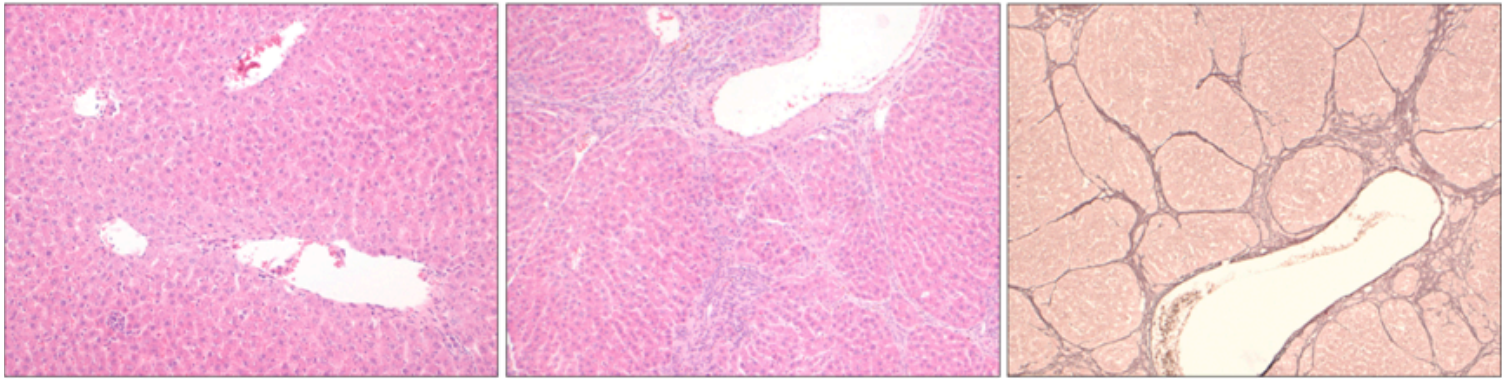


Figure 3.3: Representative sections of rat liver (5 μ m thickness; x40 magnification) from a sham-operated rat (left panel, haematoxylin and eosin stain), BDL rat (centre panel – haematoxylin and eosin stain, right panel – reticulin stain). Sham liver demonstrates normal liver architecture, whereas BDL liver shows cross-linking of fibrous septa, representative of bridging fibrosis.

3.2.5 Quantification of DDAH-1 expression in healthy and cirrhotic rodent liver

As noted above, DDAH-1 levels appeared decreased in human cirrhosis, using a non-quantitative approach in immunostained human liver samples. These findings were confirmed in two rodent models of cirrhosis using western blot. Figure 3.4b demonstrates significantly decreased hepatic DDAH-1 protein expression in cirrhotic BDL rats compared with control sham-operated rats ($p < 0.01$). These results were confirmed in liver tissue from cirrhotic CCl₄ rats, which had significantly lower hepatic DDAH-1 expression than control rats (figure 3.3c, $p < 0.01$).

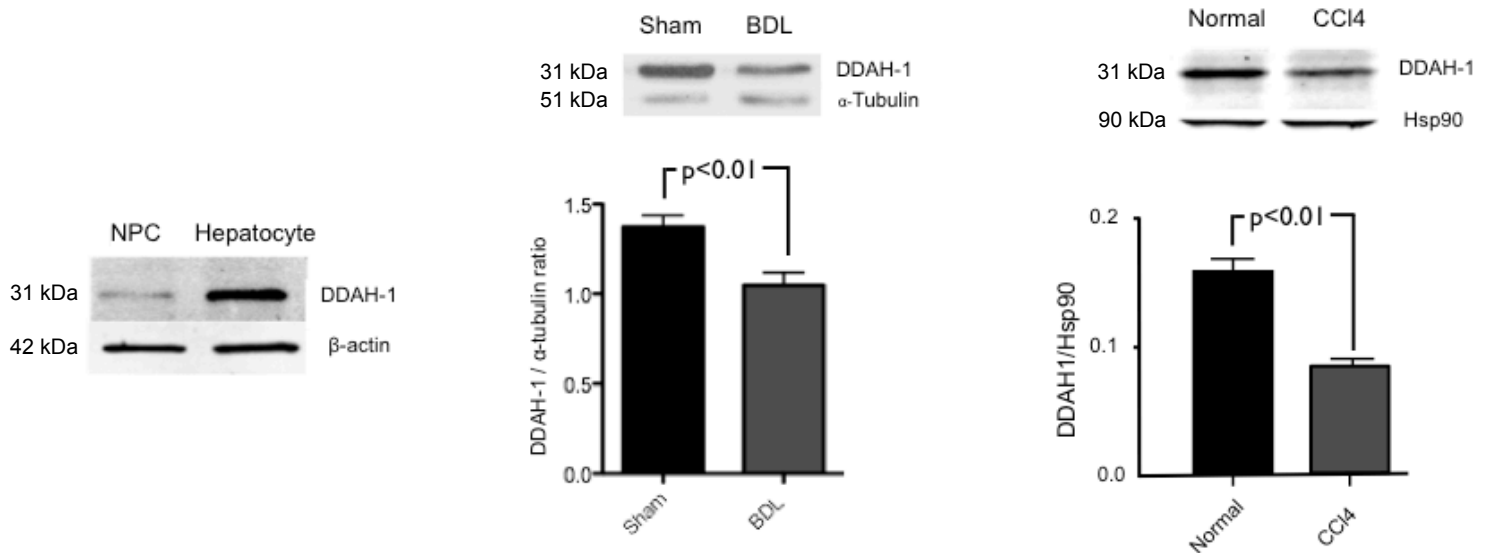


Figure 3.4a (left panel): Representative western blot on cell separation preparations from healthy rat liver (n=3). DDAH-1 protein is predominantly expressed in the hepatocyte fraction rather than the non-parenchymal cell (NPC) fraction. Figure 3.4b (centre panel): Representative western blot from rat liver demonstrates that hepatic DDAH-1 expression is significantly reduced in BDL rats compared to sham (n=6/group, Student's t-test $p < 0.01$). Figure 3.4c (right panel): Representative western blot demonstrating that hepatic DDAH-1 is also significantly reduced in CCl_4 -treated rats compared to control (n=6/group, Student's t-test $p < 0.01$).

3.2.6 Effect of ADMA on endothelial NO production

Since hepatic DDAH-1 expression is decreased in models of cirrhosis compared to control animals, it is hypothesized that hepatic ADMA metabolism is impaired leading to increased local ADMA levels and impaired eNOS function. Endogenous levels of NO for regulation of sinusoidal vasculature are low, and hence measurement of hepatic NO and determining fine changes in hepatic NO *in vivo* is problematic. Therefore, an *in vitro* model of eNOS-mediated NO production was used to demonstrate effects of exogenous ADMA on endothelial NO production.

Bovine aortic endothelial cells (BAECs) can be stimulated to produce NO by use of

the calcium ionophore Ionomycin, which results in rapid de-phosphorylation of eNOS at Threonine 497 (Thr497) and consequent functional activation¹³³. As such, this model of endothelial NO generation was used to study the effects of physiologically relevant concentrations of ADMA on eNOS-mediated NO release. After overnight culture, BAECs were pre-treated for 30 minutes with either 5uM ADMA or phosphate-buffered saline (PBS) control. Following this, BAECs were stimulated with 5uM Ionomycin or PBS control. At 30 minutes following stimulation, cell media was removed for NO measurement by chemiluminescence and cells were lysed for protein quantification and western blot.

As demonstrated in figure 3.4, Ionomycin stimulation leads to a marked increase in BAEC NO production, in association with increased eNOS phosphorylation at Ser1177, although total eNOS protein levels remain unchanged. Exogenous ADMA leads to an inhibition of BAEC NO production, reaching significance at 5uM ADMA with no further increase in inhibition of NO production at 10uM ADMA. This inhibition of NO production was not associated with any change in total eNOS or Ser1177 phospho-eNOS (figure 3.4).

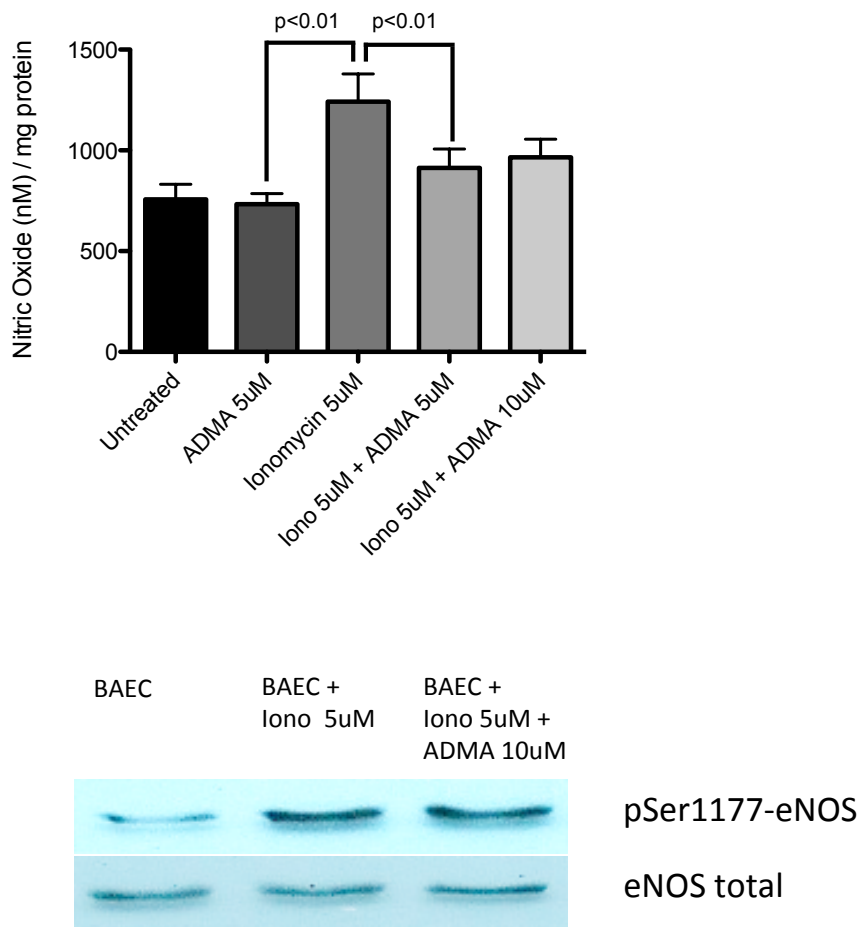


Figure 3.5. *Top panel:* Nitric oxide (NO) measurement from BAEC supernatant, normalized per mg total protein. Ionomycin treatment leads to NO generation from cultured BAECs, which is inhibited by exogenous ADMA (n=8/group, p<0.01 one way ANOVA). *Bottom panel:* Representative western blot of Ser1177 phospho-eNOS and total eNOS from cultured BAECs treated with exogenous Ionomycin and ADMA (n=6/group). Ionomycin treatment leads to enhanced phosphorylation of eNOS (Student's t-test p<0.01), which remains unchanged following addition of exogenous ADMA.

3.3 Effect of DDAH augmentation on portal pressure – gene therapy approaches

Having established that hepatic DDAH-1 protein expression is decreased in human

and rodent models of cirrhosis, and that local ADMA leads to a dose-dependent reduction in endothelial NO generation, it was hypothesized that reconstitution of hepatic DDAH-1 would lead to a reduction in portal pressure in the BDL rodent model of cirrhosis.

Despite over a decade of research into the DDAH-ADMA-NOS axis, and high-throughput screening of drug libraries, no specific agonist or activator for DDAH-1 has been developed. A non-specific activator of DDAH-1 has been demonstrated – the Farnesoid X receptor (FXR) agonist obeticholic acid (OCA). This bile salt analogue has been shown to increase DDAH-1 transcription and protein synthesis by binding to a FXR response element in exon 1 of the DDAH-1 gene, hence acting as a transcription enhancer¹³⁴. Previously, it has been demonstrated that this agonist leads to increased hepatic DDAH-1 expression and decreased portal pressure following 5 days of administration in BDL cirrhotic rats¹³⁵. However, OCA also has pluripotent effects on other pathways that could potentially alter portal pressure, such as SOCS3 signaling¹³⁶, stellate cell activation¹³⁷, and endothelin signaling¹³⁸. Therefore, the aim of this series of experiments was to demonstrate a causal relationship between increased hepatic DDAH-1 expression and decreased portal pressure in BDL cirrhotic rats.

3.3.1 Adeno-associated virus (AAV) cloning

Supplemental methods for AAV cloning and manufacture are provided in section 8.0.

A multiple cloning site *cis* plasmid with an AAV2 backbone was used to generate the

AAV_DDAH1 plasmid that was subsequently used for AAV_DDAH1 particle manufacture. An AAV2 plasmid with the LP1 hepatocyte-restricted promoter was chosen for AAV_DDAH1 cloning, to minimize off-target effects of AAV_DDAH1 transduction *in vivo*.

To construct AAV_DDAH1, the cassette expressing DDAH-1 cDNA was excised from pCMV_DDAH1 with an *EcoR1/Not1* digest, and ligated into pAAV2_LP1 with standard techniques (figure 3.5a). Following ligation, transformation and selection on an ampicillin plate, colonies were picked and grown overnight. Recombinants were checked by diagnostic restriction digest, and cloning was confirmed by sequencing.

Following construction of this pAAV2_LP1_DDAH1 plasmid, it is necessary to check that the ITRs are intact and balanced. Homologous recombination can occur between the ITRs in *E.coli* during the construction of the rAAV plasmids. As a result of this recombination, ITR sequences are often rearranged or partially deleted during subcloning. It was essential, therefore, to check the intactness of the 5' and 3' ITR sequences in all constructs. They were screened by 3 restriction enzymes including *BssHII*, *MscI* and *SmaI*.

Since the LP1 promoter has already been shown to express in rat hepatocytes, the expression of this construct in a human hepatocyte and non-hepatocyte cell line was checked to demonstrate liver specificity. The human hepatocyte cell line HepG2, and the human non-hepatocyte cell line HEK293T were used to demonstrate liver specificity of the pAAV2_LP1_DDAH1 construct. Transient transfection of the pAAV2_LP1_DDAH1 construct in HepG2 cells was performed (n=6/group), and at 24

hours cells were lysed and protein extracted for qPCR and western blot. Significantly increased DDAH-1 gene and protein expression was seen following transfection into HepG2 cells (figure 3.5). No significant increase in DDAH-1 gene or protein expression was seen following transfection into HEK293T cells (data not shown).

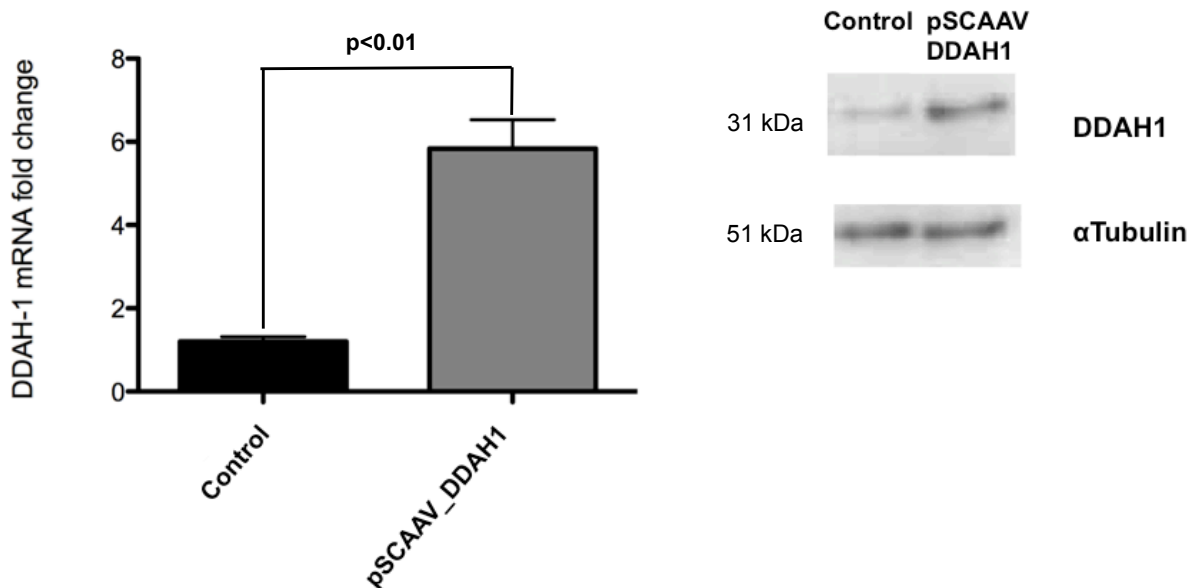


Figure 3.6: *Left panel:* Transfection of pSCAAV_DDAH1 or control salmon sperm DNA (ssDNA) into HepG2 cells (n=6/group) leads a significant 6-fold upregulation of DDAH-1 mRNA (Student's t-test, $p < 0.01$). *Right panel:* Transfection of pSCAAV_DDAH1 into HepG2 cells (n=6/group) also leads to increased DDAH-1 protein expression compared to control ssDNA (Student's t-test, $p < 0.01$) – representative western blot.

3.3.2 Adeno-associated virus particle manufacture

Following cloning and testing of the pAAV2_LP1_DDAH1 construct, this plasmid was then used for AAV particle manufacture, with a view to a pilot *in vivo* experiment.

The size of the pAAV2_LP1_DDAH1 is 5.2kb (figure 3.6), which is at the upper limit of the optimal size for efficient functional packaging of scAAV particles¹³⁹. A triple-transfection method was used to produce the virus particles (see section 3.6.1 for full details), followed by purification by iodixanol step-gradient ultracentrifugation (section 3.6.2). The virus particle titer was determined by DNA dot-blot hybridisation analysis (section 3.6.3).

Primers used for dot-blot hybridization were optimized to produce a 225bp PCR product from human DDAH-1 cDNA, which was subsequently used as a hybridization probe. The primers used were F:GGCGCCGAGCCGGAGAAGG and R: GCCACTGGCACTGTGGAGACTGC using the conditions described in section 2.2.1, with an optimized T_m of 58.4°C and MgCl₂ concentration of 2.5uM.

Following virus preparation, viral DNA was prepared for dot-blot quantification as described in section 3.6.3. A serial dilution of the pAAV2_LP1_DDAH1 vector was used as a series of standards, alongside the prepared viral DNA. These were then hybridized to the 225bp labeled DNA probe. Following development of these blots using chemiluminescence as outlined in section 3.6.3, AAV particle number in each viral preparation was calculated from densitometry of probe intensity. These preparations yielded a total yield of 4.3E11 VP.

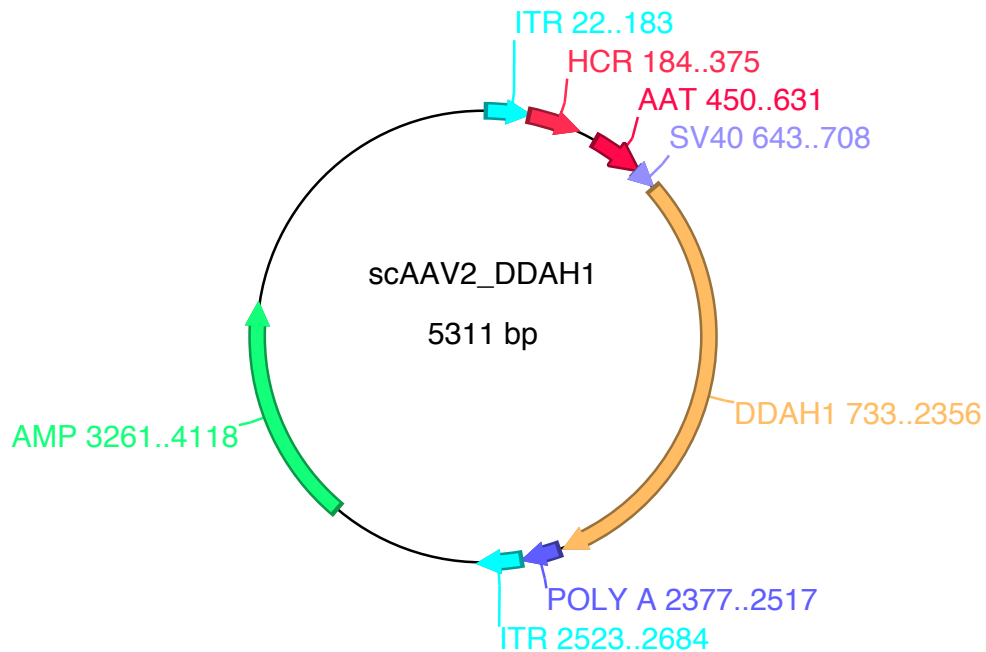


Figure 3.7. Plasmid map of the scAAV2_LP1_DDAH1 construct. ITR=inverted terminal repeat, HCR=hepatocyte control region of the human apolipoprotein promoter, AAT=human alpha-1-antitrypsin promoter, SV40= Simian vacuolating virus 40 promoter.

3.3.3 Adeno-associated virus delivery of DDAH-1 to cirrhotic rodents

Following the manufacture of AAV particles expressing human DDAH-1 (scAAV2_LP1_DDAH1), these particles were used *in vivo* in a pilot experiment to determine efficacy of gene transduction in the BDL model of cirrhosis. Four Sprague-dawley rats underwent BDL surgery as described in section 2.8.1, and were injected at day 25 following BDL surgery. Injections were performed under isoflurane anaesthesia as described in section 2.8.1, with viral particles diluted in 4mls of DMEM culture media and delivered into the jugular vein. Two animals were injected with a dose of 1E10 AAV particles, and two were injected with a dose of 1E11 AAV particles.

Two animals died within 12 hours post-injection, for reasons that were not clear. Post-mortem examination was not performed, and tissues from these animals were not retrieved.

The remaining two animals (one from the 1E10 dose and one from the 1E11 dose) were sacrificed at 5 days post-injection. Both animals displayed portal hypertension (portal pressure 15.6mmHg and 13.9mmHg respectively). However, on quantitative PCR, no discernible hepatic expression of human DDAH-1 was apparent. No other organs were analysed from these animals, and no further AAV *in vivo* experimentation was performed.

3.3.4 Hydrodynamic gene delivery of DDAH-1 in a rat model of cirrhosis

The hydrodynamic approach to gene delivery was used in these experiments, since viral mediated gene therapy was shown to be inefficient in cirrhotic rats. Hydrodynamic gene delivery using naked plasmid DNA leads temporary expression of transgene, predominantly in liver.

The pCMVSPORT6_DDAH1 plasmid was used for gene delivery. This was initially tested *in vitro* for DDAH-1 expression in hepatocytes. At 24 hours following transfection by standard techniques in HepG2 cells, cells were lysed and protein extracted for western blotting. Western blot demonstrated significantly increased DDAH-1 protein expression following transfection in HepG2 cells compared to controls transfected with salmon sperm DNA (data not shown).

Subsequently the pCMVSPORT6_DDAH1 plasmid was amplified using an endotoxin-free Gigaprep kit (Qiagen Ltd), and sequence verified. Hydrodynamic injection was performed at day 25 following BDL surgery, according to the technique described in chapter 2, in three groups of animals: a) sham+control saline injection, (b) BDL+control saline injection, (c) BDL+DDAH-1 expressing plasmid. Experiments were terminated at day 30 following BDL surgery (5 days after hydrodynamic injection) and haemodynamic measurements were performed, along with retrieval of blood for biochemistry and haematology, and liver tissue for RNA and protein extraction.

As shown in figure 3.7, BDL+saline group had significantly elevated portal pressure ($p < 0.01$) compared to the sham+saline group. Hydrodynamic injection with DDAH-1 led to a significant increase in hepatic human DDAH-1 mRNA in BDL+DDAH-1 rats, compared to saline-treated BDL+control and sham+control rats which had background levels of mRNA, similar to that noted in the no-sample qPCR control (data not shown). Hydrodynamic injection with DDAH-1 also led to a protein expression of DDAH-1 (figure 3.7), and also significantly decreased portal pressure ($P < 0.01$, figure 3.7) in BDL+DDAH-1 rats compared to BDL+control saline injection.

There is a marked rise in plasma ALT and AST at 5 days following hydrodynamic injection, however there is no difference in magnitude of ALT/AST rise between BDL+saline and BDL+DDAH-1 groups (table 3.2). Moreover, there is no significant change in mean arterial pressure with DDAH-1 gene therapy compared to saline control.

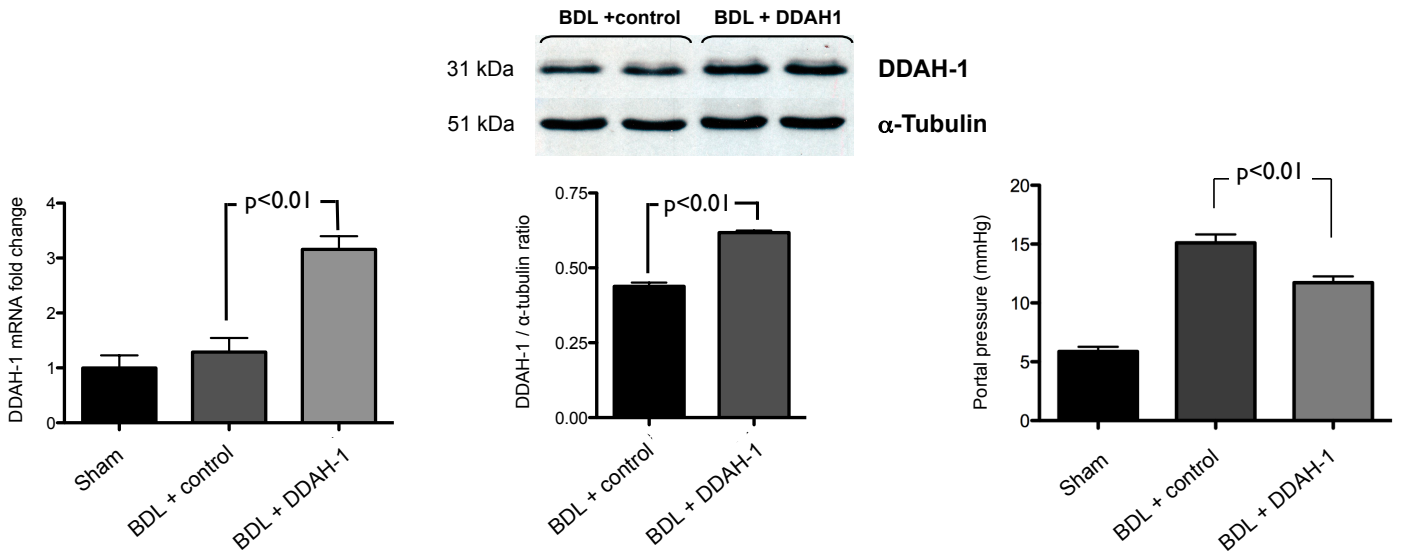


Figure 3.8: Hydrodynamic gene delivery of saline control or plasmid expressing human DDAH-1 in sham and BDL rats ($n=8/\text{group}$, all variables analysed by Student's t-test). *Left panel:* Human DDAH-1 mRNA expression in sham, BDL rats treated with control saline injection and BDL rats treated with human DDAH-1 plasmid injection. Human DDAH-1 plasmid injection led to a significant increase in human DDAH-1 mRNA expression in BDL rat liver over background level ($p<0.01$, negligible background detection – normalised to 1 in this graph by the $\Delta\Delta\text{CT}$ method). *Centre panel:* Hydrodynamic injection of human DDAH-1 plasmid also leads to a significant increase in total liver DDAH-1 protein expression compared with control saline injection ($p<0.01$) – representative Western blot and densitometry presented (Western blot with anti-DDAH-1 Abcam 2231 antibody, recognises both human and rat DDAH-1). *Right panel:* Hydrodynamic gene delivery of DDAH-1 in BDL rats leads to a significant reduction in portal pressure at 5 days following hydrodynamic injection, compared with BDL rats treated with control saline injection ($p<0.01$).

	Sham + Saline (n=8)	BDL + Saline (n=8)	BDL + DDAH1 (n=8)
Albumin (g/L)	29.3 (2.3)	25.2 (2.3)	28.0 (1.0)
AST (IU/L)	65.6 (3.7)	383.6 (35.3)*	383.1 (143.9)*
ALT (IU/L)	43.7 (3.6)	82.9 (8.5)*	74.5 (6.4)*
Bilirubin (µM/L)	1.25 (0.3)	128.2 (6.5)*	121.1 (7.3)*
MAP (mmHg)	111.3 (6.8)	91.6 (3.8)*	90.3 (3.3)*

Table 3.2 – Biochemical parameters and mean arterial pressure of sham and bile duct ligated rats treated with saline or DDAH-1 plasmid hydrodynamic injection; mean (SEM). * p<0.01 vs sham group.

3.4 Discussion

The experiments leading up to this thesis suggested that the DDAH-ADMA axis was associated with disease severity in cirrhosis and portal hypertension, but a causal relationship signifying pathophysiological relevance had not been confirmed. A major limiting factor to the study of hepatic DDAH-1 was the lack of antibodies with sufficient specificity for high quality immunohistochemical studies, particularly in rats, to determine the cell type expressing hepatic DDAH-1 and to give insights into pathobiology. This initial hurdle was overcome through two strategies. Initially, *in situ* hybridization for DDAH-1 mRNA on rodent and human liver sections was attempted, to overcome the problems of DDAH-1 antibody specificity – this work is detailed in chapter 4. Subsequently, we obtained human liver tissue sections from patients with cirrhosis and a healthy control, and performed a series of steps to optimize immunohistochemistry conditions with different antibodies and different approaches to antigen retrieval. Previous studies have demonstrated decreased hepatic DDAH in patients with cirrhosis and superimposed hepatic inflammation, with associated exaggerated portal hypertension⁷², although considerable debate exists regarding specificity for DDAH enzyme subtype of the antibodies used in this study. The antibodies used at that time were non-commercial from a collaborating laboratory (Dr J Leiper, UCL); over recent years the gradual emergence of commercially available and validated antibodies has improved the specificity of these antibodies for DDAH subtype. Following microwave-based antigen retrieval techniques, we were able to demonstrate sensitive DDAH-1 antigen staining, demonstrating clear hepatocyte-restricted expression of DDAH-1. Moreover, these studies suggested decreased hepatic DDAH-1 expression with advanced liver disease. To confirm the hepatocyte-specific expression of hepatic DDAH-1, we performed cell separation in healthy

rodent liver, and subsequently evaluated DDAH-1 expression by western blot. These studies confirmed that hepatic DDAH-1 expression is predominantly hepatocyte restricted in rodents. Subsequently, we sought to confirm previous findings of decreased hepatic DDAH-1 immunostaining in patients with cirrhosis, and demonstrated significantly decreased hepatic DDAH-1 protein expression in both BDL and CCl₄ cirrhotic rats with elevated portal pressure, compared to non-cirrhotic controls rats.

Measurement of ADMA for these experiments was not possible, due to temporary unavailability of mass-spectrometry at the Royal Free Campus due to laboratory restructuring. The majority of liver homogenate and plasma/serum samples were used for other assays, although aliquots were saved for future ADMA measurement. However, regrettably, due to a subsequent freezer failure these retained aliquots are no longer suitable for analysis. However, DDAH-1 has been shown to efficiently metabolize ADMA, with a Km value of 68.7uM and Vmax value of 356 nmol/mg/min *in vitro*¹⁴⁰, so one would expect DDAH-1 expression to linearly correlate with DDAH activity and inversely correlate with local ADMA concentration at physiological/pathophysiological concentrations of ADMA (5-10uM), and with no known endogenous inhibitors of DDAH activity.

Measurements of NO *in vivo* are also subject to technical factors. Since NO is a diatomic free radical with an extremely short half life, in many cases measurement of peripheral blood NO does not accurately reflect the corresponding NO status in tissues of interest. Moreover, NO and NO-derived metabolites rapidly interact with protein thiols, secondary amines, and metals to form S-nitrosothiols (RSNOs), N-

nitrosamines (RNNOs), and nitrosyl-heme respectively. Additionally, NO may also rapidly interact with the free radical superoxide (O_2^-) to yield the potent oxidants peroxynitrite ($ONOO^-$) and its conjugate acid peroxynitrous acid ($ONOOH$). Thus, free NO and NO-metabolite levels are rapidly altered *in vivo*. The major pathway for NO metabolism is the stepwise oxidation to nitrite and nitrate. In plasma or other physiological fluids or buffers NO is oxidized almost completely to nitrite (NO_2^-), where it remains stable for several hours. However, in blood, the half life of NO_2^- is about 110 seconds, due to rapid conversion to nitrate (NO_3^-). This is thought to be a consequence of oxidation by certain oxyhemoproteins such as oxyhemoglobin or oxymyoglobin. Typical methods for estimation NOS activity *in vivo* therefore rely on quantification of nitrate and nitrite in peripheral blood. However, there is a significant contribution of both nitrite and nitrate from dietary sources, including experimental animal chow. Sample preparation can also introduce artifactually create NO products or metabolites – ideally blood/tissues should be perfused with an isotonic solution containing N-ethylmaleimide (NEM) and EDTA to block SH-groups and inhibit artificial nitrosation, as well as thiolate- and ascorbate- mediated degradation of endogenous RSNOs and nitrite. For these reasons, *in vivo* measurements of NO were not performed, but *in vitro* endothelial studies were performed to demonstrated effects of exogenous ADMA on endothelial NO generation.

Previous *in vitro* studies in BAECs demonstrate that NO production is increased by DDAH-1 overexpression and decreased by DDAH-1 silencing. Moreover, DDAH-1 silencing is associated with a reduction in L-arginine/ADMA ratio and partially restored by L-arginine supplementation, suggesting that DDAH-1 is responsible for

modulating ADMA-dependent inhibition of NO generation⁸⁴. Following on from this work, it was sought to confirm that ADMA is an inhibitor of endothelial NO generation, and a similar *in vitro* model of BAEC-mediated NO generation was utilized. Following stimulation of BAECs with the calcium ionophore Ionomycin, a significant induction of NO production into cell media was demonstrated by the chemiluminescence method. This induction of NO production was robust, and was inhibited by ADMA at physiologically relevant concentrations. Typically, intracellular levels of ADMA are in the low micromolar range and, in a similar manner to the experiments described here, Pope and colleagues found dose-dependent inhibition of NO formation with extracellular ADMA concentrations of 5 μ M⁸⁴.

Torondel et al have also demonstrated that overexpression of DDAH-1 in endothelial cells *in vitro* leads to a reduction in ADMA concentration, and improvement in NO production¹⁴¹. However, our data from human and rodent hepatic tissue suggests that hepatic DDAH-1 is located in the parenchymal hepatocyte, rather than sinusoidal endothelial cells which are responsible for eNOS-mediated NO production. This suggests that within the liver, the mechanisms of action of DDAH-1 may be in acting to reduce local ADMA levels in a paracrine fashion. There is evidence to support this; Fickling et al showed that ADMA made in one cell is capable of diffusing and inhibiting NOS in an adjacent cell¹⁴². Moreover, Luo et al noted that DDAH-1 expression in the kidney is seen in pre-glomerular vascular smooth muscle cells, without any NOS expression in these cells, suggesting that this DDAH-1 may act to alter local ADMA levels and eNOS activity in adjacent endothelium¹⁴³. Therefore, on the basis that exogenous ADMA leads to inhibition of endothelial NO generation, and DDAH-1 has previously been shown to be a key

regulator of local ADMA levels, we proceeded to reconstitute hepatic DDAH-1 *in vivo* in a rodent model of cirrhosis. This route of experimentation was chosen rather than further *in vitro* studies of DDAH-1 over-expression, which would require a complex co-culture system to recapitulate the physiological environment of paracrine metabolism of local ADMA, hepatocyte DDAH-1 and endothelial eNOS.

To assert a causal association between hepatic DDAH-1 expression and portal hypertension, we initiated a gene therapy experiment to reconstitute hepatic DDAH-1 in the BDL rodent model of cirrhosis. Despite a precedent for viral-mediated gene delivery in rodent models of cirrhosis^{50, 76}, significant transgene expression could not be demonstrated in the livers of BDL rats treated with intravenous administration of two doses (1E10vp and 1E11vp) of scAAV2_LP1-DDAH1.

The reasons for inefficient hepatic transduction of transgene, or for early death in two animals, are unclear. In terms of transduction, the dose of AAV used was comparable to that used by intravenous injection in mice to transduce healthy liver^{144, 145}. Moreover, the route and dose of administration was similar to that used in rats with non-cirrhotic liver disease and in cirrhotic rats^{146, 147}. High-level liver-mediated transgene expression has been reported at 1 day and 4 days post AAV injection in healthy mice, with a dose of 1e11 viral genomes per animal¹⁴⁴. However, the earliest reported expression from a reporter AAV (eg luciferase) in studies with cirrhotic rats is 7 days¹⁴⁷. Hence, it is unclear if 5 days is sufficient time for high-level expression of transgene in a cirrhotic liver. The rationale for a 5-day duration for transgene expression in these experiments was to balance the time required for transgene expression, with the risk that earlier administration of AAV into the BDL animals (ie

prior to 21 days) may alter the evolution and phenotype of the model. Moreover, as outlined in the introduction to this chapter, the BDL animals demonstrate organ failure with a considerable mortality following 28 days, hence a prolonged period for transgene expression may lead to excess mortality in the AAV treated animals.

Regarding the mortality seen in the AAV-treated animals in this pilot experiment, there was no apparent immediate post-operative reason for early death in 2 animals. As mentioned above, there is excess mortality after 28 days following BDL surgery, and in the absence of a control non-AAV treated group it is impossible to determine if this mortality is a consequence of liver failure or of the AAV infection. Nevertheless, it is apparent from human trials that high doses of scAAV particles can induce a mild elevation in liver enzymes in hemophilia patients *without* cirrhosis, the reasons for which remained unclear. Therefore, it can be conjectured that in the context of liver disease, superimposed hepatic inflammation, albeit mild, may induce worsening liver disease akin to acute-on-chronic liver failure.

There are no prior studies of AAV use in BDL cirrhotic rats. Using adenoviral vectors, Smith et al demonstrated that luciferase expression was 10,000 fold lower compared to healthy rats¹⁴⁸. Regarding AAVs, Sobrevals et al found efficient transduction of CCl₄ cirrhotic rat liver when the vector was administered through the hepatic artery or portal vein¹⁴⁷. A peripheral venous route was not studied in this paper. Therefore, the possible reasons for inadequate transduction of BDL rats seen in this study include inadequate duration for transgene expression, suboptimal route of administration, inadequate dose for BDL cirrhosis. Since it was clear that extensive optimization would be required for adequate AAV mediate transgene delivery in BDL

rats, this method of gene therapy was abandoned in favour of non-viral methods.

Hydrodynamic injection of plasmid DNA via tail vein has been demonstrated to lead to efficient, temporary hepatic transgene expression in rodents¹⁴⁹. Rapid, high volume, high pressure injection is thought to lead to transgene expression by causing retrograde flow in the inferior vena cava and hepatic vein, leading to transient permeation of cell membranes of hepatic parenchymal and non-parenchymal cells, and subsequent uptake and expression of plasmid DNA. Viral vectors are thought to have decreased efficiency in cirrhosis due to a decreased ability to accessing the space of Disse due to collagen deposition and loss of endothelial fenestrae. However, in the BDL model fibrosis typically progresses from the peri-portal region, due to portal myofibroblast activation. Hence, retrograde injection of plasmid may in theory lead to permeation of peri-venous hepatocytes where fibrosis is typically less advanced, leading to passive uptake of plasmid DNA, which is also much smaller than the diameter of an AAV particle.

Typically, following hydrodynamic injection of plasmid, liver enzymes are transiently elevated and liver histology shows minimal damage that resolves within a week¹⁵⁰,¹⁵¹. In these experiments, a degree of elevation of serum AST and ALT was noted in BDL animals following hydrodynamic injection, but the degree of elevation was similar in both the plasmid-injected and saline control groups, suggesting that the inflammation was a consequence of high-pressure injection rather than the presence of plasmid DNA. Indeed, the absence of a marked rise in plasma AST and ALT in the sham group that also underwent hydrodynamic injection also suggests that the

pressure of the injection is the likely cause, since these animals would have far greater liver compliance to withstand high-pressure injection.

These experiments demonstrated hepatic transduction with hydrodynamic injection in BDL rats, as shown by a significant increase in hepatic human DDAH-1 mRNA in treated BDL rats compared to untreated BDL and sham rats which had background levels, and a significant increase in DDAH-1 protein. Unfortunately, neither immunohistochemistry nor *in situ* hybridization could be applied to these treated tissues to demonstrate location of transgene expression. This is because immunohistochemistry techniques for rat antigen retrieval for DDAH-1 have not been optimized, and there remain no published data demonstrating successful immunostaining of rodent liver for DDAH-1. Similarly, as described in chapter 4, initial attempts at *in situ* hybridization for human mRNA in rat liver was unsuccessful. Nevertheless, these experiments demonstrate a significant reduction in portal pressure associated with the increased hepatic DDAH-1 gene and protein expression, supporting the assertion that DDAH-1 is key in the local regulation of hepatic ADMA and eNOS activity in cirrhosis, and that maintaining hepatic DDAH-1 through liver specific targeting provides a novel approach to therapy in portal hypertension.

Chapter 4 – Hepatic DDAH-1 Expression is Post-Transcriptionally Regulated by MicroRNAs in Cirrhosis

4.1 Introduction

In this chapter the mechanism of decreased hepatocyte DDAH-1 expression in cirrhosis is explored. Since DDAH-1 is expressed in a cell- and tissue-restricted fashion, it was anticipated that the transcriptional regulation of DDAH-1 gene expression would be complex. Moreover, it can be hypothesized that a protein involved in ADMA metabolism, and hence partially responsible for control of tissue blood flow and vascular tone, may be regulated in a post-transcriptional or post-translational manner for rapid response to changing physiology. Therefore, following initial experiments characterizing hepatic DDAH-1 mRNA expression in cirrhosis, the post-transcriptional regulation of DDAH-1 mRNA, and effects of oxidative stress and microRNA-mediated mechanisms in particular, were explored in detail.

4.1.1 MicroRNAs and post-transcriptional regulation

MicroRNAs (miRNAs) are a large class of short (≈ 22 nt) noncoding RNAs (ncRNAs), which function as important regulators of a wide range of cellular processes by modulating gene expression. The role of ncRNAs in mammals was unclear until the 1990s. Up to this point, ncRNAs were thought to have a relevant function in plant species only. Ambros and colleagues changed this dogma with the seminal observation that the *lin-4* and *lin-14* genes play a key role in the temporal control of development of *Caenorhabditis elegans* (*C. Elegans*)^{152, 153}. They noted that the *lin-4* gene product was not protein encoding, but was a ncRNA, and levels were inversely proportional to levels of *lin-14* mRNA. Sequence analysis revealed that the *lin-4* RNA has sequence complementarity to the 3' untranslated region (UTR) of the

lin-14 gene, leading to the hypothesis that *lin-4* regulated LIN-14 protein expression, in part through Watson–Crick base pairing. Over the following decade other examples of regulatory ncRNAs in *C. Elegans* were described, and the basic concepts of miRNA biosynthesis and function were delineated¹⁵⁴⁻¹⁵⁶.

The generation of miRNAs is a multistage process (Figure 4.1)¹⁵⁷. Briefly, the primary miRNA (pri-miRNA) transcript, produced by RNA polymerase II or III, is transcribed as a hairpin double-stranded RNA structure in the nucleus. This structure contains the mature 22 nt miRNA sequence, and hence the miRNA must be excised during its biogenesis to elicit gene silencing. Two endoribonucleolytic enzymes are responsible for this excision - the nuclear endoribonuclease Drosha, in complex with the dsRNA-binding protein DiGeorge critical region 8 (DGCR8) is responsible for the first endonucleolytic reaction. DGCR8, also known as Pasha, functions as a molecular ruler that positions the Drosha cut site 11 bp from the base of the hairpin stem. This releases a ≈70nt stem-loop precursor miRNA (pre-miRNA) that possesses a 3' overhang. The pre-miRNA is exported to the cytoplasm via Exportin-5 in complex with Ran-GTP. Once exported, the pre-miRNA is processed by a second endoribonucleolytic reaction, catalyzed by Dicer, yielding a ≈22nt RNA duplex with protruding 3' overhangs at both ends (Figure 4.1). The duplex is loaded onto an Argonaute protein where one strand is selected, the “guide strand” - complementary to the target mRNA, and subsequently forms the miRNA effector as part of a miRNA-induced silencing complex (miRISC), while the remaining strand, the “passenger strand”, is released and degraded.

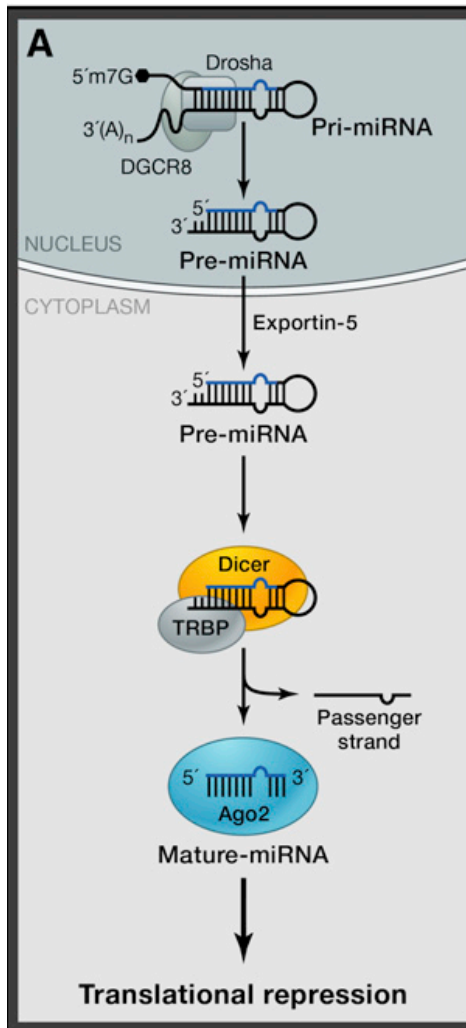


Figure 4.1 (adapted from Yates et al¹⁵⁷). The canonical pathway of miRNA maturation includes the production of the primary miRNA transcript (pri-miRNA) by RNA polymerase II or III and cleavage of the pri-miRNA by the microprocessor complex Drosha–DGCR8 (Pasha) in the nucleus. The resulting precursor hairpin, the pre-miRNA, is exported from the nucleus by Exportin-5–Ran-GTP. In the cytoplasm, the RNase Dicer, in complex with the double-stranded RNA-binding protein TRBP, cleaves the pre-miRNA hairpin to its mature length. The functional strand of the mature miRNA is loaded together with Argonaute (Ago2) proteins into the miRNA-induced silencing complex (miRISC), which targets mRNAs through mRNA cleavage, translational repression or deadenylation, whereas the passenger strand is degraded.

Typically, miRNA-binding sites of animal mRNAs reside in the 3' untranslated regions (UTRs) where recognition occurs through base pairing of the seed sequence (nucleotide positions 2 to 8) of a miRNA. Subsequently, the mRNA-miRNA

interaction guides the RISC to these transcripts, leading to silencing of transcription. However, the mechanism of transcriptional silencing remains unresolved, with mechanism such as translational inhibition¹⁵⁸, mRNA deadenylation¹⁵⁹, and decay¹⁶⁰ being proposed.

In terms of degree of complementarity, one would expect that it is relatively straightforward to identify miRNA target sites if the sequence of all the miRNAs and mRNAs are known. However, in animals and humans it is very rare that an mRNA contains a perfect complementary target site for any miRNA. The only known exception is the *HOXB8* mRNA, which is recognized with complete complementarity by miR-196¹⁶¹. All other human miRNAs silence mRNAs with target sites that are *not* perfectly complementary – indeed the overall degree of miRNA:mRNA complementarity is considered a determinant of mechanism of mRNA regulation.

Thus, identifying these target sites by a similarity search is difficult, because by allowing mismatches between miRNAs and mRNAs in a database search, hundreds or thousands of potential target sites will be identified due to the small size of the miRNAs. Furthermore, the positions of the mismatches are important although, typically, nucleotides in the seed sequence (positions 2–8) of the miRNA are perfectly complementary to the target mRNA (see figure 4.2)^{162, 163}.

Therefore, a three-step approach needs to be adopted when searching for evolutionarily conserved miRNA target sites; (i) identify 7nt matches to the miRNA seed sequence of interest, (ii) use available whole-genome alignments to compile orthologous 3' UTRs, (iii) search within the orthologous UTRs for conserved occurrence of a 7nt match¹⁶⁴. However, as noted above, there is considerable

heterogeneity with the degree of mismatch observed, with some experimentally verified miRNAs that would not necessarily be predicted by searching for perfect seed-sequence matching. Most current miRNA prediction software operates on the basis of perfect seed sequence complementarity. When evaluated on the basis of proteomic changes after miRNA addition or deletion, tools that require stringent Watson–Crick seed pairing perform better than those that do not^{160, 165}.

Prediction tools vary in their algorithms to account for the following: (i) 5' seed pairing, (ii) 3' compensatory pairing, (iii) evolutionary conservation, (iv) free energy of the miRNA-mRNA duplex, and local factors of the mRNA UTR such as (v) positioning of the target site within the UTR, (vi) degree of AU composition near the predicted site, and (vii) proximity to sites for coexpressed miRNAs. Since each prediction tool uses a slightly different algorithm, the predicted target lists often show little overlap with each other; e.g. TargetScan focuses on finding predicted sites with perfect 5' seed matching, whereas MiRanda preferentially predicts sites with 3'-compensatory matching. Prediction tools thereby order the predicted sites by rank, with varied weighting to the listed factors above. There is some evidence to suggest that TargetScan trends towards better performance with this ranking compared to other prediction tools, when verified experimentally by proteomics¹⁶⁵.

The aim of this series of experiments was to determine if DDAH-1 undergoes miRNA-mediated post-transcriptional regulation in cirrhosis.

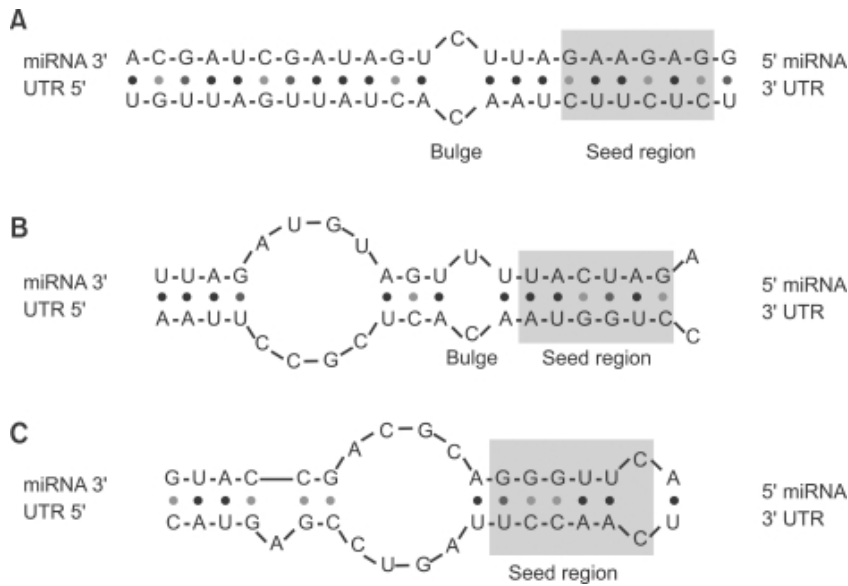


Figure 4.2 (adapted from Maziere and Enright¹⁶⁶): Approximate secondary structures of the three main types of target site duplex. (A) Canonical sites have perfect base pairing in seed region, a bulge in the middle and extensive base pairing in the 3' end of the miRNA. (B) Dominant seed sites form perfect complementarity in the seed, but poor complementarity in the 3' end of the miRNA. (C) Compensatory sites have a mismatch or G:U wobble in the seed region, but have extensive base pairing to the 3' end of the miRNA.

4.2 Results

4.2.1 mRNA expression in rats and humans with cirrhosis

As noted in the previous chapter, DDAH-1 protein expression is significantly decreased in rodent models of cirrhosis, and also decreased on semi-quantitative analysis of immunohistochemical staining of human cirrhotic tissue.

Initially liver tissue from BDL rats from the experiment in section 3.4 was used for analysis of expression of native (rat) DDAH-1 mRNA using qPCR. Figure 4.3 demonstrates no significant change on DDAH-1 mRNA between BDL and sham rats at 4 weeks following BDL surgery.

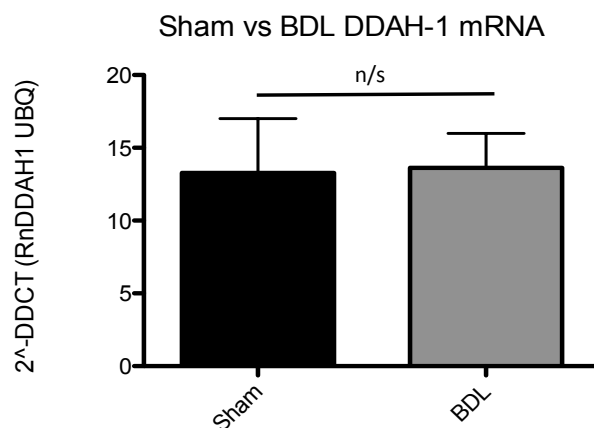


Figure 4.3: Rat hepatic DDAH-1 mRNA expression is unchanged at 4 weeks following BDL surgery compared with sham-operated animals (n=8/group, Student's t-test).

Subsequently, RNA extracted from human liver tissue from patients with end-stage cirrhosis at the time of liver transplantation, and from paired non-cirrhotic donor livers, was obtained for gene expression analysis. Briefly, biopsies of liver tissue were taken peri-operatively, from the recipient cirrhotic liver prior to explantation, and

from the donor non-cirrhotic liver after complete implantation in the recipient, and immediately snap frozen in liquid nitrogen and processed as in chapter 2. Details for these patients are provided in table 4.1.

Study no.	Recipient Details			Donor Details	
	Age	Gender	Liver disease	Age	Gender
1	55	M	ALD	27	M
2	42	F	ALD	46	M
3	67	M	NASH	54	F
4	53	M	Hepatitis C	23	M
5	65	F	NASH	49	F
6	51	M	Hepatitis C	25	M
7	28	M	AIH	27	F
8	57	M	ALD	55	F

Table 4.1: Patient characteristics from 8 cirrhotic liver transplant recipients, and their respective liver donors, from whom peri-operative liver biopsies were taken for RNA analysis. ALD= alcoholic liver disease; NASH= non-alcoholic liver disease.

As shown in figure 4.4, although a trend to a lower DDAH1 mRNA in cirrhotic recipient liver is seen, there was no significant difference between these groups to explain the previously described lower hepatic DDAH1 protein expression in rodent and human cirrhosis.

DDAH-1 mRNA Expression in Non-Cirrhotic Liver Transplant Donors and Cirrhotic Liver Transplant Recipients

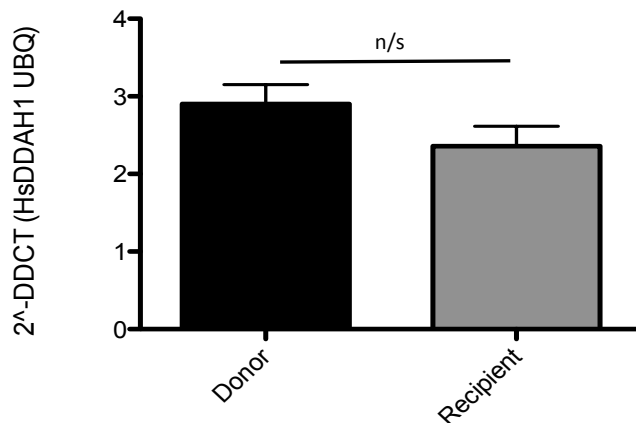


Figure 4.4: Human hepatic DDAH-1 mRNA expression is similar between non-cirrhotic human liver transplant donors and cirrhotic liver transplant recipients (n=8/group, Mann-Whitney U test).

4.2.2 miRNA expression in BDL cirrhotic rats

The data demonstrated thus far in this chapter demonstrate that hepatic DDAH-1 mRNA expression is unchanged in human cirrhosis and the BDL rat model of cirrhosis, yet as we demonstrated in chapter 3 hepatic DDAH-1 protein expression is significantly decreased in cirrhosis. As such, miRNA expression analysis was performed in BDL rats to explore candidate miRNA targets that may account for the observed discordance between hepatic DDAH-1 mRNA and protein expression in cirrhosis.

The GeneChip miRNA 2.0 array was used to demonstrate changes in miRNAs and non-coding RNAs between sham and BDL cirrhotic liver (n=4/group). One RNA sample from BDL liver failed to hybridize during the running of the chip, hence

results are only available for 7 animals (4 sham, 3 BDL). Figure 4.5 demonstrates miRNAs that are significantly altered from sham to BDL liver.

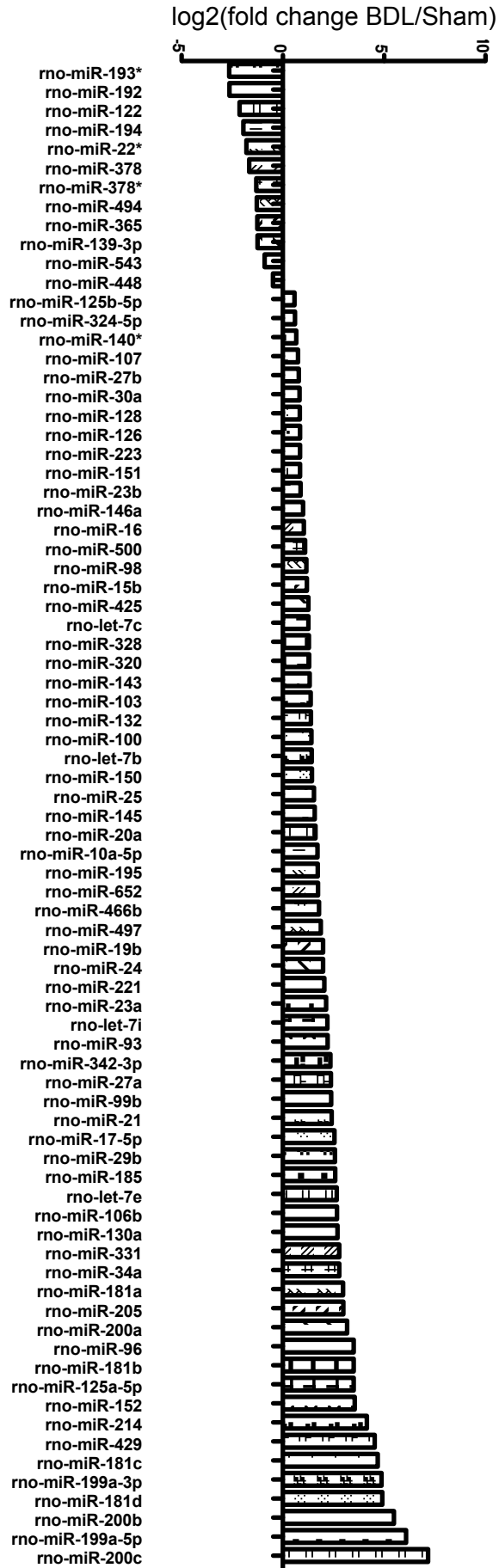


Figure 4.5: All significantly altered (adjusted $p < 0.05$) hepatic miRNAs from Genechip 2.0 miRNA microarray in BDL ($n=3$) vs sham ($n=4$) rats. Data presented as \log_2 transformed ratio of fold change BDL/Sham. Adjusted p -value calculated by Westfall–Young correction¹⁶⁷.

Quantitative PCR was used to confirm the changes in expression of a subset of miRs from sham and BDL rat liver, as shown in figure 4.6.

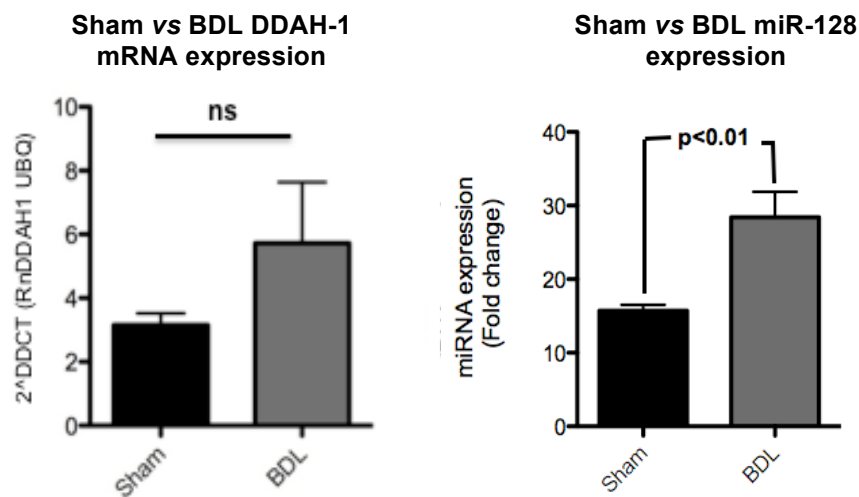


Figure 4.6. *Left panel:* Hepatic expression of rat DDAH-1 mRNA is unchanged between sham-operated and BDL rats ($n=6/\text{group}$, $p=\text{ns}$ Student's t -test). *Right panel:* Hepatic expression of mir-128 is significantly elevated in BDL rats compared with sham-operated rats ($n=6/\text{group}$, $p < 0.01$ Student's t -test).

4.2.3 Bioinformatic analysis of DDAH-1 3'UTR

As noted above, computational methods of determining potential binding sites for miRNA seed sequences exist, yet they are limited since perfect mRNA-miRNA complementarity is not absolutely required, and an extremely large number of potential target sites exists for any given miRNA. A computational approach to

prediction of miRNA targets facilitates the process of narrowing down potential target sites for experimental validation. These computational predictions utilise several aspects for algorithms of site prediction: (i) complementarity to the miRNA seed region; (ii) evolutionary conservation of the miRNA recognition element; (iii) free energy of the miRNA-mRNA duplex; and (iv) mRNA sequence features outside the target site as listed above¹⁶⁴.

The TargetScan algorithm focuses on the seed region in miRNA targeting, requiring an exact match to ≥ 7 bases of the seed sequence. Targetscan also includes a special class of seed matches with a hexamer match in positions 2–7, plus an adenosine at position 1. Additionally, TargetScan improves predictions by taking into account evolutionary conservation, and also adds a ‘context score’, which considers features in the surrounding mRNA UTR mentioned above, including local A-U content and location (near either end of the 3’UTR is preferred). When evaluated independently, each of the parameters used to rank TargetScan predictions— site conservation, site number, site type (with 8mer > 7mer-m8 > 7mer-A1), and site context - correlate with targeting efficacy^{160, 165, 168-170}.

TargetScan version 5.2 was used to interrogate the human DDAH-1 3’UTR for predicted miRNA recognition elements. The sequence used was that listed on the NCBI Genbank database – transcript NM_012137.3.

TargetScan provided a series of predicted miRNA recognition elements, and additionally a table of likelihood of biological relevance of miRNAs based on the probability of conserved targeting score (Pct) described by Friedman et al¹⁷⁰. This

score ranks the likely biological relevance of a predicted miRNA recognition elements as a function of orthologous conservation, miRNA complementarity and mRNA sequence features. This analysis demonstrated two putative regulatory areas in the DDAH-1 3'UTR – one at the 5' end of the 3'UTR containing predicted sites for miRs 219, 128, and 30, and a further cluster at the 3' end of the 3'UTR containing predicted sites for miRs 96, 148, 182, 101 (figure 4.7). These were also the most likely miRNA recognition elements in the TargetScan ranking on the basis of Pct score.

Human DDAH1 3' UTR

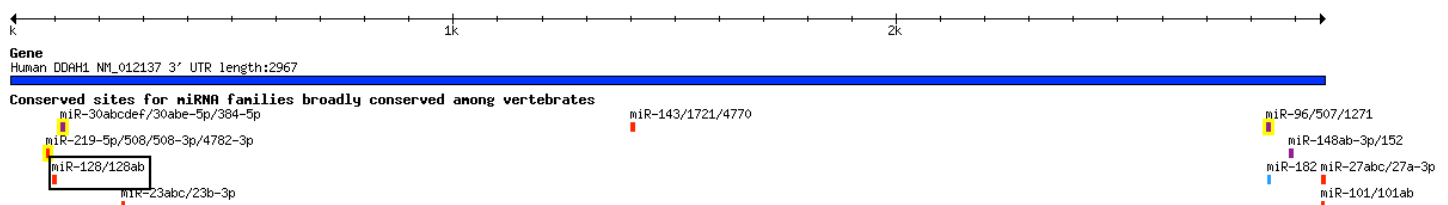


Figure 4.7: TargetScan (v5.2) analysis of the human DDAH-1 3'UTR (length 2.97kb). this figure demonstrates predicted miRNA binding sites for miR families 219, 128, 30, 23, 143, 96, 148, 182, 101.

The miRanda site was also used as a computational tool to predict DDAH-1 miRNA recognition elements. This tool uses similar parameters for analysis, although with slightly different weighting. Initially, Watson-Crick base pair matching of the seed sequence is searched for, and subsequently the free energy of each miRNA:mRNA target pair is calculated, and each target that has a predicted free energy below a threshold is passed to the last step. Matches are allowed to contain limited G-U wobble pairs with insertions or deletions. Free energy is calculated by predicting the folding of the miRNA:mRNA hybrid using the Vienna package calculation ¹⁷¹.

Orthologous conservation is used as a final filter, although unlike TargetScan, miRanda considers conservation of both binding site and position of binding site within the UTR.

Using miRanda (August 2010 release) to interrogate the DDAH-1 3'UTR, a number of predicted miRNA recognition elements were demonstrated and ranked according to the SVR score which takes into account the above aspects along with mRNA features such as site accessibility, AU flanking content, position of the target site within the 3' UTR, and UTR length. When ranked by SVR score, the miRNA recognition elements predicted by miRanda followed a similar pattern to those predicted by TargetScan. As demonstrated in figure 4.8, the above-mentioned clusters at the 5' and 3' ends of the 3'UTR contain predicted sites, although other sites in the centre of the DDAH-1 mRNA are also predicted.

Figure 4.8: miRanda (August 2010) analysis of the human DDAH-1 3'UTR. This figure demonstrates multiple predicted miRNA binding sites for miR families (in blue text above coding sequence in black text), including the segment containing sites for miRs 219, 128, 30.

On the basis of these findings, and the findings of differential hepatic DDAH-1 mRNA and protein expression, functional genomic studies were undertaken to test the hypothesis that the miRNA seed sequences identified by Targetscan and miRanda are regulatory within the human DDAH-1 3'UTR.

4.2.4 Luciferase reporter assays of the DDAH-1 3'UTR

In order to confirm the above *in silico* findings, an *in vitro* approach was adopted to test the regulatory function of the DDAH-1 3'UTR. The reporter vector pMirReport was used for this series of experiments. Briefly, the human DDAH-1 3'UTR was amplified from human cDNA using the PCR primers F: CGTGAGCATGTCTGAACTGG and R: CATGATTGGTTTTGGCACAC, and subcloned into the pMirReport luciferase reporter vector (Life Technologies, USA). Either this construct, or the control pMirReport vector, was co-transfected with a pRL-CMV Renilla expressing vector (Promega, USA) into HepG2 cells or HEK293T cells by standard techniques. At 24 hours following transfection, cells were lysed and Firefly and Renilla luciferase expression measured using the Dual-Luciferase Reporter assay (Promega, USA). Data is expressed as Firefly/Renilla luciferase expression, and all measurements were performed in triplicate

As seen in figure 4.9 the pMirReport_DDAH1 construct lead to a significant repression of luciferase expression compared to the empty control pMirReport vector, suggesting that this 3'UTR has regulatory functionality.

Further experiments were undertaken to characterise the predicted sites identified by bioinformatics studies above. Specifically, the predicted cluster of three miRNAs (219, 128, 30) at the 5' end of the 3'UTR were chosen for site-directed mutagenesis experiments, since they ranked highly on both Targetscan and miRanda prediction tools, and since they are within 100bp of the STOP codon, hence favourably located within the 3'UTR.

Briefly, synthetic oligonucleotides containing the wild-type 50bp region highlighted in figure 4.9, or containing site-specific mutations in the predicted miRNA binding sites, were designed and purchased. Subsequently, these oligonucleotides were annealed, and with 'sticky' ends were subcloned into pMirReport in a similar fashion to previously. As above, co-transfection of either the construct or the empty control pMirReport vector was performed with a pRL-CMV Renilla expressing vector into HepG2 cells. As above, cells were lysed at 24 hours, and Firefly and Renilla luciferase expression measured using the Dual-Luciferase Reporter assay.

Wild type sequence	CTAGTCCTT GACAATC TACTGTGC CACTGTG CTACTAACTCT TGTTTACA
Mutated miR-219 site	CTAGTCCTT GAGAATT CACTGTGCCACTGTGCTACTAACTCTT TGTTTACA
Mutated miR-128 site	CTAGTCCTT GACAATC TACTGTGC GACGTTG CTACTAACTCTT TGTTTACA
Mutated miR-30 site	CTAGTCCTT GACAATC TACTGTGCCACTGTGCTACTAACTCT TGTTGACA

Table 4.2: 50bp oligonucleotides of a section of the wild type DDAH-1 UTR (from nucleotides 71-120 of the UTR sequence) and similar oligonucleotides with mutations in miR bindings sites for miR-219 (yellow), miR-128 (green) and miR-30 (blue).

These data, presented in figure 4.9, demonstrates that the 50bp region has a repressive effect on luciferase expression of similar magnitude to that exerted by the full-length DDAH-1 UTR.

Point mutations were introduced into the predicted miR 219, 128 and 30 binding sites, through design of similar length 50bp oligonucleotides, and annealing and subcloning into the pMirReport vector as described above, and summarised in table 4.2. As shown in figure 4.9, despite mutation of the predicted miR 219 and 30 sites, significant repression of luciferase expression is still seen. However, with mutation of the miR-128 site a complete loss of repression is seen, with luciferase expression returned to baseline.

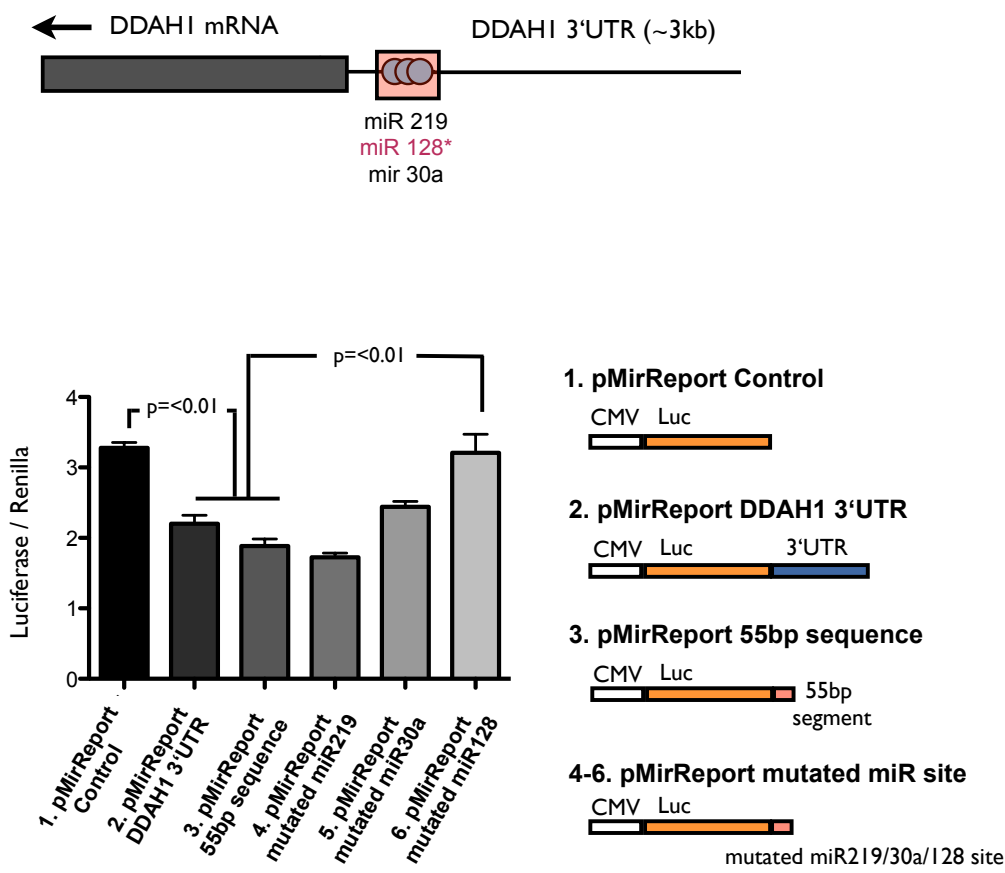


Figure 4.9a (*top panel*). Pictorial representation of the 3'UTR of DDAH-1, with a 55bp region of interest highlighted containing predicted binding sites for miRs 219, 128 and 30. This area was subcloned into the pMirReport luciferase vector (see figure 4.9b).

Figure 4.9b (*bottom panel*). Six constructs of the pMirReport luciferase reporter vector were transfected into HepG2 cells according to the schematic diagrams on the right of the figure, and cells were lysed at 24 hours. Firefly luciferase reporter expression, normalized for renilla luciferase expression as a transfection control, is depicted in the graph (n=8/group; all measurements performed in triplicate). The graph demonstrates that construct 2 containing the full-length DDAH-1 3'UTR significantly decreases luciferase expression, as does construct 3 containing the 55bp sequence highlighted in figure 4.9a with predicted binding sites for miRs 219, 128 and 30 (p<0.01 one way ANOVA). Mutation of the mir-128 binding site (construct 6) causes a significant de-repression of luciferase expression to baseline levels, which is not seen with mutation of miR-219 and miR-30 sites (constructs 4 and 5) (p<0.01 one way ANOVA).

4.2.5 Effect of hydrogen peroxide on hepatocyte DDAH-1 expression

Oxidative stress is a feature of chronic liver disease, and ACLF in particular. Increased markers of lipid peroxidation and markers of hepatic mitochondrial respiratory dysfunction have also been found in the livers of BDL cirrhotic rats. Therefore, a model of oxidative stress applied to HepG2 cells was used to evaluate effects on DDAH-1 protein expression and on DDAH-1 3'UTR function.

HepG2 cells were exposed to increasing concentrations of H_2O_2 as in figure 4.10. Protein expression of DDAH-1 was significantly reduced with H_2O_2 in a dose-dependent fashion at 24 hours following exposure, however there was no change in DDAH-1 mRNA with increasing H_2O_2 levels in HepG2 cells. To determine if this reduction in DDAH-1 protein expression was partially due to a post-transcriptional regulatory mechanism, pMirReport_DDAH1 luciferase reporter vector was transfected into HepG2 cells and exposed to similar increasing concentrations of H_2O_2 . A significant decrease in luciferase expression was seen following exposure to 10uM H_2O_2 at 24 hours (figure 4.10), although no further reduction in luciferase expression was seen at a concentration of 100uM H_2O_2 .

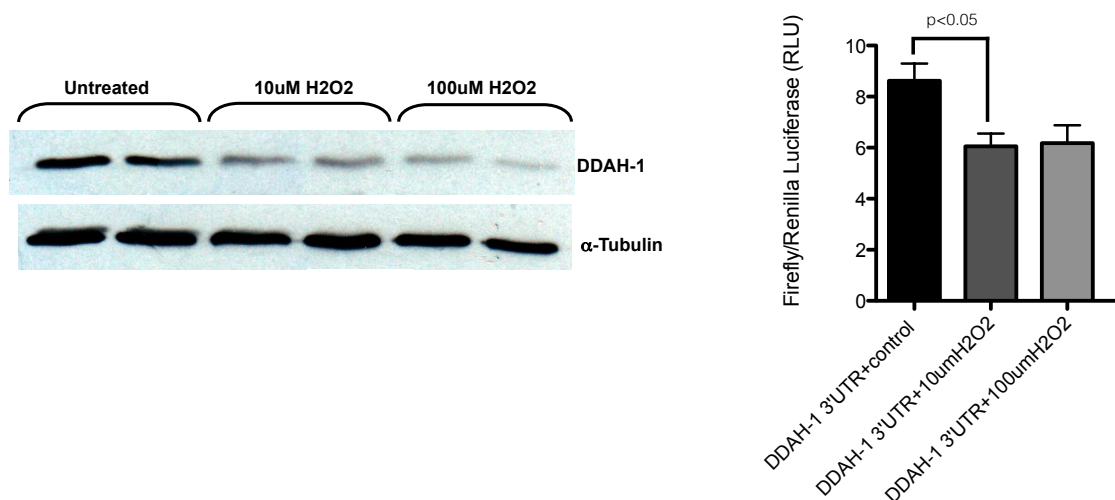


Figure 4.10a (*left panel*) – Representative western blot of HepG2 cells (n=6/group) exposed to control, 10uM or 100uM of H₂O₂ for 24 hours. HepG2 cells demonstrate a concentration-dependent decrease in DDAH-1 protein expression after 24 hours of exposure to H₂O₂.

Figure 4.10b (*right panel*) – HepG2 cells were transfected with the pMirReport_DDAH1 3'UTR reporter vector or control vector, and after 16 hours cells were exposed to H₂O₂ at the concentrations stated for 24 hours. Cells were then lysed and luciferase expression measured (n=6/group; all measurements performed in triplicate). Exposure of cells to 10uM H₂O₂ leads to a significant reduction in luciferase activity compared to control (p<0.01, one way ANOVA). No further decrease in luciferase activity is seen with exposure to 100uM H₂O₂.

4.2.6 Transfection of miRNA mimics and effects on DDAH-1 expression

To further demonstrate an effect of the predicted miRNAs on human DDAH-1 expression, transfection studies were undertaken to over-express mature miRNAs in a human cell line to ascertain effects on DDAH-1 expression compared to transfection of control, scrambled RNA controls.

To optimise transfection conditions, a selection of transfection conditions were tried in both HepG2 and HEK293T cells using the Qiagen Allstars cell death control RNA oligonucleotides. These siRNA oligonucleotides inhibit key genes required for cell

survival, and cell death observed microscopically is a sign of successful transfection, hence these conditions can be extrapolated for use in subsequent experiments.

Following optimisation of transfection conditions, miRNA mimics for human miRs 219, 128 or 30 were transfected into HEK293T cells, alongside a control group transfected with a scrambled miRNA mimic. At 24 hours, cells were lysed and DDAH-1 protein expression was determined by western blot. As shown in figure 4.11, transfection of each of these three human miRNAs (miR-219, miR-128, miR-30) led to a significant reduction in DDAH-1 protein expression in HEK293T cells.

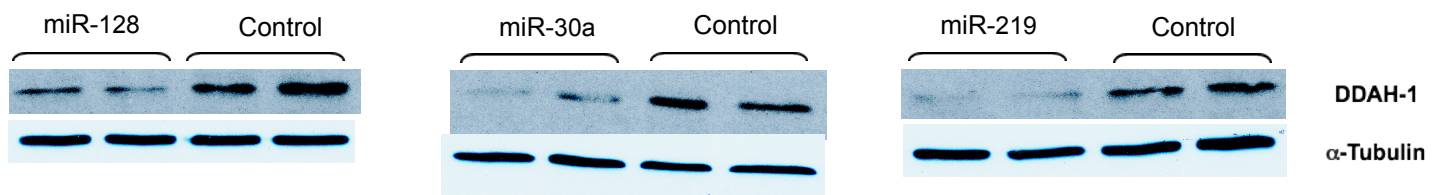


Figure 4.11: Representative western blots for DDAH-1 expression in HEK293T cells, 72 hours following transfection with synthetic miRNAs (n=6/group). Synthetic miRNA mimics for miR-128 (left panel), miR-30a (centre panel) and miR-219 (right panel) all significantly reduce DDAH-1 protein expression ($p < 0.05$, each test by Student's t-test).

4.2.7 *In situ* hybridisation for DDAH-1 and miR-128 in liver tissue

Initially, *in situ* hybridisation was chosen as a technique to map hepatic DDAH-1 expression, due to poor specificity of commercially available antibodies for

immunohistochemistry for DDAH-1 as described in chapter 3. The same primers as used in section 3.3.2 were used to amplify a 225bp PCR product from human DDAH-1 cDNA, which was subsequently used as a DIG-labelled hybridization probe (see supplemental methods for further detail). The primers used were F:GGCGCCGAGCCGGAGAAGG and R: GCCACTGGCACTGTGGAGACTGC.

DIG labelling of riboprobes was carried out according to the protocol in supplemental methods S4.1, and *in situ* hybridization was performed on frozen sections cut from frozen human liver tissue from the samples used in section 4.2.1. These samples were from subjects with end-stage cirrhosis at the time of liver transplantation, and from the healthy donor livers – the details for these patients is provided in appendix 1.

In situ hybridisation of anti-DDAH-1 DIG-labelled riboprobes, and of a DIG-labelled poly (dT) oligonucleotide positive control (recognising mRNA poly A tails), was performed on cirrhotic and control liver sections (n=3/group). Despite systematically altering conditions of temperature for hybridisation and stringency of washing, as listed in supplemental methods section S4.2, no staining was visible for either DDAH-1 or the positive control probe in these sections.

Subsequently, formalin fixed and paraffin embedded (FFPE) sections from naive and BDL cirrhotic rats were used for *in situ* hybridisation characterisation. The Affymetrix Quantigene *in situ* hybridisation kit was used for detection of rat DDAH-1 and miR-128 as described in supplemental methods S4.2.

As shown in figure 4.12 these images validate the findings described in chapter 3, and earlier in this chapter. These images demonstrate that DDAH-1 is expressed in

a hepatocyte-restricted fashion in rat liver, predominantly in a peri-venular distribution mirroring the expression of DDAH-1 protein in rat liver identified by immunostaining in chapter 3. Additionally, these images confirm no demonstrable change in DDAH-1 mRNA expression, despite a previously noted decrease in DDAH-1 protein expression in cirrhotic rodents characterised in chapter 3. Finally, these images demonstrate a marked upregulation of miR-128 expression in cirrhotic rat liver, as noted in studies with microarray and qPCR earlier in this chapter. Moreover, the distribution of miR-128 expression in cirrhotic liver also appears to be in a peri-venular fashion.

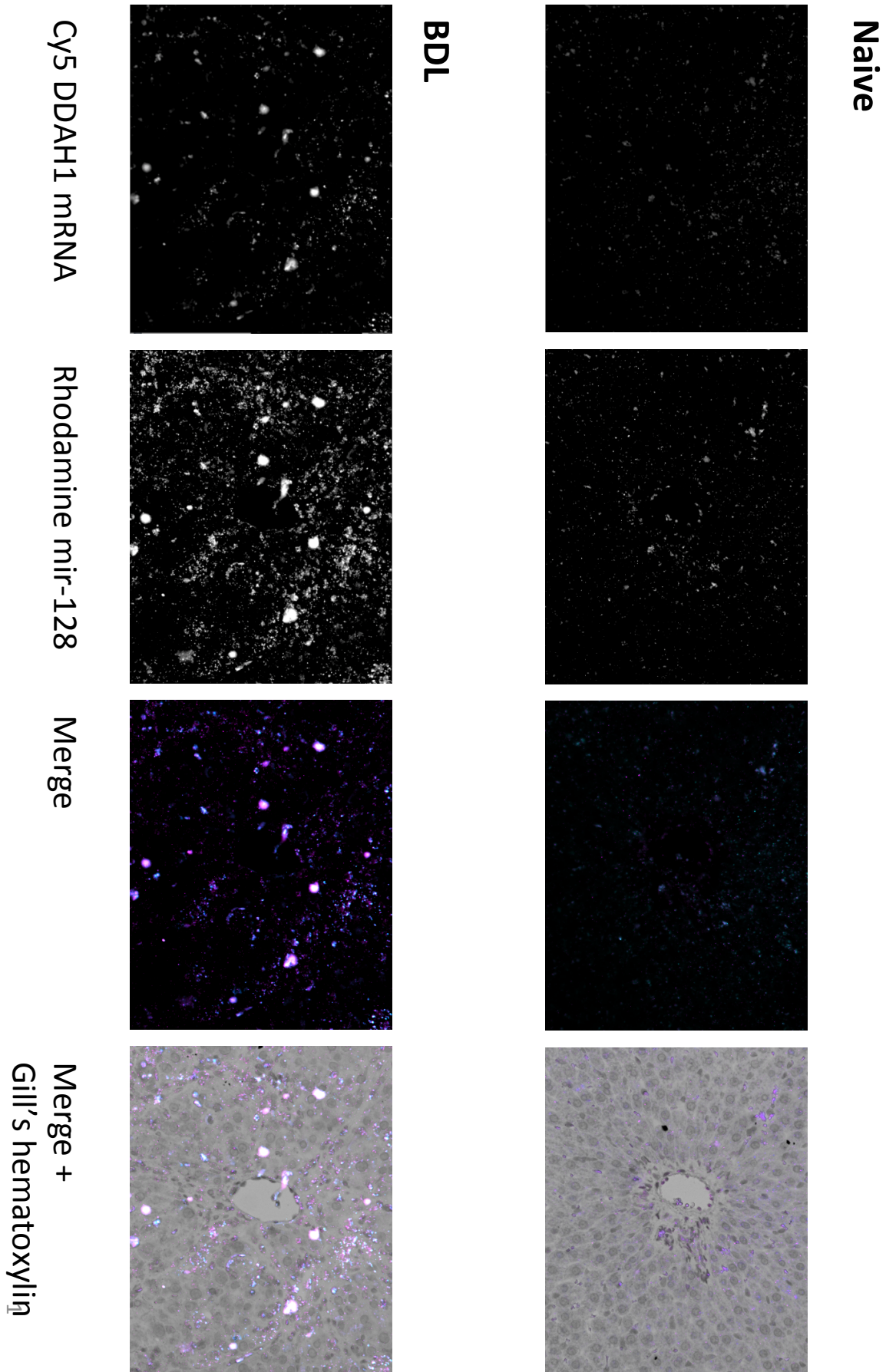


Figure 4.12: *In situ* hybridisation images (x40) of DDAH-1 mRNA and miR-128 expression from naïve (top panel) and BDL (bottom panel) rat liver.

4.3 Discussion

In this chapter we demonstrate through several lines of evidence that hepatic DDAH-1 is post-transcriptionally regulated in cirrhosis by an altered miRNA profile. The initial data leading to the hypothesis that DDAH-1 is post-transcriptionally regulated took the form of a discrepancy between DDAH-1 gene and protein expression in rat and human cirrhotic liver. This finding was confirmed by *in situ* hybridisation experiments in rat liver, demonstrating unchanged hepatocyte DDAH-1 mRNA in cirrhosis.

Subsequent bioinformatic analyses demonstrated several highly-conserved miRNA binding sites within the DDAH-1 3'UTR. Moreover, these sites are located in regions optimal for miRNA-mediated regulation, specifically near the 5' end of the UTR within 100bp of the STOP codon, since this facilitates access of the miRNA to the mRNA 3'UTR with less likelihood of hindrance due to tertiary RNA structures¹⁶⁴. It was also postulated that since ADMA has a role in the minute-to-minute regulation of organ blood flow, as the main regulator of tissue ADMA levels DDAH-1 may be regulated in a post-transcriptional manner to facilitate rapid responsiveness to changing physiological conditions.

The first experiment to determine the ability of the DDAH-1 3'UTR to confer regulation was through *in vitro* luciferase reporter assays. For these experiments, the DDAH-1 UTR expressing luciferase construct was transfected into a hepatocyte cell line (HepG2), since miRNA-mediated gene regulation is likely to be tissue-specific, and a hepatocyte cell line is therefore most likely to recapitulate the cellular microenvironment within human hepatocytes. These experiments demonstrated a robust and reproducible suppression of luciferase expression compared to the empty vector control. Subsequently, on the basis of the results of two miRNA prediction

tools, a short (50bp) segment was also subcloned into the luciferase reporter vector. These experiments demonstrated that this shorter section of the 3'UTR has a similar regulatory effect to the full-length 3'UTR in HepG2 cells.

The initial experiments were performed with a virtually full-length (>2.8kb) UTR aside from the last 114bp at the 3' end (due to the lack of suitable primers to amplify this section for subsequent sub-cloning). As noted by Bartel, the complete UTR sequence should be tested to ensure that endogenous sequences that enhance or inhibit miRNA binding and gene regulation located distal to the predicted miRNA-binding site are also present in the reporter construct¹⁶⁴. Therefore it is possible, although unlikely, that inclusion of the terminal 114bp could change the dynamics of the DDAH-1 mRNA to alter responsiveness to endogenous miRNAs.

As discussed above, the context of the miRNA binding site within the UTR has relevance for determining the miRNA-mRNA interaction. Genome-wide analyses of site conservation, site efficacy, and site depletion, all indicate that 7–8 nt seed sequences within the 3' UTR tend to be most effective if they do *not* fall in the middle of long UTRs¹⁶⁸. One explanation for these results is that sites in the middle of long UTRs may be less accessible to the RISC silencing complex due to the possibility of occlusive RNA-RNA interactions with segments from either side, whereas sites near the UTR ends would not. Similarly, local nucleotide composition in the immediate vicinity of the site, has been shown to be important, with those sites within high local AU content performing best¹⁶⁸. Several methods have been proposed for predicting accessible UTR secondary structure favourable for miRNA targeting¹⁷²⁻¹⁷⁶. Although some of these methods have predictive value, when experimentally evaluated they are less successful in predicting responsive targets than scoring local AU content alone^{165, 168}. The reasons for this are unclear, but when orthologous 3' UTRs are

analyzed, conserved 7-mers are preferentially found in local AU-rich contexts, in predicted accessible secondary structure, away from the first 15 nt of the 3' UTR, and away from the centre of long UTRs^{168, 177, 178}. Thus, these results support the accessibility of the chosen 46pb region of the DDAH-1 UTR, since it occurs in an A-U rich area, is away from the centre of the UTR and towards the STOP codon (but not within 15nt of the STOP codon) and contains highly orthologously conserved miRNA sites.

Subsequent experiments were performed to mutate the predicted miRNA binding sites within the 46bp sequence cloned into the luciferase reporter. These experiments firstly confirmed that the short 46bp sequence is sufficient to induce repression of translation of luciferase in HepG2 cells. Moreover, these experiments suggested that the predicted miR-128 site was necessary for this translational repression, since mutation of this site caused a loss of repression back to baseline levels, unlike mutation of the other predicted miR-219 and miR-30 sites.

However, these results are not completely consistent with subsequent experiments where miRs 128, 219 and 30 were overexpressed in HEK293T cells, and all three miRs were found to significantly repress DDAH-1 protein expression. Thus, it is unclear why overexpression of miRs 219 and 30 led to significant repression of DDAH-1 expression in HEK293T cells, whereas mutation of predicted miR-219 and miR-30 binding sites did not lead to a de-repression of luciferase expression in HepG2 cells.

One possibility is that HepG2 cells do not express enough endogenous miR-219 or miR-30 to contribute to repression of a luciferase reporter, but may exhibit repression in the context of over-expression. Other authors have demonstrated that mir-219-5p

is expressed in HepG2 cells, albeit at lower levels than in other hepatocyte cell lines¹⁷⁹. Similarly, previous studies have demonstrated that HepG2 cells also express miR-30a, but at lower levels than the breast cancer line MSF7¹⁸⁰. Thus it is likely that the HepG2 cells used in these experiments express miRs 219 and 30a, although this was not tested in the experiments described above.

A further possibility is that the sites were not adequately mutated to reduce miR function. Taking miR219-5p, only 2 nucleotides were changed from the wild type seed sequence. (GACAATC → GAGAATT). Since it is possible that miR-219-5p acts through having compensatory 3' matching (see above), this would explain the lack of de-repression on mutating only 2 sites in the seed sequence. A recent study (published subsequent to the experiments described in this thesis) demonstrated that mutation of 6 nucleotides in the miR219-5p seed sequence leads to a significant de-repression of target gene lending credence to this hypothesis¹⁸¹. Similarly, only one nucleotide was altered in the mutant miR-30 construct (TGTTTAC→TGTTGAC). For similar reasons, this may not have been sufficient to alter miR-30 function, particularly if significant compensatory 3' binding is present.

Finally, it is possible that cell-specific cofactors are required, that are *permissive* for subsequent miR-219 or miR-30 binding, possibly by involving other mRNA binding proteins. An example is the Pumilio proteins, which have been shown to induce a permissive change in p27 mRNA to allow access of the miR221/222 –RISC complex to its target site to enable translational repression and play a role in cell cycle regulation¹⁸². Thus, it is possible that cell-specific cofactors are responsible for the differential effect of miR-219 and miR-30 seen between HEK293T and HepG2 cells.

In this chapter, we also show for the first time that hepatocyte DDAH-1 is sensitive to oxidative stress, with a concentration-dependent decrease in DDAH-1 protein expression. Previous investigators have shown that DDAH-1 is sensitive to TNF α -mediated inflammation and oxidative stress – Ito et al demonstrated decreased DDAH activity in endothelial cells exposed to TNF α or oxidized LDL¹⁸³. More recently, Luo et al showed that renal preglomerular vascular smooth muscle cells (VSMCs) exposed to oxidative stress with H₂O₂ showed a marked decrease in DDAH-1 protein expression, but *increased* DDAH-1 mRNA expression¹⁴³, thus echoing our findings of discordant DDAH-1 mRNA and protein expression following H₂O₂ exposure in hepatocytes. Interestingly, these authors found that proteosomal inhibition led to partial but not complete reversal of this effect, suggesting that the decrease in DDAH-1 protein expression is partially due to protein degradation but the remainder of this effect remained unexplained. In the experiments outlined above, we found that the 3'UTR mediated some of the effects of H₂O₂ on DDAH-1 protein expression, since 10uM concentrations of H₂O₂ lead to a repression of luciferase expression that was not enhanced at the higher 100uM concentration. Thus, it is likely that post-transcriptional regulation of DDAH-1 mRNA is partially responsible for the decrease in DDAH-1 protein expression seen in hepatocytes at lower levels of oxidative stress, and at higher levels protein degradation may be the predominant mechanism.

From the experiments presented here, it is unclear if H₂O₂ mediated oxidative stress leads to decreased DDAH-1 expression through increasing miRNA regulation or through a parallel signalling mechanism. Clearly, measurement of miR-128 (or indeed other candidate miRs such as miR-219 or miR-30) in HepG2 cells exposed to H₂O₂ would have lent support to the hypothesis that oxidative stress modulates

hepatocyte DDAH-1 expression through altered miR regulation. However, this experiment was not performed, primarily due to the chronological order in which the experiments in this thesis took place. Prior investigators have shown that miR-128 is induced by H₂O₂ in a dose-dependent fashion in cardiac myocytes¹⁸⁴, however as yet this experiment has not been performed in hepatocytes.

Other possibilities are that H₂O₂ acts in parallel with miRNAs to decrease hepatocyte DDAH-1 expression. Indeed, post-transcriptional protein-mRNA interactions in the 3'UTR have been shown to account for decreased protein expression in response to H₂O₂-mediated oxidative stress in other cell types¹⁸⁵. Thus, aside from miRNA regulation, possible mechanisms of redox signalling on the DDAH-1 3'UTR include: (i) by direct oxidation of a mRNA-binding stabilising protein, (ii) by activation of a mRNA-inhibiting target protein upon dissociation of an oxidized inhibitor, (iii) activation of target proteins through an intermediate signalling pathway, such as the peroxiredoxin-thioredoxin axis¹⁸⁶ (Day et al Mol Cell 2012).

Thus, taking the data presented above together, miR-128 appears to be an attractive target for therapeutic intervention in portal hypertension, since it is elevated in BDL cirrhotic liver, is located in hepatocytes and co-localises with DDAH-1 mRNA, and has regulatory function on DDAH-1 through loss-of-function and gain-of-function experiments. Mechanisms of oxidative stress acting through post-transcriptional mechanisms on DDAH-1 expression also merit further investigation.

Chapter 5 – DDAH-1 is Differentially Expressed as an Alternative Truncated mRNA Transcript in Human Placenta

5.1 Introduction

In addition to miRNA-mediated regulation of gene expression, a further recognized aspect of genomic complexity is the generation of alternative gene products from a single gene locus, which can occur through transcriptional or post-transcriptional (splicing) mechanisms^{187, 188}. The use of alternative transcriptional initiation and/or termination (transcriptional events) can give rise to different pre-mRNAs, which can further undergo alternative splicing (splicing events), leading to multiple mRNA/transcript variants from the same gene. Therefore, a gene can potentially yield an extensive array of gene products - alternative transcript (transcriptome) and alternative protein (proteome) isoforms - thereby expanding the repertoire of the gene products in the mammalian genome. Although the functional consequence of differential expression of alternative isoforms is known for some genes, the magnitude of alternative isoform expression at the genome scale remains unknown, although recent evidence suggests that almost all multi-exon human genes generate multiple RNA variants that differ either in protein-coding regions and/or regulatory untranslated regions (UTR)¹⁸⁹⁻¹⁹².

The role of alternative promoters is particularly critical in transcriptional regulation, since alternative sites of transcription initiation allows tissue-specific or context-specific expression of different transcript variants. An example of this is the gene *LEF1*, which encodes lymphoid enhancer factor proteins that mediate the transcriptional regulation of Wnt/ β -catenin target genes. *LEF1* is transcribed by two alternative promoters (P1 and P2). The most 5' promoter P1 produces full-length

LEF1 protein (LEF1), which recruits β -catenin to Wnt target genes. However, an intronic promoter P2 drives transcription of the shorter LEF1 protein (Δ NLEF1), which cannot interact with β -catenin and instead *suppresses* Wnt regulation of target genes¹⁹³. Thus, the two proteins from the *LEF1* gene have opposing biological activities, adding a further layer of complexity to gene regulatory networks. Moreover, this switch in *LEF1* promoter and transcript has functional consequences - *LEF1* is not normally expressed in the human colon or in embryonic mouse intestine. However, in colon cancer tissue and cell lines, the promoter that produces full-length LEF1 is aberrantly activated, and the second promoter that drives the shorter protein is silent producing different biological outcomes¹⁹⁴.

Since in chapter 3 it was demonstrated that hepatocyte DDAH-1 is reduced in cirrhosis, and there is a discrepancy between hepatocyte DDAH-1 mRNA and protein expression in cirrhosis, a further possibility exists that transcription of an alternative non-protein coding DDAH-1 transcript is responsible for these findings. This hypothesis was explored further in this chapter.

5.2 Results

5.2.1 Bioinformatic analysis of an alternative DDAH-1 transcript

As a first step in characterizing alternative DDAH-1 transcripts in the *homo sapiens* transcriptome, the NCBI Nucleotide database was interrogated for alternative DDAH-1 transcripts. This revealed a curated DDAH-1 transcript 2 (NM_001134445.1)(figure 5.1). This transcript was submitted directly to NCBI for curation by the DNA sequencing consortium of the German Genome Project in 2005, from an endometrial cancer cell line. However, no further characterization of this transcript had been performed, and, at the time of the experiments presented in this thesis, had not been studied in any peer-reviewed publications.

This transcript, although a longer mRNA with 2 non-coding exons and a longer 5'UTR, lacks the coding exon 1 of the protein coding DDAH-1 transcript 1.

Subsequently, a process of comparative regulatory genomics was performed, whereby this genome sequence was interrogated by comparison with orthologous genomic loci from a number of other species in multiple mammalian and non-mammalian lineages, looking for evolutionarily conserved sequences. Comparative regulatory genomics describes the comparison of orthologous genomic sequences from multiple species in order to identify putative promoters or other functional *cis* regulatory modules (CRMs). This comparative process, also commonly referred to as “phylogenetic footprinting”, is based on the premise that some function of regulatory elements will be conserved between species, and this functional conservation will be reflected in similar nucleotide sequences¹⁹⁵.

The assumption is made that the sequences being aligned are derived from a common ancestor, and that the time since their divergence has enabled a significant accumulation of mutations within both genomes and that selection has occurred¹⁹⁵.¹⁹⁶ It is crucial however that the genomes compared still maintain sufficient sequence similarity so that the homologous regions can be easily identified. Comparing closely related species, for example mouse and rat which diverged 41 million years ago (mya), will highlight genomic sequences where divergence is most readily tolerated, by highlighting *differences* rather than similarities between the two species. Conversely when one compares distantly related species, for example rat and chicken (species diverged 310 mya), sequences under positive selection (genomic sequences constrained during evolutionary selection) are more easily identified (Ureta-Vidal et al, 2003). Sequence comparisons between human and opossum, which diverged ~180mya, have been empirically shown to be suitable for identification of functional CRMs in many cases¹⁹⁷.

Homo sapiens mRNA; cDNA DKFZp686N2176 (from clone DKFZp686N2176)

GenBank: BX648145.1

[FASTA](#) [Graphics](#)

LOCUS BX648145 3908 bp mRNA linear HTC 16-OCT-2008
DEFINITION Homo sapiens mRNA; cDNA DKFZp686N2176 (from clone DKFZp686N2176).
ACCESSION BX648145
VERSION BX648145.1 GI:34367304
KEYWORDS HTC.
SOURCE Homo sapiens (human)
ORGANISM [Homo sapiens](#)
Eukaryota; Metazoa; Chordata; Craniata; Vertebrata; Euteleostomi;
Mammalia; Eutheria; Euarchontoglires; Primates; Haplorrhini;
Catarrhini; Hominidae; Homo.
REFERENCE 1 (bases 1 to 3908)
AUTHORS Ansoorge,W., Krieger,S., Regiert,T., Rittmueller,C., Schwager,B.,
Mewes,H.W., Weil,B., Amid,C., Osanger,A., Fobo,G., Han,M. and
Wiemann,S.
CONSRMT The German cDNA Consortium
TITLE Direct Submission
JOURNAL Submitted (20-JAN-2005) MIPS, Ingolstaedter Landstr.1, D-85764
Neuherberg, GERMANY
COMMENT Clone from S. Wiemann, Molecular Genome Analysis, German Cancer
Research Center (DKFZ); Email s.wiemann@dkfz-heidelberg.de;
sequenced by EMBL (European Molecular Biology Laboratories,
Heidelberg/Germany) within the cDNA sequencing consortium of the
German Genome Project.
This clone (DKFZp686N2176) is available at the RZPD Deutsches
Ressourcenzentrum fuer Genomforschung GmbH in Berlin, Germany.
Please contact RZPD for ordering:
<http://www.rzpd.de/cgi-bin/products/cl.cgi?CloneID=DKFZp686N2176>
Further information about the clone and the sequencing project is
available at <http://mips.gsf.de/projects/cdna/>
FEATURES Location/Qualifiers
source 1..3908
/organism="Homo sapiens"
/mol_type="mRNA"
/db_xref="taxon:9606"
/clone="DKFZp686N2176"
/tissue_type="endometrium carcinoma cell line"
/clone_lib="686 (synonym: hlcc3). Vector pSport1_Sfi; host
DH10B; sites SfiIA + SfiIB"
/dev_stage="adult"
/note="NG,NG-dimethylarginine dimethylaminohydrolase 1,
alternative start, differentially spliced"
gene 1..3908
/gene="DKFZp686N2176"
CDS 390..938
/gene="DKFZp686N2176"
/codon_start=1
/product="hypothetical protein"
/protein_id="CAI45988.1"
/db_xref="GI:57997565"
/db_xref="GOA:Q5HYC8"
/db_xref="HGNC:HGNC:2715"
/db_xref="InterPro:IPR003198"
/db_xref="UniProtKB/TrEMBL:Q5HYC8"
/translation="MMKEALEKLQLNIVEMKDENATLDGGDVLFTGREFFVGLSKRTN
QRGAELADTFKDYAVSTVPVADGLHLKSFCSMAGPNLIAIGSSESAQKALKIMQQMS
DHRVDKLTVPDDIAANCYLNIPNKGHVLLHRTPEEYEPESAKVYEKLDHMLIPVMS
ELEKVDGLLTCCSVLTKKRVDS"
misc feature <390..920
/gene="DKFZp686N2176"
/note="Amidinotransferase; Region: Amidinotransf; c119186"
/db_xref="CDD:267539"

Figure 5.1: NCBI entry for DDAH-1 transcript 2 (NM_001134445.1) – accessed 4th June 2012.

The human sequence comprising ≈ 100 kb area upstream of the DDAH-1 transcript 1 (termed T1) encompassing the 2 non-coding exons of DDAH-1 transcript 2 (termed T2) as well as further ≈ 50 kb upstream of the T2 transcript, was compared with orthologous *loci* from multiple species, including both mammalian and non-mammalian lineages. As described in the methods, the ECR browser was used for these comparisons. ECR utilises a widely employed technique to graphically display sequence conservation profiles in reference to the base DNA sequence (Homo sapiens 1p22 150kb *DDAH-1* genomic interval) that is linear along the horizontal axis (Figure 5.2) while the vertical axis displays percent identity with respect to the chosen secondary sequence (Figure 5.2 multiple-species). Regions of significant non-coding conservation are graphically displayed as **red** peaks, with exonic and untranslated coding sequences depicted by **blue** and **yellow** peaks respectively.

A pre-defined cut-off for significant conservation of non-coding elements was employed – >350 bp long with $>77\%$ sequence homology. These filters have been shown to identify 90% of non-coding conserved elements between human and Fugu genomes, and subsequently used a filter to identify functional human/mouse regulatory elements¹⁹⁸. Using this threshold, our analysis demonstrates only a single evolutionarily conserved non-coding region, just upstream of the transcription start site (TSS) of the DDAH-1 T2 transcript. This ≈ 700 bp area is conserved across mammalian species to opossum, but is lost when chicken or fugu genomes are included. The level of conservation, maintained in the 180 million years since human and opossum diverged, suggests that this area is likely to be of functional importance. Moreover, the spatial conservation of this area just upstream of the DDAH-1 T2 TSS, suggests this area may represent a putative core promoter.

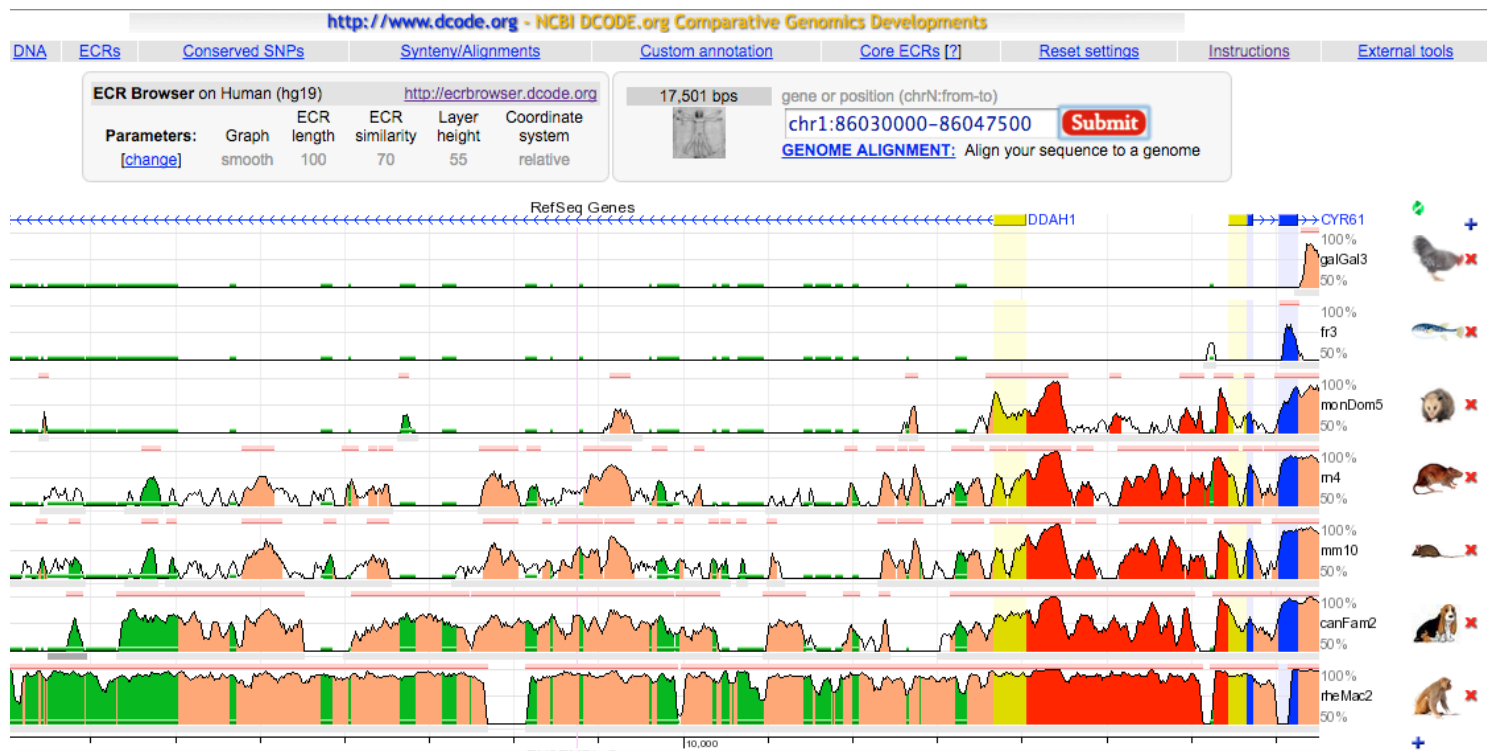


Figure 5.2: Conservation of homo sapiens chromosome 1 DDAH-1 5' flanking region across mammalian species. Screenshot of ECR browser – accessed 21st May 2011. Regions of significant non-coding conservation are graphically displayed as red peaks. DDAH-1 is expressed on the negative strand of chromosome 1, hence transcription proceeds from right to left ('5' to 3') across this figure, and the area in red is immediately 5' to the coding region. The area in red has significant conservation (>77% sequence homology) across the species depicted in the right panel compared to the human sequence (in ascending order: rhesus macaque, canine, mouse, rat, opossum). Conservation of this area is lost for the non-mammalian species depicted in the upper part of the right panel (chicken and fugu).

5.2.2 Determination of human tissue expression of alternate DDAH-1 transcript

Quantitative PCR was used to determine the expression of both the full-length T1 transcript and the alternate T2 transcript in a human tissue cDNA panel (Clontech Laboratories, USA). This cDNA panel from a variety of human tissues is normalized to several different house-keeping genes to ensure accurate relative assessment of

target mRNA abundance.

Taqman qPCR probes (Life Tech Inc, USA) were used to distinguish the two transcripts – an initial probe detecting a 77bp amplicon across the exon 2-3 boundary was used to detect *both* the T1 and T2 transcripts, and a second probe detecting a 71bp amplicon across the exon 1-2 boundary of the T2 transcript was also used – this was selective for the T2 transcript (Figure 5.3).

As shown in figure 5.4 although a broad distribution of expression for the full length T1 DDAH-1 transcript was seen, no expression of the T2 transcript was seen in the tissues represented in the cDNA panel. Additionally, no expression of the T2 transcript was seen in human liver samples from patients with cirrhosis (the same samples as examined in chapter 4 section – data not shown).

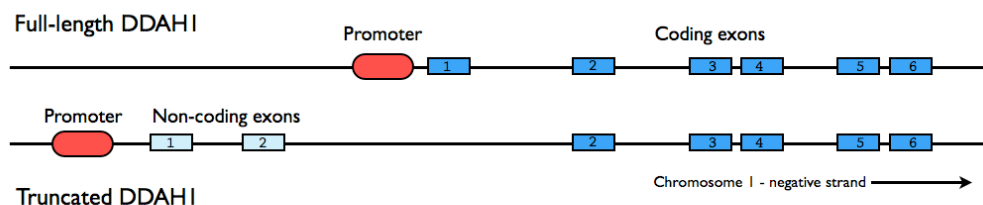


Figure 5.3: Schematic diagram of promoters and exons of DDAH-1 T1 and T2 transcripts. The T1 transcript is a shorter mRNA, but with 6 coding exons encoding a longer protein. The T2 transcript is a longer mRNA but has only 5 coding exons, with 2 non-coding exons, and is therefore predicted to encode a shorter protein.

Since, endometrial tissue was not represented in this cDNA panel, and the original curated NCBI entry for this transcript was from an endometrial cancer cell line, RNA from the Ishikawa endometrial cell line was also analysed by qPCR for the T2

transcript. As seen in figure 5.4 low level expression of the T2 transcript is evident. Although a direct comparison with the mRNA expression of the T1 transcript is not possible since the $\Delta\Delta\text{CT}$ method was used for RNA quantification, rather than standard curve method, it is clearly lower than the full-length T1 transcript. No expression of T2 was seen in the negative controls for this experiment.

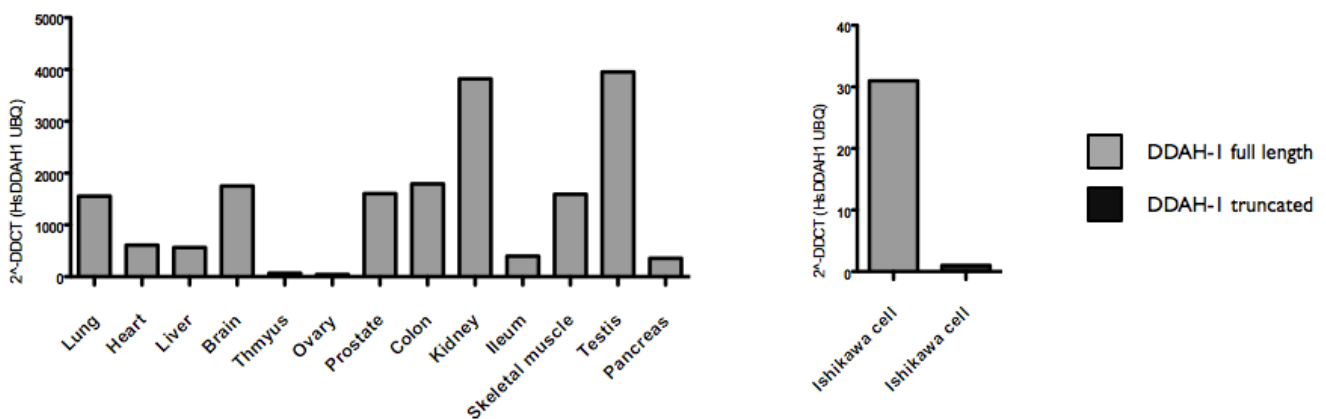


Figure 5.4: *Left panel:* DDAH-1 T1 transcript mRNA expression in human tissue cDNA panel (pooled cDNA from n=6 tissues/group) . No DDAH-1 T2 transcript expression was detectable in this tissue panel. *Right panel:* Expression of both DDAH-1 T1 and T2 transcript mRNA is detectable in the Ishikawa cell line (pooled RNA from n=4 experiments).

To confirm these findings, healthy human placental tissue (n=4) was obtained from healthy mothers at the time of caesarean section. Non-targeted samples were taken, snap frozen in liquid nitrogen, and RNA extracted for qPCR as in section 2.4.1. As shown in figure 5.5 there is similarly low-level expression of the T2 mRNA transcript seen in healthy placenta, although again direct comparison with the expression level of the T1 transcript is not possible with the $\Delta\Delta\text{CT}$ method of quantification. Again, no expression of T2 was seen in the negative controls for this experiment.

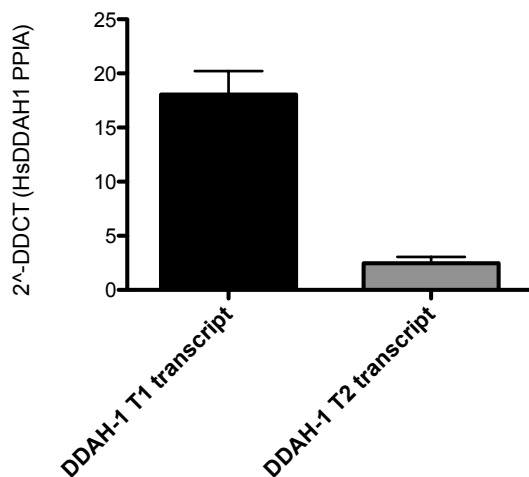


Figure 5.5: DDAH-1 T1 and T2 transcript mRNA expression in healthy human placenta (n=4).

The core promoter is required for the transcription of eukaryotic RNA polymerase II (RNA pol II) transcribed genes. The promoter is typically defined as the area of genomic DNA approximately 35-40 bp upstream and downstream of the TSS. The core promoter is also defined in functional terms, since this region is usually sufficient to mediate gene expression in a reporter gene assay. The core promoter contains sequence elements, referred to as “core promoter motifs,” which interact with the basal transcription machinery, including RNA polymerase II and the TFIID complex^{199, 200}. Although a number of prevalent core promoter motifs have been defined, there is no universal motif common to all promoters. However, the traditional model of a eukaryotic promoter driven by RNA pol II is an AT-rich DNA sequence (the TATA box) approximately 30 bp upstream of an initiator (Inr) sequence that contains the TSS. Assembly of a pre-initiation complex (PIC), which includes the transcription factor TFIIA-H along with RNA pol II, is initiated by TFIID binding to the TATA box, Inr sequences and/or other sites, and bending the DNA through a 90° angle. The next step involves recruitment other general transcription factors, after

which transcription is initiated 30 bp downstream.

Transcription is further regulated by interactions of the PIC with three additional components: the TATA-associated factors, the so-called mediator complex(es), and positive and negative cofactors. Coordination of chromatin modification, mainly through the control of post-translational modification of histones, also has an important role in transcription initiation. The recruitment of all of these co-activators and co-repressors of transcription initiation is controlled by transcription factor binding to cis-acting DNA sequences that can lie within the core promoter or in more remote locations (enhancers and repressors).

Using the Genomatix Gene2Promoter and Matinspector software, a number of transcription factor binding sites were mapped to this putative promoter using default parameters for core and matrix similarity thresholds (matrix similarity values of 0.75 and core similarity values of 0.7)^{201, 202}.

The graphical output identifies 251 significantly conserved TFBS according the above parameters, within the conserved ≈ 700 bp area upstream of the T2 transcript TSS. Specifically, binding sites for important initiators of transcription such as the TATA box (O\$VTBP) and TFIID (O\$TF2D) are present in this conserved area (Figure 5.6).

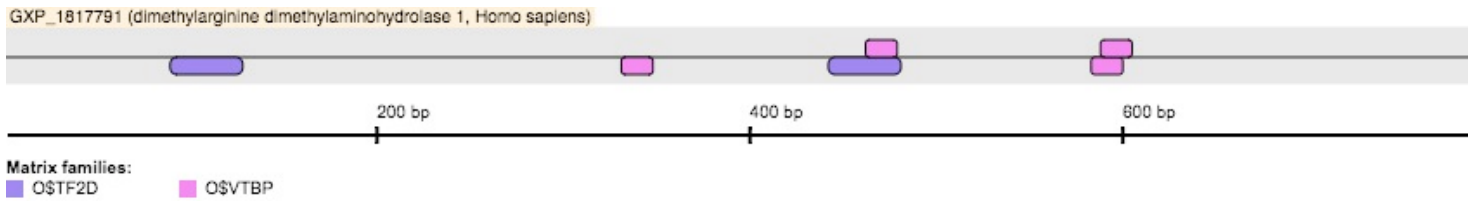


Figure 5.6 Identification of putative promoter elements within conserved non-coding element using Genomatix Gene2Promoter. TATA= O\$VTBP, TFIID =O\$TF2D.

As mentioned above, the TATA box is not a ubiquitous feature of core promoters, but tends to be prevalent in ‘sharp’ or ‘narrow’ promoters. Large-scale mapping studies have revealed that the TSS is usually not a single distinct genomic position; instead, a typical core promoter may consist of an array of closely located TSSs spread over 50–100 bp. Thus, ‘sharp’ or ‘narrow’ peak promoters are distinguished by a tight cluster of TSSs spanning only one or several bps, whereas ‘broad’, or ‘wide’ peak promoters the TSSs are distributed over a wide range, up to 100 bp²⁰³. Sharp promoters are typically involved in tissue-specific regulation of expression rather than ‘broad’ promoters which are common in constitutively expressed genes. Therefore, this TATA box located 34bp upstream of the TSS for the T2 DDAH-1 transcript, in a highly evolutionarily conserved non-coding region, supports the hypothesis that this region represents a promoter involved in the tissue-specific regulation of this transcript.

```

LOCUS      GXP_1817791(dimethylarginine dimethylaminohydrolase 1/human)      818 bp
DNA  DEFINITION      loc=GXL_77723|sym=dimethylarginine dimethylaminohydrolase 1|
geneid=23576|acc=GXP_1817791|taxid=9606|spec=Homo sapiens|
chr=1|ctg=NC_000001|str=(-)|start=86043733|end=86044550|

```

```

len=818|descr=DDAH1|comm=CompGen promoter ACCESSION GXP_1817791 BASE COUNT 207
a 173 c 220 g 218 t ORIGIN
    1 GACGGGGGGC GGGAGGGGGG AGGAGGGGTG CAGGGACAGT ACTGGTTGAA CTAGAGAGAG
   61 AATGGAGAGG AGGGTTCCTG GCTTCTGTTG TGGCGTCTTT TCTATTTGAC TTCATGTTTG
  121 TAAGTATTTT CAGATGGTGA ATCAGACACC AGACGTAACA ATATTTCCAT ATTTGGGTAT
  181 AGCAGTAGCC TCGTTTTTTA ACATTTTCTT GCCTCTGTTA TCCAACCACA AAGCATTCTT
  241 GACAGCTTCA AATGTTGTTA AATATAGATT TAACTTCTCT TCCCAGAGCA GGAAATTCTT
  301 TGGAAATCCT TGTTTTTTCAC GCAATCTGTC CATCATGATT TAAAATAAAA GCACAGTGGA
  361 TCATCCAACT GGCCGTATAT ACCTTAATTG GAGGTTGGGG ATGGGGGACG GCAGAGATCC
  421 AGTCTGCCGC ACTGCGTTCA AACACACGCC ATTCCAGAGA TTCCTTTAAA ATCACATTA
  481 AGTTTTTTTA ACAAGGGTGT GTGGGTTTTG TTCTGGACTT CAACTGGGGA ATCTTGAGGA
  541 TCAGTTTGCC CCAGAAGAGA AATTTAGAGA ACCTTACCCT CAGCTGCCCA TTTAAAGCAG
  601 GGGGTGTGTT GTGGGATGGG GGTGGGAAGC TGGAGCAACA GGGCCACCAG GTGTGGGACC
  661 GGGAGACACT AGAGTAACCT ATGTGCACAG CCTCTCCATA TACCATGTGC TGTTCGCCCT
  721 GCTAGTAATC GACGACATTA GGCAAGAGAA ACAGCGGCTC CTCGAATCCT GCCCAAGAC
  781 CGTCAGAAA CCCAGCCTC CGTGGCCTT CTCGCCGC

```

Figure 5.7: Sequence of putative promoter of DDAH-1 T2 transcript. Purple=TATA box. Green= coding sequence.

To further explore the hypothesis of endometrial/placental restricted expression of this T2 transcript, the putative promoter was interrogated for transcription factor binding sites that are upregulated in placental tissue in pre-eclampsia. Since pre-eclampsia is a condition characterized by placental vascular dysfunction, elevated placental ADMA and decreased placental DDAH activity, it was hypothesized that pre-eclampsia may be associated with a switch in transcription of full-length DDAH-1 to truncated, non-functional T2 DDAH-1 through the putative alternative promoter of T2.

The transcription factor profile of pre-eclampsia has been previously defined - Vaiman et al recently analysed data from publicly available microarray analyses of pre-eclamptic and normal placentae, to obtain a consensus list of modified genes²⁰⁴. Subsequently, they demonstrated 67 up-regulated and 31 down-regulated genes, and went on to find over-represented transcription factor binding sites in the promoters of these genes. This group found that the promoters of up-regulated genes are enriched in putative binding sites for NFkB, cAMP responsive element binding protein 1 (CREB), RAS-responsive element binding protein 1 (RREB1), and activator protein-2 (AP-2).

When these specific transcription factor sites were searched for in the putative DDAH-1 T2 promoter, several predicted binding sites for CREB and RREB1 are found within the region +/-100bp of the TSS, in the vicinity of the proposed TFIID binding site (figure 5.8).

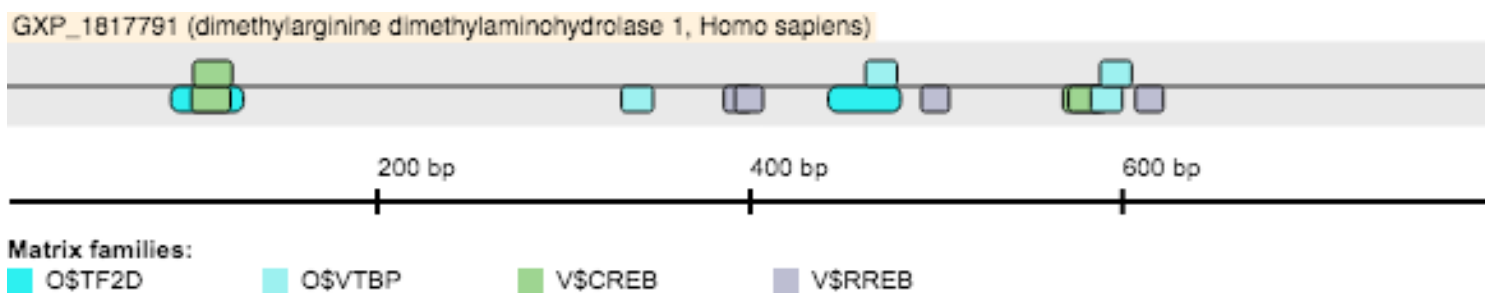


Figure 5.8 Identification of putative transcription factor binding sites within the conserved predicted promoter site of the DDAH-1 T2 transcript using Genomatix Gene2Promoter (accessed May 2016). TFIID=O\$TF2D, TATA=\$VTBP, CREB=V\$CREB, RREB1=V\$RREB.

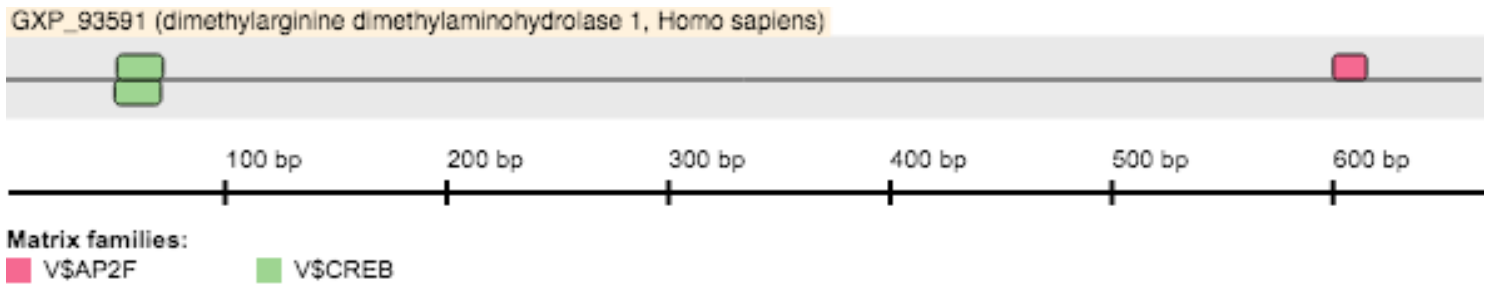


Figure 5.9 Identification of putative transcription factor binding sites within the promoter site of the DDAH-1 T1 transcript using Genomatix Gene2Promoter (accessed May 2016). CREB=V\$CREB, AP-2=V\$AP2F.

By contrast, in the DDAH-1 T1 transcript promoter, from the above list of transcription factor binding sites, there are no predicted binding sites for RREB and fewer predicted CREB binding sites (figure 5.9).

5.2.3 *In vitro* translation of the predicted protein of the alternate DDAH-1 transcript

To determine if the alternate, truncated DDAH-1 T2 transcript is protein-coding, a cell-free *in vitro* translation system was utilized to identify a protein product from the cDNA for this transcript. As such, both the T1 and T2 DDAH-1 RNA transcripts were generated from linearized vectors, using the protocol for *in vitro* transcription outlined in section S4.1. The DNA template was then removed by DNase digestion, and the RNA products from this reaction were run on an RNA gel, and subsequently used for *in vitro* translation.

The rabbit reticulocyte lysate cell-free expression system was used for *in vitro* translation. This system is prepared as a crude extract containing all the macromolecular components (70S or 80S ribosomes, tRNAs, aminoacyl-tRNA

synthetases, initiation, elongation and termination factors, etc.) required for translation of exogenous RNA. The initial *in vitro* translation reaction was performed with labeled [35S]methionine in the translation mix for subsequent protein product identification. Following the *in vitro* translation reaction, RNase digestion was performed and the reaction product was analysed by SDS-PAGE and autoradiography.

As seen in figure 5.9, the T1 transcript was, as expected, translated with high efficiency into a 33kDa protein product. Additionally, a further band of lesser intensity is seen at 27kDa as a product of the T2 transcript. This band is not seen in the minus-RNA control reaction.

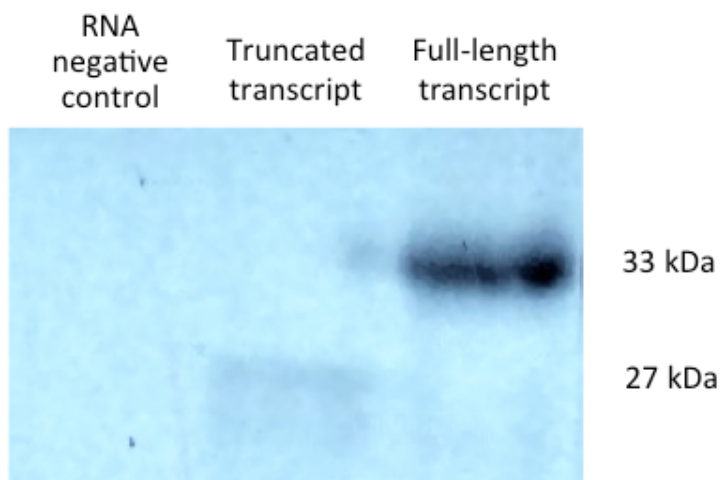


Figure 5.9: *In vitro* translation and autoradiography of full-length DDAH-1 protein (right lane 33kDa) and truncated DDAH-1 (centre lane 27kDa). No band is visible in the RNA-negative control lane (left lane).

5.3 Discussion

The results in this chapter demonstrate for the first time that a novel truncated DDAH-1 RNA transcript exists in human placental tissue from healthy mothers. Subsequent *in vitro* experiments demonstrate that this novel transcript is protein coding, and therefore may potentially be translated in human placenta. Moreover, bioinformatics analysis strongly suggests that this transcript has a TATA-containing promoter, with predicted binding sites for transcription factors that are upregulated in placenta from patients with pre-eclampsia (PE).

The predicted lack of exon 1 in transcript T2 is important, since the presence of exon 1 has been shown to be essential for hydrolase activity. The *Ddah1*^{+/-} heterozygote knockout mouse described by Leiper et al has a global reduction of DDAH activity by approximately half, although *Ddah1*^{-/-} homozygotes are not viable⁸⁸. Thus, although not tested here, it is likely that a truncated DDAH-1 protein lacking exon 1 would not have DDAH activity, yet may still have (patho)physiological relevance through protein-protein interactions as suggested in chapter 1.

Subsequent to the experiments presented in this thesis, the group of Sun et al have similarly demonstrated the presence of the T2 truncated DDAH-1 transcript in HUVEC cells, as well as peripheral blood mononuclear cells from healthy human subjects and patients with acute ischaemic stroke²⁰⁵. Although no experiments are performed in this paper to characterize the promoter of this transcript, or the protein-coding nature of this transcript, they do note that unlike the full-length (T1) transcript there is no correlation between T2 expression levels and DDAH activity in HUVEC cells, further suggesting that the T2 transcript has no DDAH activity.

As noted above, the initial hypothesis preceding the early experiments outlined in this chapter was that a switch to an alternative non-functional/no-coding transcript of DDAH-1 may be responsible for the discrepancy noted earlier in this thesis between DDAH-1 mRNA and protein expression. However, no hepatic expression of the T2 DDAH-1 transcript was noted in healthy or cirrhotic human liver tissue, or indeed in any healthy tissues from a broad panel of human cDNAs. Subsequently, an endometrial adenocarcinoma cell line, Ishikawa, was used to replicate the original curated observation of the T2 transcript submitted by the German Genome Project. This experiment replicated this original observation, and the T2 transcript was detected in Ishikawa cells at low levels, albeit that direct comparison of mRNA expression levels with other transcripts is not possible since the $\Delta\Delta\text{CT}$ method of mRNA quantification was used, and factors such as PCR efficiency may affect the relative cycle threshold with different taqman probes. To validate this observation, human placental tissue – which develops from the endometrial decidual layer – was obtained from healthy mothers with no evidence of PE. Similar levels of the DDAH-1 T2 transcript were found by qPCR in this tissue across all samples.

Although protein characterisation was not performed in these placental tissues, *in vitro* studies demonstrated that the T2 transcript is protein coding in a cell-free translation system. Although the level of expression determined by autoradiography following cell-free translation was low for this transcript, this does not necessarily reflect the translation efficiency of this transcript *in vivo*. Firstly, since radiolabelled methionine was used to detect the protein product, the shorter transcript would be expected to have lower intensity since it contains fewer methionine residues.

Secondly, mRNA generated by *in vitro* transcription from linearized plasmid DNA may lack necessary post-transcriptional modifications for efficient translation, such as a 5'-7 methyl-GTP cap and a 3' poly(A) tail. Both these modifications contribute to the stability of the mRNA by preventing degradation. Additionally, the 5' cap structure enhances the translation of mRNA by helping to bind the eukaryotic ribosome and assuring recognition of the proper AUG initiator codon. Further, the consensus sequence 5'-GCCACCAUGG-3', also known as the "Kozak" sequence, is considered to be the strongest ribosomal binding signal in eukaryotic mRNA. An mRNA that lacks the Kozak consensus sequence may not be translated efficiently in cell-free systems, particularly if secondary structures form in the 5'-UTR. Thus, any signal from the *in vitro* translation of the T2 transcript can be regarded as evidence that this transcript is protein coding, the relative expression of which is likely to depend on tissue and pathological state.

Thus, although the T2 transcript was translated into protein *in vitro*, there is as yet no evidence that this occurs *in vivo*. Nevertheless, it is not absolutely necessary for an alternate transcript to be protein-coding to have a regulatory role, as has been recently described for a non-coding transcript of the murine proteinase 3 gene. However, it is tempting to hypothesize that under certain conditions transcription of a truncated DDAH-1 protein lacking exon 1 occurs, with no hydrolase activity, but alternative functions through direct protein-protein interactions as mentioned above. This hypothesis deserves further attention, although protein characterization with antibodies able to distinguish T1 and T2 transcript proteins will be required.

The relevance of the T2 transcript in the pathogenesis of PE is suggested by

literature demonstrating altered placental DDAH activity amongst patients with PE. The process of placental vascular development is a key process during fetal development, and placental vascular dysfunction is implicated in several pathologies such as pregnancy induced hypertension (PIH) and PE. In a similar fashion to the intrahepatic circulation, NO is a key regulator of placental vascular tone, and is essential for the processes of implantation and trophoblast invasion.

Elevated systemic ADMA levels have been described in patients with PE, and two SNPs in the DDAH1 gene have been associated with elevated risk of PE. More recently, Anderssohn et al have described markedly decreased DDAH activity in placental tissue from patients with PE compared to healthy controls²⁰⁶. Importantly, these authors found no change in DDAH-1 mRNA, eNOS mRNA or PRMT1 mRNA. Although protein levels of DDAH-1 and DDAH-2 were not measured, the authors attributed the marked decrease in DDAH activity to a marginally significant decrease in DDAH-2 gene expression. However, since DDAH-2 has limited hydrolase activity, a far more likely explanation is a change in DDAH-1 activity. Since the authors used qPCR primers that would be unable to distinguish the T1 and T2 DDAH-1 transcripts, it is possible that the observed marked decrease in DDAH activity can be explained by a switch in transcription to the truncated T2 transcript.

This hypothesis is further supported by the bioinformatic analysis of the putative T2 promoter that demonstrates predicted binding sites for a series transcription factors that are overexpressed in placentae from patients with PE. Of course these predictions need experimental verification, ideally through luciferase reporter studies demonstrating promoter activity for this putative promoter sequence in Ishikawa

cells, and subsequent mutation of predicted transcription factor binding sites as 'loss-of-function' experiments. However, these experiments were unable to be performed during the course of this thesis, since a nationwide shortage of Ishikawa cells was declared by the major cell line suppliers which remains ongoing.

A further possibility is that DDAH-1 undergoes post-transcriptional regulation by miRNAs in PE. Other groups have demonstrated decreased DDAH-1 protein expression in PE, but DDAH-1 mRNA is unchanged in disease, suggesting post-transcriptional regulation of DDAH-1 in PE in a similar manner to cirrhosis. Although several placental miRNAs have been shown to be differentially expressed in PE compared to healthy controls, miR-128 has not been shown to be elevated in PE placenta.

Thus, the work presented in this chapter demonstrates for the first time a novel, truncated, protein-coding transcript of DDAH-1 in human placenta. This is likely to be non-functional, but may represent a tier of transcriptional regulation of DDAH-1 through an alternative promoter, which may be of pathophysiological relevance in pre-eclampsia or other conditions with elevated placental ADMA. This hypothesis deserves further attention, through quantification of this alternative transcript in tissues from patients with pre-eclampsia and healthy controls, and functional characterisation of the putative alternative promoter outlined above.

Chapter 6 – Discussion and Future Work

It is well recognized that portal hypertension is a grave step in the progression of cirrhosis, associated with the development of complications and a close predictor of mortality. Although the pathobiology of portal hypertension involves fibrosis as well as increased intrahepatic vascular tone, recent work has focussed on the role of infection and inflammation in portal hypertension and complications in cirrhosis⁷⁸.

Pro-inflammatory cytokines tumor necrosis factor (TNF)- α and interleukin (IL)-6 are elevated in cirrhosis, and are further elevated in cirrhotic patients with infection²⁰⁷. This dysregulated inflammatory response is associated with severity of portal hypertension and complications – serum bacterial DNA level, as a surrogate marker of bacterial translocation in cirrhosis, is correlated with systemic inflammation and portal hypertension²⁰⁸. Indeed, recently a panel of biomarkers for of pro-inflammatory cytokines was found to be highly predictive for the presence of portal hypertension and oesophageal varices in a prospective cohort²⁰⁹. A causal relationship between systemic inflammation and portal hypertension in ACLF is also inferred by studies in alcoholic hepatitis, demonstrating a rapid and sustained reduction in portal pressure with anti-TNF α therapy²¹⁰.

As outlined in chapter 1, initial clinical observations implicated the DDAH-ADMA pathway in the pathobiology of portal hypertension, particularly in states of systemic inflammation. Plasma ADMA levels were found to be elevated in cirrhosis with superimposed inflammation, and hepatic ADMA correlated with portal pressure⁷².

Experiments from our group leading up to this thesis had demonstrated that anti-TNF α therapy also produces a clinically significant reduction in portal pressure in cirrhotic rodents, associated with reduced NF κ B-mediated inflammation and increased hepatic DDAH-1 expression. Additionally, the DDAH-ADMA pathway has recently been implicated as the pathway for the therapeutic reduction in portal pressure seen with Farnesoid X receptor (FXR) agonists in cirrhotic rodents and humans²¹¹.

It is on this background that the aim of this thesis was to further characterise the role of DDAH-1 in a rodent model of portal hypertension, establishing a relationship between hepatic DDAH-1 protein expression and portal pressure. Although both anti-TNF α therapy and FXR agonists lead to an increase in hepatic DDAH-1 expression in cirrhosis, they are both associated with myriad 'off-target' effects, hence a selective DDAH-1 'gain-of-function' experiment was performed to assert a causal relationship between DDAH-1 expression and hepatic haemodynamic phenotype.

Thus in chapter 3, we validate the previous finding that hepatic DDAH-1 expression is decreased in cirrhosis, and proceed to demonstrate that hydrodynamic gene delivery of DDAH-1 in cirrhotic rodents leads to a significant increase in hepatic DDAH-1 expression and a clinically significant reduction in portal pressure with no adverse effect on systemic haemodynamics. A major limitation of the *in vivo* work presented in this thesis is the lack of *in vivo* ADMA measurements. This was due to technical problems with mass spectrometry in our laboratory during the course of the experiments presented in this thesis. Since ADMA is not a protein, but is a

methylated arginine residue, initial methods for the quantification of ADMA relied upon HPLC or MS to allow differentiation between the structurally similar isomers ADMA and SDMA. More recently, ELISA based methods for the measurement of ADMA have been developed, but have not been validated, and indeed antibody-based methods for the detection and discrimination of methylated arginine residues may be envisaged to be problematic. Thus, for these reasons ADMA measurements were not performed in the experiments presented here. However, *in vitro* work was carried out on primary endothelial cells to demonstrate that ADMA is an inhibitor of NO generation at pathophysiological levels, and several investigators have previously demonstrated that DDAH-1 is a major pathway of ADMA elimination *in vivo*.

In chapter 3 we also demonstrate for the first time that DDAH-1 is primarily located in hepatocyte cytoplasm within the liver. If the major effect of DDAH-1 on the hepatic vasculature is through metabolism of local ADMA, this implies a paracrine mechanism of action, since ADMA acts to competitively inhibit the action of eNOS located in the SEC. In chapter 4 we proceeded to show for the first time that hepatocyte DDAH-1 is sensitive to oxidative stress, with a H₂O₂ concentration-dependent decrease in DDAH-1 protein expression. Furthermore, the mechanism for this decrease in protein expression was found to be partially related to the DDAH-1 3'UTR.

Further studies in chapter 4 demonstrated the presence of predicted miRNA binding sites in the DDAH-1 3'UTR, and indeed miR-128 was found to be elevated in

cirrhotic rat liver compared with sham controls, as well as being found to be an active regulator of DDAH-1 protein expression through both gain-of-function and loss-of-function experiments.

As discussed in chapter 4, it is unclear whether the H₂O₂ mediated changes in DDAH-1 expression are due to alterations in miRNA expression, or through alternate mechanisms relating to the DDAH-1 3'UTR. Nevertheless, the finding of post-transcriptional regulation of hepatic DDAH-1 through miRNAs raises the possibility of therapeutic targeting of miRNAs for portal hypertension in ACLF.

As noted in chapter 2, currently there is no licensed therapy for portal hypertension. Non-licensed therapy includes non-selective beta-blockers used in stable portal hypertension, and the vasopressin analogue terlipressin for acute variceal bleeding. However, both these agents compromise liver blood flow and an 'ideal' agent for treatment of portal hypertension would aim to lower intra-hepatic resistance without compromising liver blood flow. From the results presented in chapter 3, an agent to selectively increase hepatic DDAH-1 in ACLF would be predicted to decrease intrahepatic ADMA, thus decreasing intrahepatic resistance and lowering portal pressure without any deleterious effect on liver blood flow or systemic haemodynamics. Since no specific agonist for DDAH-1 currently exists, modulation of hepatic DDAH-1 expression in ACLF through miRNA targeting is a possible avenue for translation. FXR agonists have been shown to upregulate hepatic DDAH-1 expression, through an FXR responsive element in DDAH-1 exon 1,¹³⁴ and also been shown to reduce portal pressure in cirrhotic rodents^{211, 212}. However, FXR

signalling has pleotropic effects, and translation of these agents may be limited by concerns surrounding pruritus, dyslipidemia and cholangiocyte proliferation. Therefore, selective targetting of DDAH-1 remains an attractive therapeutic route.

Antisense oligonucleotides, such as locked nucleic acids (LNAs), have been shown to successfully target miRNAs in the context of liver disease, and have been shown to be safe and well tolerated in man²¹³. As shown in chapter 3, viral-mediated gene therapy is challenging in cirrhosis, but oligonucleotide based therapies are likely to be more successful at delivery, since they are much smaller than viral particles hence able to access hepatocytes in cirrhotic liver. Moreover, modified oligonucleotides such as LNAs are resistant to nuclease digestion, and have been shown to be safe and efficacious in the knockdown of hepatic miRNAs in humans with intermittent parenteral administration. The next steps to build on the work discussed in this thesis would be to use LNAs to target miR-128 in a rodent model of cirrhosis, to demonstrate changes in hepatic DDAH-1 expression and portal haemodynamics, as well gene expression arrays to screen for off-target effects that may limit broader translational use.

The final observation noted in the experiments detailed in this thesis was the first characterisation of a novel, truncated transcript of DDAH-1 in human placenta. As discussed in chapter 5, transcription of alternate transcripts through alternative promoters is a recognized aspect of genomic complexity and regulation. Although this alternate transcript was not found in healthy or diseased human liver, it was found in human placenta, and can be hypothesized to play a role in the pathobiology

of pre-eclampsia. Further study is required to experimentally characterise the putative promoter for this transcript found through *in silico* analysis – these experiments were not carried out during the course of this thesis due to a limitation on the availability of Ishikawa cells which were used for the early experiments detecting this novel transcript. Nevertheless, a switch to transcription of this truncated, protein-coding transcript under certain pathological conditions may play a role in the development pre-eclampsia, and studies of placental specimens from well-characterised patients and healthy controls should be undertaken to explore this hypothesis.

During the course of the experiments presented in this thesis, the result so of a large international collaborative effort to determine the functional importance of non-coding DNA was published (the ENCyclopedia Of DNA Elements – ENCODE). This landmark project aimed to annotate the entire genomic sequence for functional non-coding elements. The background to this project was the disappointingly low ‘hit rate’ from genome-wide association studies (GWAS) for biological targets in disease cohorts. The human genome project had ushered in the concept of ‘personalized medicine’ whereby genomic sequence would highlight propensity to disease as well as candidate proteins as therapeutic targets. However, from the over 1500 GWAS studies in the NIH GWAS catalogue, it is apparent that the vast majority (88%) of disease associated SNPs are not related to coding regions – 45% are intronic and 43% are intergenic²¹⁴. The implication is that variance in the *regulatory* elements of the genome carry a large burden of the risk of complex diseases. The ENCODE project aimed to characterise these regulatory elements, and in the flagship paper in September 2012, as well as 30 other simultaneously published research papers,

ENCODE demonstrated with a variety of methodologies that 80% of non-coding 'junk' DNA contains elements with biochemical function²¹⁵. In particular, these areas of non-coding DNA contain gene enhancers, alternative promoters and regions that encode non-coding RNA transcripts.

Included in the wealth of data from ENCODE is the recognition of biochemical signatures characterising promoters as well as alternate RNA transcripts. Examples include promoter regions that are rich in predictable binding sites for DNA binding proteins, which can be experimentally verified by site-specific occupancy assays such as ChIP^{216, 217}. Promoter regions also have alterations in chromatin structure giving rise to nuclease hypersensitivity of the underlying DNA²¹⁸. Other characteristics of functional elements are histone modifications suggesting transcription factor occupancy of adjacent DNA, and DNA methylation as an epigenetic modulator of gene expression^{216, 219}. All of these biochemical signatures were experimentally assayed in the ENCODE project. Overall, 636,336 binding regions covering 231 megabases (8.1% of the genome) were enriched for regions bound by DNA-binding proteins across all cell types. Additionally, ENCODE demonstrated with ultra-deep RNA sequencing that about 75% of the genome is transcribed to RNA at some point in certain cell types²²⁰. Therefore, the majority of RNA in a cell is never translated to protein, but may play important regulatory functions. Moreover, the expression of RNA transcripts from genes is not uniform – most genes express more than one isoform of a transcript, with an average of 10-12 expressed isoforms per gene per cell line. Thus, in concert with the results of this thesis delineated above, these findings highlight that transcription is a lot widespread than previously thought, with large numbers of non-coding RNA molecules

with potential regulatory roles.

The immediate implications are that genome-wide approaches to determining disease risk and finding targets for therapy require re-evaluation in this light. ENCODE demonstrates that non-coding regions must be considered when interpreting GWAS findings, and provides a strong basis for reinterpreting previous GWAS results. Furthermore, as mentioned above, the results of ENCODE suggest that exome-sequencing studies focusing on protein-coding sequences risk missing crucial parts of the genome and the ability to identify true causal variants.

The implication for liver diseases is the prospect of transcriptional modulation as a therapeutic strategy. Knowledge of regulatory elements will point us toward new therapeutic approaches and expand the 'druggable genome'. Although the prospect of characterization and validation of this new tier of genomic control is daunting, novel technologies of gene editing such as zinc-finger and TAL effector-like nucleases are now scalable, and thus functional elements can be validated on a large scale. The manipulation of DDAH-1 through anti-miRNA strategies or targeting of an alternate placental RNA transcript are just examples of this application of molecular therapeutics. Thus, the paradigm shift in genomic data provided by ENCODE, along with improved chemistry for the delivery of nucleic acid based therapies to the liver, has provided the opportunity for novel genome and epigenome targeted therapies. As William Ford Gibson famously said, "the future already exists, it's just not very evenly distributed".

7.0 References:

1. Ripoll C, Groszmann R, Garcia-Tsao G, et al. Hepatic venous pressure gradient predicts clinical decompensation in patients with compensated cirrhosis. *Gastroenterology* 2007;133:481-8.
2. Statistics OfN. Health service quarterly. Winter 2008. 2009;40:59-60.
3. D'Amico G, Garcia-Tsao G, Pagliaro L. Natural history and prognostic indicators of survival in cirrhosis: a systematic review of 118 studies. *J Hepatol* 2006;44:217-31.
4. Groszmann RJ, Garcia-Tsao G, Bosch J, et al. Beta-blockers to prevent gastroesophageal varices in patients with cirrhosis. *N Engl J Med* 2005;353:2254-61.
5. Fede G, D'Amico G, Arvaniti V, et al. Renal failure and cirrhosis: a systematic review of mortality and prognosis. *J Hepatol* 2012;56:810-8.
6. Arnold WP, Mittal CK, Katsuki S, et al. Nitric oxide activates guanylate cyclase and increases guanosine 3':5'-cyclic monophosphate levels in various tissue preparations. *Proc Natl Acad Sci U S A* 1977;74:3203-7.
7. Furchgott RF, Zawadzki JV. The obligatory role of endothelial cells in the relaxation of arterial smooth muscle by acetylcholine. *Nature* 1980;288:373-6.
8. Ignarro LJ, Buga GM, Wood KS, et al. Endothelium-derived relaxing factor produced and released from artery and vein is nitric oxide. *Proc Natl Acad Sci U S A* 1987;84:9265-9.
9. Mittal MK, Gupta TK, Lee FY, et al. Nitric oxide modulates hepatic vascular tone in normal rat liver. *Am J Physiol* 1994;267:G416-22.
10. Rockey DC, Chung JJ. Reduced nitric oxide production by endothelial cells in cirrhotic rat liver: endothelial dysfunction in portal hypertension. *Gastroenterology* 1998;114:344-51.
11. Schuman EM, Madison DV. A requirement for the intercellular messenger nitric oxide in long-term potentiation. *Science* 1991;254:1503-6.
12. Khan BV, Harrison DG, Olbrych MT, et al. Nitric oxide regulates vascular cell adhesion molecule 1 gene expression and redox-sensitive transcriptional events in human vascular endothelial cells. *Proc Natl Acad Sci U S A* 1996;93:9114-9.
13. Pantopoulos K, Hentze MW. Nitric oxide signaling to iron-regulatory protein: direct control of ferritin mRNA translation and transferrin receptor mRNA stability in transfected fibroblasts. *Proc Natl Acad Sci U S A* 1995;92:1267-71.
14. Liu XB, Hill P, Haile DJ. Role of the ferroportin iron-responsive element in iron and nitric oxide dependent gene regulation. *Blood Cells Mol Dis* 2002;29:315-26.
15. Brune B, Dimmeler S, Molina y Vedia L, et al. Nitric oxide: a signal for ADP-ribosylation of proteins. *Life Sci* 1994;54:61-70.
16. Forstermann U, Sessa WC. Nitric oxide synthases: regulation and function. *Eur Heart J*.
17. Togashi H, Sakuma I, Yoshioka M, et al. A central nervous system action of nitric oxide in blood pressure regulation. *J Pharmacol Exp Ther* 1992;262:343-7.
18. Rajfer J, Aronson WJ, Bush PA, et al. Nitric oxide as a mediator of relaxation of the corpus cavernosum in response to nonadrenergic, noncholinergic neurotransmission. *N Engl J Med* 1992;326:90-4.
19. Forstermann U, Closs EI, Pollock JS, et al. Nitric oxide synthase isozymes. Characterization, purification, molecular cloning, and functions. *Hypertension* 1994;23:1121-31.
20. Nathan CF, Hibbs JB, Jr. Role of nitric oxide synthesis in macrophage antimicrobial activity. *Curr Opin Immunol* 1991;3:65-70.
21. Wink DA, Kasprzak KS, Maragos CM, et al. DNA deaminating ability and genotoxicity of nitric oxide and its progenitors. *Science* 1991;254:1001-3.
22. McNaughton L, Puttagunta L, Martinez-Cuesta MA, et al. Distribution of nitric oxide synthase in normal and cirrhotic human liver. *Proc Natl Acad Sci U S A* 2002;99:17161-6.

23. Rafikov R, Fonseca FV, Kumar S, et al. eNOS activation and NO function: structural motifs responsible for the posttranslational control of endothelial nitric oxide synthase activity. *J Endocrinol*;210:271-84.
24. Sessa WC, Barber CM, Lynch KR. Mutation of N-myristoylation site converts endothelial cell nitric oxide synthase from a membrane to a cytosolic protein. *Circ Res* 1993;72:921-4.
25. Liu J, Garcia-Cardena G, Sessa WC. Biosynthesis and palmitoylation of endothelial nitric oxide synthase: mutagenesis of palmitoylation sites, cysteines-15 and/or -26, argues against depalmitoylation-induced translocation of the enzyme. *Biochemistry* 1995;34:12333-40.
26. Drab M, Verkade P, Elger M, et al. Loss of caveolae, vascular dysfunction, and pulmonary defects in caveolin-1 gene-disrupted mice. *Science* 2001;293:2449-52.
27. Fulton D, Gratton JP, McCabe TJ, et al. Regulation of endothelium-derived nitric oxide production by the protein kinase Akt. *Nature* 1999;399:597-601.
28. Dimmeler S, Fleming I, Fisslthaler B, et al. Activation of nitric oxide synthase in endothelial cells by Akt-dependent phosphorylation. *Nature* 1999;399:601-5.
29. Ackah E, Yu J, Zoellner S, et al. Akt1/protein kinase B α is critical for ischemic and VEGF-mediated angiogenesis. *J Clin Invest* 2005;115:2119-27.
30. Iwakiri Y, Satoh A, Chatterjee S, et al. Nitric oxide synthase generates nitric oxide locally to regulate compartmentalized protein S-nitrosylation and protein trafficking. *Proc Natl Acad Sci U S A* 2006;103:19777-82.
31. Braet F, Wisse E. Structural and functional aspects of liver sinusoidal endothelial cell fenestrae: a review. *Comp Hepatol* 2002;1:1.
32. Limmer A, Ohl J, Kurts C, et al. Efficient presentation of exogenous antigen by liver endothelial cells to CD8⁺ T cells results in antigen-specific T-cell tolerance. *Nat Med* 2000;6:1348-54.
33. Mori T, Okanoue T, Sawa Y, et al. Defenestration of the sinusoidal endothelial cell in a rat model of cirrhosis. *Hepatology* 1993;17:891-7.
34. Shah V, Haddad FG, Garcia-Cardena G, et al. Liver sinusoidal endothelial cells are responsible for nitric oxide modulation of resistance in the hepatic sinusoids. *J Clin Invest* 1997;100:2923-30.
35. Mookerjee RP, Wiesenthal A, Icking A, et al. Increased gene and protein expression of the novel eNOS regulatory protein NOSTRIN and a variant in alcoholic hepatitis. *Gastroenterology* 2007;132:2533-41.
36. Goh BJ, Tan BT, Hon WM, et al. Nitric oxide synthase and heme oxygenase expressions in human liver cirrhosis. *World J Gastroenterol* 2006;12:588-94.
37. Sarela AI, Mihaimeed FM, Batten JJ, et al. Hepatic and splanchnic nitric oxide activity in patients with cirrhosis. *Gut* 1999;44:749-53.
38. Iwakiri Y, Grisham M, Shah V. Vascular biology and pathobiology of the liver: Report of a single-topic symposium. *Hepatology* 2008;47:1754-63.
39. Rockey DC, Weisiger RA. Endothelin induced contractility of stellate cells from normal and cirrhotic rat liver: implications for regulation of portal pressure and resistance. *Hepatology* 1996;24:233-40.
40. Fiorucci S, Antonelli E, Mencarelli A, et al. The third gas: H₂S regulates perfusion pressure in both the isolated and perfused normal rat liver and in cirrhosis. *Hepatology* 2005;42:539-48.
41. Bataller R, Gines P, Nicolas JM, et al. Angiotensin II induces contraction and proliferation of human hepatic stellate cells. *Gastroenterology* 2000;118:1149-56.
42. Graupera M, March S, Engel P, et al. Sinusoidal endothelial COX-1-derived prostanoids modulate the hepatic vascular tone of cirrhotic rat livers. *Am J Physiol Gastrointest Liver Physiol* 2005;288:G763-70.
43. Taura K, De Minicis S, Seki E, et al. Hepatic stellate cells secrete angiotensin 1 that induces angiogenesis in liver fibrosis. *Gastroenterology* 2008;135:1729-38.

44. Fernandez M, Mejias M, Garcia-Pras E, et al. Reversal of portal hypertension and hyperdynamic splanchnic circulation by combined vascular endothelial growth factor and platelet-derived growth factor blockade in rats. *Hepatology* 2007;46:1208-17.
45. Harbrecht BG, Billiar TR, Stadler J, et al. Inhibition of nitric oxide synthesis during endotoxemia promotes intrahepatic thrombosis and an oxygen radical-mediated hepatic injury. *J Leukoc Biol* 1992;52:390-4.
46. Harbrecht BG, Wu B, Watkins SC, et al. Inhibition of nitric oxide synthase during hemorrhagic shock increases hepatic injury. *Shock* 1995;4:332-7.
47. Saetre T, Gundersen Y, Thiemermann C, et al. Aminoethyl-isothiourrea, a selective inhibitor of inducible nitric oxide synthase activity, improves liver circulation and oxygen metabolism in a porcine model of endotoxemia. *Shock* 1998;9:109-15.
48. Thiemermann C, Ruetten H, Wu CC, et al. The multiple organ dysfunction syndrome caused by endotoxin in the rat: attenuation of liver dysfunction by inhibitors of nitric oxide synthase. *Br J Pharmacol* 1995;116:2845-51.
49. Van de Casteele M, Omasta A, Janssens S, et al. In vivo gene transfer of endothelial nitric oxide synthase decreases portal pressure in anaesthetised carbon tetrachloride cirrhotic rats. *Gut* 2002;51:440-5.
50. Yu Q, Shao R, Qian HS, et al. Gene transfer of the neuronal NO synthase isoform to cirrhotic rat liver ameliorates portal hypertension. *J Clin Invest* 2000;105:741-8.
51. Abraldes JG, Rodriguez-Vilarrupla A, Graupera M, et al. Simvastatin treatment improves liver sinusoidal endothelial dysfunction in CCl4 cirrhotic rats. *J Hepatol* 2007;46:1040-6.
52. Abraldes JG, Albillos A, Banares R, et al. Simvastatin lowers portal pressure in patients with cirrhosis and portal hypertension: a randomized controlled trial. *Gastroenterology* 2009;136:1651-8.
53. Vallance P, Moncada S. Hyperdynamic circulation in cirrhosis: a role for nitric oxide? *Lancet* 1991;337:776-8.
54. Jalan R, Olde Damink SW, Ter Steege JC, et al. Acute endotoxemia following transjugular intrahepatic stent-shunt insertion is associated with systemic and cerebral vasodilatation with increased whole body nitric oxide production in critically ill cirrhotic patients. *J Hepatol*;54:265-71.
55. Iwakiri Y, Cadelina G, Sessa WC, et al. Mice with targeted deletion of eNOS develop hyperdynamic circulation associated with portal hypertension. *Am J Physiol Gastrointest Liver Physiol* 2002;283:G1074-81.
56. Theodorakis NG, Wang YN, Skill NJ, et al. The role of nitric oxide synthase isoforms in extrahepatic portal hypertension: studies in gene-knockout mice. *Gastroenterology* 2003;124:1500-8.
57. Moreau R, Barriere E, Tazi KA, et al. Terlipressin inhibits in vivo aortic iNOS expression induced by lipopolysaccharide in rats with biliary cirrhosis. *Hepatology* 2002;36:1070-8.
58. Kajita M, Murata T, Horiguchi K, et al. iNOS expression in vascular resident macrophages contributes to circulatory dysfunction of splanchnic vascular smooth muscle contractions in portal hypertensive rats. *Am J Physiol Heart Circ Physiol* 2011;300:H1021-31.
59. Jalan R, Gines P, Olson JC, et al. Acute-on chronic liver failure. *J Hepatol* 2013;57:1336-48.
60. Moreau R, Jalan R, Gines P, et al. Acute-on-chronic liver failure is a distinct syndrome that develops in patients with acute decompensation of cirrhosis. *Gastroenterology* 2013;144:1426-37, 1437 e1-9.
61. Rincon D, Lo Iacono O, Ripoll C, et al. Prognostic value of hepatic venous pressure gradient for in-hospital mortality of patients with severe acute alcoholic hepatitis. *Aliment Pharmacol Ther* 2007;25:841-8.
62. Mookerjee RP, Lackner C, Stauber R, et al. The role of liver biopsy in the diagnosis and prognosis of patients with acute deterioration of alcoholic cirrhosis. *J Hepatol* 2011;55:1103-11.

63. Schwabe RF, Seki E, Brenner DA. Toll-like receptor signaling in the liver. *Gastroenterology* 2006;130:1886-900.
64. Zhu Q, Zou L, Jagavelu K, et al. Intestinal decontamination inhibits TLR4 dependent fibronectin-mediated cross-talk between stellate cells and endothelial cells in liver fibrosis in mice. *J Hepatol* 2012;56:893-9.
65. Seki E, De Minicis S, Osterreicher CH, et al. TLR4 enhances TGF-beta signaling and hepatic fibrosis. *Nat Med* 2007;13:1324-32.
66. Jagavelu K, Routray C, Shergill U, et al. Endothelial cell toll-like receptor 4 regulates fibrosis-associated angiogenesis in the liver. *Hepatology* 2010;52:590-601.
67. Mandrekar P, Szabo G. Signalling pathways in alcohol-induced liver inflammation. *J Hepatol* 2009;50:1258-66.
68. Wheeler MD, Kono H, Yin M, et al. The role of Kupffer cell oxidant production in early ethanol-induced liver disease. *Free Radic Biol Med* 2001;31:1544-9.
69. Steib CJ, Hartmann AC, v Hesler C, et al. Intraperitoneal LPS amplifies portal hypertension in rat liver fibrosis. *Lab Invest* 2010;90:1024-32.
70. Steib CJ, Bilzer M, op den Winkel M, et al. Treatment with the leukotriene inhibitor montelukast for 10 days attenuates portal hypertension in rat liver cirrhosis. *Hepatology* 2010;51:2086-96.
71. Waidmann O, Brunner F, Herrmann E, et al. Macrophage activation is a prognostic parameter for variceal bleeding and overall survival in patients with liver cirrhosis. *J Hepatol* 2013;58:956-61.
72. Mookerjee RP, Malaki M, Davies NA, et al. Increasing dimethylarginine levels are associated with adverse clinical outcome in severe alcoholic hepatitis. *Hepatology* 2007;45:62-71.
73. Shah V, Toruner M, Haddad F, et al. Impaired endothelial nitric oxide synthase activity associated with enhanced caveolin binding in experimental cirrhosis in the rat. *Gastroenterology* 1999;117:1222-8.
74. Matei V, Rodriguez-Vilarrupla A, Deulofeu R, et al. The eNOS cofactor tetrahydrobiopterin improves endothelial dysfunction in livers of rats with CCl4 cirrhosis. *Hepatology* 2006;44:44-52.
75. Gracia-Sancho J, Lavina B, Rodriguez-Vilarrupla A, et al. Increased oxidative stress in cirrhotic rat livers: A potential mechanism contributing to reduced nitric oxide bioavailability. *Hepatology* 2008;47:1248-56.
76. Lavina B, Gracia-Sancho J, Rodriguez-Vilarrupla A, et al. Superoxide dismutase gene transfer reduces portal pressure in CCl4 cirrhotic rats with portal hypertension. *Gut* 2009;58:118-25.
77. Karaa A, Kamoun WS, Clemens MG. Oxidative stress disrupts nitric oxide synthase activation in liver endothelial cells. *Free Radic Biol Med* 2005;39:1320-31.
78. Mehta G, Gustot T, Mookerjee RP, et al. Inflammation and portal hypertension - the undiscovered country. *J Hepatol* 2014;61:155-63.
79. Gary JD, Clarke S. RNA and protein interactions modulated by protein arginine methylation. *Prog Nucleic Acid Res Mol Biol* 1998;61:65-131.
80. Clarke S. Protein methylation. *Curr Opin Cell Biol* 1993;5:977-83.
81. Miyake M, Kakimoto Y. Synthesis and degradation of methylated proteins of mouse organs: correlation with protein synthesis and degradation. *Metabolism* 1976;25:885-96.
82. Tsikas D, Boger RH, Sandmann J, et al. Endogenous nitric oxide synthase inhibitors are responsible for the L-arginine paradox. *FEBS Lett* 2000;478:1-3.
83. Shin S, Mohan S, Fung HL. Intracellular L-arginine concentration does not determine NO production in endothelial cells: Implications on the "L-arginine paradox". *Biochem Biophys Res Commun*;414:660-3.
84. Pope AJ, Karrupiah K, Kearns PN, et al. Role of dimethylarginine dimethylaminohydrolases in the regulation of endothelial nitric oxide production. *J Biol Chem* 2009;284:35338-47.

85. Ogawa T, Kimoto M, Sasaoka K. Dimethylarginine:pyruvate aminotransferase in rats. Purification, properties, and identity with alanine:glyoxylate aminotransferase 2. *J Biol Chem* 1990;265:20938-45.
86. Ogawa T, Kimoto M, Sasaoka K. Purification and properties of a new enzyme, NG,NG-dimethylarginine dimethylaminohydrolase, from rat kidney. *J Biol Chem* 1989;264:10205-9.
87. Leiper JM, Santa Maria J, Chubb A, et al. Identification of two human dimethylarginine dimethylaminohydrolases with distinct tissue distributions and homology with microbial arginine deiminases. *Biochem J* 1999;343 Pt 1:209-14.
88. Leiper J, Nandi M, Torondel B, et al. Disruption of methylarginine metabolism impairs vascular homeostasis. *Nat Med* 2007;13:198-203.
89. Pawlak MR, Scherer CA, Chen J, et al. Arginine N-methyltransferase 1 is required for early postimplantation mouse development, but cells deficient in the enzyme are viable. *Mol Cell Biol* 2000;20:4859-69.
90. Krause CD, Yang ZH, Kim YS, et al. Protein arginine methyltransferases: evolution and assessment of their pharmacological and therapeutic potential. *Pharmacol Ther* 2007;113:50-87.
91. Nijveldt RJ, Teerlink T, Siroen MP, et al. The liver is an important organ in the metabolism of asymmetrical dimethylarginine (ADMA). *Clin Nutr* 2003;22:17-22.
92. Stuhlinger MC, Tsao PS, Her JH, et al. Homocysteine impairs the nitric oxide synthase pathway: role of asymmetric dimethylarginine. *Circulation* 2001;104:2569-75.
93. Tokuo H, Yunoue S, Feng L, et al. Phosphorylation of neurofibromin by cAMP-dependent protein kinase is regulated via a cellular association of N(G),N(G)-dimethylarginine dimethylaminohydrolase. *FEBS Lett* 2001;494:48-53.
94. Zhang P, Hu X, Xu X, et al. Dimethylarginine dimethylaminohydrolase 1 modulates endothelial cell growth through nitric oxide and Akt. *Arterioscler Thromb Vasc Biol* 2011;31:890-7.
95. Boulton JK, Walker-Samuel S, Jamin Y, et al. Active site mutant dimethylarginine dimethylaminohydrolase 1 expression confers an intermediate tumour phenotype in C6 gliomas. *J Pathol* 2011;225:344-52.
96. Tran CT, Fox MF, Vallance P, et al. Chromosomal localization, gene structure, and expression pattern of DDAH1: comparison with DDAH2 and implications for evolutionary origins. *Genomics* 2000;68:101-5.
97. O'Dwyer MJ, Dempsey F, Crowley V, et al. Septic shock is correlated with asymmetrical dimethyl arginine levels, which may be influenced by a polymorphism in the dimethylarginine dimethylaminohydrolase II gene: a prospective observational study. *Crit Care* 2006;10:R139.
98. Lambden S, Kelly P, Ahmetaj-Shala B, et al. Dimethylarginine dimethylaminohydrolase 2 regulates nitric oxide synthesis and hemodynamics and determines outcome in polymicrobial sepsis. *Arterioscler Thromb Vasc Biol* 2015;35:1382-92.
99. Caplin B, Leiper J. Endogenous nitric oxide synthase inhibitors in the biology of disease: markers, mediators, and regulators? *Arterioscler Thromb Vasc Biol* 2012;32:1343-53.
100. Livak KJ, Schmittgen TD. Analysis of relative gene expression data using real-time quantitative PCR and the 2(-Delta Delta C(T)) Method. *Methods* 2001;25:402-8.
101. Laemmli UK. Cleavage of structural proteins during the assembly of the head of bacteriophage T4. *Nature* 1970;227:680-5.
102. Lluch P, Torondel B, Medina P, et al. Plasma concentrations of nitric oxide and asymmetric dimethylarginine in human alcoholic cirrhosis. *J Hepatol* 2004;41:55-9.
103. Nijveldt RJ, Teerlink T, Siroen MP, et al. Elevation of asymmetric dimethylarginine (ADMA) in patients developing hepatic failure after major hepatectomy. *JPEN J Parenter Enteral Nutr* 2004;28:382-7.

104. Mookerjee RP, Dalton RN, Davies NA, et al. Inflammation is an important determinant of levels of the endogenous nitric oxide synthase inhibitor asymmetric dimethylarginine (ADMA) in acute liver failure. *Liver Transpl* 2007;13:400-5.
105. Siroen MP, van der Sijp JR, Teerlink T, et al. The human liver clears both asymmetric and symmetric dimethylarginine. *Hepatology* 2005;41:559-65.
106. Hu X, Xu X, Zhu G, et al. Vascular endothelial-specific dimethylarginine dimethylaminohydrolase-1-deficient mice reveal that vascular endothelium plays an important role in removing asymmetric dimethylarginine. *Circulation* 2009;120:2222-9.
107. Arrigoni FI, Vallance P, Haworth SG, et al. Metabolism of asymmetric dimethylarginines is regulated in the lung developmentally and with pulmonary hypertension induced by hypobaric hypoxia. *Circulation* 2003;107:1195-201.
108. Onozato ML, Tojo A, Leiper J, et al. Expression of NG,NG-dimethylarginine dimethylaminohydrolase and protein arginine N-methyltransferase isoforms in diabetic rat kidney: effects of angiotensin II receptor blockers. *Diabetes* 2008;57:172-80.
109. Dayoub H, Achan V, Adimoolam S, et al. Dimethylarginine dimethylaminohydrolase regulates nitric oxide synthesis: genetic and physiological evidence. *Circulation* 2003;108:3042-7.
110. Proctor E, Chatamra K. High yield micronodular cirrhosis in the rat. *Gastroenterology* 1982;83:1183-90.
111. Hernandez-Munoz R, Diaz-Munoz M, Suarez-Cuenca JA, et al. Adenosine reverses a preestablished CCl4-induced micronodular cirrhosis through enhancing collagenolytic activity and stimulating hepatocyte cell proliferation in rats. *Hepatology* 2001;34:677-87.
112. Sieber CC, Lopez-Talavera JC, Groszmann RJ. Role of nitric oxide in the in vitro splanchnic vascular hyporeactivity in ascitic cirrhotic rats. *Gastroenterology* 1993;104:1750-4.
113. Vorobioff J, Bredfeldt JE, Groszmann RJ. Increased blood flow through the portal system in cirrhotic rats. *Gastroenterology* 1984;87:1120-6.
114. Lee SS, Girod C, Braillon A, et al. Hemodynamic characterization of chronic bile duct-ligated rats: effect of pentobarbital sodium. *Am J Physiol* 1986;251:G176-80.
115. Kountouras J, Billing BH, Scheuer PJ. Prolonged bile duct obstruction: a new experimental model for cirrhosis in the rat. *Br J Exp Pathol* 1984;65:305-11.
116. Franco D, Gigou M, Szekely AM, et al. Portal hypertension after bile duct obstruction: effect of bile diversion on portal pressure in the rat. *Arch Surg* 1979;114:1064-7.
117. Heller J, Shiozawa T, Trebicka J, et al. Acute haemodynamic effects of losartan in anaesthetized cirrhotic rats. *Eur J Clin Invest* 2003;33:1006-12.
118. Sikuler E, Buchs AE, Yaari A, et al. Hemodynamic characterization of conscious and ketamine-anesthetized bile duct-ligated rats. *Am J Physiol* 1991;260:G161-6.
119. Wright G, Davies NA, Shawcross DL, et al. Endotoxemia produces coma and brain swelling in bile duct ligated rats. *Hepatology* 2007;45:1517-26.
120. Fallon MB, Abrams GA, McGrath JW, et al. Common bile duct ligation in the rat: a model of intrapulmonary vasodilatation and hepatopulmonary syndrome. *Am J Physiol* 1997;272:G779-84.
121. Hendrickson H, Chatterjee S, Cao S, et al. Influence of caveolin on constitutively activated recombinant eNOS: insights into eNOS dysfunction in BDL rat liver. *Am J Physiol Gastrointest Liver Physiol* 2003;285:G652-60.
122. Christ M, Louis B, Stoeckel F, et al. Modulation of the inflammatory properties and hepatotoxicity of recombinant adenovirus vectors by the viral E4 gene products. *Hum Gene Ther* 2000;11:415-27.
123. Asokan A, Schaffer DV, Samulski RJ. The AAV vector toolkit: poised at the clinical crossroads. *Mol Ther* 2012;20:699-708.
124. Xiao W, Chirmule N, Berta SC, et al. Gene therapy vectors based on adeno-associated virus type 1. *J Virol* 1999;73:3994-4003.

125. Brown BD, Venneri MA, Zingale A, et al. Endogenous microRNA regulation suppresses transgene expression in hematopoietic lineages and enables stable gene transfer. *Nat Med* 2006;12:585-91.
126. Nathwani AC, Gray JT, Ng CY, et al. Self-complementary adeno-associated virus vectors containing a novel liver-specific human factor IX expression cassette enable highly efficient transduction of murine and nonhuman primate liver. *Blood* 2006;107:2653-61.
127. Hirata RK, Russell DW. Design and packaging of adeno-associated virus gene targeting vectors. *J Virol* 2000;74:4612-20.
128. McCarty DM, Monahan PE, Samulski RJ. Self-complementary recombinant adeno-associated virus (scAAV) vectors promote efficient transduction independently of DNA synthesis. *Gene Ther* 2001;8:1248-54.
129. Duan D, Sharma P, Yang J, et al. Circular intermediates of recombinant adeno-associated virus have defined structural characteristics responsible for long-term episomal persistence in muscle tissue. *J Virol* 1998;72:8568-77.
130. Nakai H, Yant SR, Storm TA, et al. Extrachromosomal recombinant adeno-associated virus vector genomes are primarily responsible for stable liver transduction in vivo. *J Virol* 2001;75:6969-76.
131. Wang W, Soroka CJ, Mennone A, et al. Radixin is required to maintain apical canalicular membrane structure and function in rat hepatocytes. *Gastroenterology* 2006;131:878-84.
132. Gao L, Utsumi T, Tashiro K, et al. Reticulon 4B (Nogo-B) facilitates hepatocyte proliferation and liver regeneration in mice. *Hepatology* 2013;57:1992-2003.
133. Lin MI, Fulton D, Babbitt R, et al. Phosphorylation of threonine 497 in endothelial nitric-oxide synthase coordinates the coupling of L-arginine metabolism to efficient nitric oxide production. *J Biol Chem* 2003;278:44719-26.
134. Ghebremariam YT, Yamada K, Lee JC, et al. FXR agonist INT-747 upregulates DDAH expression and enhances insulin sensitivity in high-salt fed Dahl rats. *PLoS One* 2013;8:e60653.
135. Balasubramanian V SV, Winstanley A, Davies N, Shah N, Jalan R, . Modulation of the DDAH-ADMA pathway with the Farnesoid X receptor (FXR) agonist INT-747 restores hepatic eNOS activity and lowers portal pressure in cirrhotic rats. . *Hepatology* 2009;50 336A-337A.
136. Xu Z, Huang G, Gong W, et al. FXR ligands protect against hepatocellular inflammation via SOCS3 induction. *Cell Signal* 2012;24:1658-64.
137. Fiorucci S, Antonelli E, Rizzo G, et al. The nuclear receptor SHP mediates inhibition of hepatic stellate cells by FXR and protects against liver fibrosis. *Gastroenterology* 2004;127:1497-512.
138. He F, Li J, Mu Y, et al. Downregulation of endothelin-1 by farnesoid X receptor in vascular endothelial cells. *Circ Res* 2006;98:192-9.
139. Dong JY, Fan PD, Frizzell RA. Quantitative analysis of the packaging capacity of recombinant adeno-associated virus. *Hum Gene Ther* 1996;7:2101-12.
140. Hong L, Fast W. Inhibition of human dimethylarginine dimethylaminohydrolase-1 by S-nitroso-L-homocysteine and hydrogen peroxide. Analysis, quantification, and implications for hyperhomocysteinemia. *J Biol Chem* 2007;282:34684-92.
141. Torondel B, Nandi M, Kelly P, et al. Adenoviral-mediated overexpression of DDAH improves vascular tone regulation. *Vasc Med* 2010;15:205-13.
142. Fickling SA, Holden DP, Cartwright JE, et al. Regulation of macrophage nitric oxide synthesis by endothelial cells: a role for NG,NG-dimethylarginine. *Acta Physiol Scand* 1999;167:145-50.
143. Luo Z, Teerlink T, Griendling K, et al. Angiotensin II and NADPH oxidase increase ADMA in vascular smooth muscle cells. *Hypertension* 2010;56:498-504.
144. Inagaki K, Fuess S, Storm TA, et al. Robust systemic transduction with AAV9 vectors in mice: efficient global cardiac gene transfer superior to that of AAV8. *Mol Ther* 2006;14:45-53.
145. Wang L, Wang H, Bell P, et al. Systematic evaluation of AAV vectors for liver directed gene transfer in murine models. *Mol Ther* 2010;18:118-25.

146. Montenegro-Miranda PS, Pichard V, Aubert D, et al. In the rat liver, Adenoviral gene transfer efficiency is comparable to AAV. *Gene Ther* 2014;21:168-74.
147. Sobrevals L, Enguita M, Rodriguez C, et al. AAV vectors transduce hepatocytes in vivo as efficiently in cirrhotic as in healthy rat livers. *Gene Ther* 2012;19:411-7.
148. Smith JS, Tian J, Muller J, et al. Unexpected pulmonary uptake of adenovirus vectors in animals with chronic liver disease. *Gene Ther* 2004;11:431-8.
149. Maruyama H, Higuchi N, Nishikawa Y, et al. High-level expression of naked DNA delivered to rat liver via tail vein injection. *J Gene Med* 2002;4:333-41.
150. Herweijer H, Wolff JA. Progress and prospects: naked DNA gene transfer and therapy. *Gene Ther* 2003;10:453-8.
151. Brunetti-Pierrri N, Lee B. Gene therapy for inborn errors of liver metabolism. *Mol Genet Metab* 2005;86:13-24.
152. Ambros V. A hierarchy of regulatory genes controls a larva-to-adult developmental switch in *C. elegans*. *Cell* 1989;57:49-57.
153. Lee RC, Feinbaum RL, Ambros V. The *C. elegans* heterochronic gene *lin-4* encodes small RNAs with antisense complementarity to *lin-14*. *Cell* 1993;75:843-54.
154. Lee RC, Ambros V. An extensive class of small RNAs in *Caenorhabditis elegans*. *Science* 2001;294:862-4.
155. Pasquinelli AE, Reinhart BJ, Slack F, et al. Conservation of the sequence and temporal expression of *let-7* heterochronic regulatory RNA. *Nature* 2000;408:86-9.
156. Reinhart BJ, Slack FJ, Basson M, et al. The 21-nucleotide *let-7* RNA regulates developmental timing in *Caenorhabditis elegans*. *Nature* 2000;403:901-6.
157. Yates LA, Norbury CJ, Gilbert RJ. The long and short of microRNA. *Cell* 2013;153:516-9.
158. Petersen CP, Bordeleau ME, Pelletier J, et al. Short RNAs repress translation after initiation in mammalian cells. *Mol Cell* 2006;21:533-42.
159. Mathonnet G, Fabian MR, Svitkin YV, et al. MicroRNA inhibition of translation initiation in vitro by targeting the cap-binding complex eIF4F. *Science* 2007;317:1764-7.
160. Selbach M, Schwanhaussner B, Thierfelder N, et al. Widespread changes in protein synthesis induced by microRNAs. *Nature* 2008;455:58-63.
161. Yekta S, Shih IH, Bartel DP. MicroRNA-directed cleavage of *HOXB8* mRNA. *Science* 2004;304:594-6.
162. Lewis BP, Burge CB, Bartel DP. Conserved seed pairing, often flanked by adenosines, indicates that thousands of human genes are microRNA targets. *Cell* 2005;120:15-20.
163. Krek A, Grun D, Poy MN, et al. Combinatorial microRNA target predictions. *Nat Genet* 2005;37:495-500.
164. Bartel DP. MicroRNAs: target recognition and regulatory functions. *Cell* 2009;136:215-33.
165. Baek D, Villen J, Shin C, et al. The impact of microRNAs on protein output. *Nature* 2008;455:64-71.
166. Maziere P, Enright AJ. Prediction of microRNA targets. *Drug Discov Today* 2007;12:452-8.
167. Westfall P, Young S. Resampling-Based Multiple Testing: Examples and Methods for p-value Adjustment. New York, USA: John Wiley & Sons, Inc., 1993.
168. Grimson A, Farh KK, Johnston WK, et al. MicroRNA targeting specificity in mammals: determinants beyond seed pairing. *Mol Cell* 2007;27:91-105.
169. Nielsen CB, Shomron N, Sandberg R, et al. Determinants of targeting by endogenous and exogenous microRNAs and siRNAs. *RNA* 2007;13:1894-910.
170. Friedman RC, Farh KK, Burge CB, et al. Most mammalian mRNAs are conserved targets of microRNAs. *Genome Res* 2009;19:92-105.
171. Hofacker IL, W. Fontana, P. F. Stadler, S. Bonhoeffer, M. Tacker, P. Schuster. Fast folding and comparison of RNA secondary structures. *Monatshefte für Chemie* 1994;25:167-188.
172. Robins H, Li Y, Padgett RW. Incorporating structure to predict microRNA targets. *Proc Natl Acad Sci U S A* 2005;102:4006-9.

173. Zhao Y, Samal E, Srivastava D. Serum response factor regulates a muscle-specific microRNA that targets Hand2 during cardiogenesis. *Nature* 2005;436:214-20.
174. Kertesz M, Iovino N, Unnerstall U, et al. The role of site accessibility in microRNA target recognition. *Nat Genet* 2007;39:1278-84.
175. Long D, Lee R, Williams P, et al. Potent effect of target structure on microRNA function. *Nat Struct Mol Biol* 2007;14:287-94.
176. Hammell M, Long D, Zhang L, et al. mirWIP: microRNA target prediction based on microRNA-containing ribonucleoprotein-enriched transcripts. *Nat Methods* 2008;5:813-9.
177. Gaidatzis D, van Nimwegen E, Hausser J, et al. Inference of miRNA targets using evolutionary conservation and pathway analysis. *BMC Bioinformatics* 2007;8:69.
178. Majoros WH, Ohler U. Spatial preferences of microRNA targets in 3' untranslated regions. *BMC Genomics* 2007;8:152.
179. Zhou B, Chen H, Wei D, et al. A novel miR-219-SMC4-JAK2/Stat3 regulatory pathway in human hepatocellular carcinoma. *J Exp Clin Cancer Res* 2014;33:55.
180. Zou Z, Wu L, Ding H, et al. MicroRNA-30a sensitizes tumor cells to cis-platinum via suppressing beclin 1-mediated autophagy. *J Biol Chem* 2012;287:4148-56.
181. Rao SA, Arimappamagan A, Pandey P, et al. miR-219-5p inhibits receptor tyrosine kinase pathway by targeting EGFR in glioblastoma. *PLoS One* 2013;8:e63164.
182. Kedde M, van Kouwenhove M, Zwart W, et al. A Pumilio-induced RNA structure switch in p27-3' UTR controls miR-221 and miR-222 accessibility. *Nat Cell Biol* 2010;12:1014-20.
183. Ito A, Tsao PS, Adimoolam S, et al. Novel mechanism for endothelial dysfunction: dysregulation of dimethylarginine dimethylaminohydrolase. *Circulation* 1999;99:3092-5.
184. Li J, Donath S, Li Y, et al. miR-30 regulates mitochondrial fission through targeting p53 and the dynamin-related protein-1 pathway. *PLoS Genet* 2010;6:e1000795.
185. Backlund M, Paukku K, Daviet L, et al. Posttranscriptional regulation of angiotensin II type 1 receptor expression by glyceraldehyde 3-phosphate dehydrogenase. *Nucleic Acids Res* 2009;37:2346-58.
186. Day AM, Brown JD, Taylor SR, et al. Inactivation of a peroxiredoxin by hydrogen peroxide is critical for thioredoxin-mediated repair of oxidized proteins and cell survival. *Mol Cell* 2012;45:398-408.
187. Hollstein M, Hainaut P. Massively regulated genes: the example of TP53. *J Pathol* 2010;220:164-73.
188. Schmucker D. Molecular diversity of Dscam: recognition of molecular identity in neuronal wiring. *Nat Rev Neurosci* 2007;8:915-20.
189. Davuluri RV, Suzuki Y, Sugano S, et al. The functional consequences of alternative promoter use in mammalian genomes. *Trends Genet* 2008;24:167-77.
190. Pan Q, Shai O, Lee LJ, et al. Deep surveying of alternative splicing complexity in the human transcriptome by high-throughput sequencing. *Nat Genet* 2008;40:1413-5.
191. Wang ET, Sandberg R, Luo S, et al. Alternative isoform regulation in human tissue transcriptomes. *Nature* 2008;456:470-6.
192. Trapnell C, Williams BA, Pertea G, et al. Transcript assembly and quantification by RNA-Seq reveals unannotated transcripts and isoform switching during cell differentiation. *Nat Biotechnol* 2010;28:511-5.
193. Arce L, Yokoyama NN, Waterman ML. Diversity of LEF/TCF action in development and disease. *Oncogene* 2006;25:7492-504.
194. Li TW, Ting JH, Yokoyama NN, et al. Wnt activation and alternative promoter repression of LEF1 in colon cancer. *Mol Cell Biol* 2006;26:5284-99.
195. Lenhard B, Sandelin A, Mendoza L, et al. Identification of conserved regulatory elements by comparative genome analysis. *J Biol* 2003;2:13.
196. Ureta-Vidal A, Ettwiller L, Birney E. Comparative genomics: genome-wide analysis in metazoan eukaryotes. *Nat Rev Genet* 2003;4:251-62.

197. Bagheri-Fam S, Ferraz C, Demaille J, et al. Comparative genomics of the SOX9 region in human and *Fugu rubripes*: conservation of short regulatory sequence elements within large intergenic regions. *Genomics* 2001;78:73-82.
198. Ovcharenko I, Stubbs L, Loots GG. Interpreting mammalian evolution using *Fugu* genome comparisons. *Genomics* 2004;84:890-5.
199. Juven-Gershon T, Hsu JY, Kadonaga JT. Perspectives on the RNA polymerase II core promoter. *Biochem Soc Trans* 2006;34:1047-50.
200. Juven-Gershon T, Hsu JY, Theisen JW, et al. The RNA polymerase II core promoter - the gateway to transcription. *Curr Opin Cell Biol* 2008;20:253-9.
201. Fu Y, Weng Z. Improvement of TRANSFAC matrices using multiple local alignment of transcription factor binding site sequences. *Genome Inform* 2005;16:68-72.
202. Knuppel R, Dietze P, Lehnberg W, et al. TRANSFAC retrieval program: a network model database of eukaryotic transcription regulating sequences and proteins. *J Comput Biol* 1994;1:191-8.
203. Carninci P, Sandelin A, Lenhard B, et al. Genome-wide analysis of mammalian promoter architecture and evolution. *Nat Genet* 2006;38:626-35.
204. Vaiman D, Calicchio R, Miralles F. Landscape of transcriptional deregulations in the preeclamptic placenta. *PLoS One* 2013;8:e65498.
205. Sun T, Zhou JP, Kuang DB, et al. Correlations of DDAH1 transcript variants with human endothelial asymmetric dimethylarginine metabolizing activity. *Am J Hypertens* 2013;26:1437-44.
206. Anderssohn M, Maass LM, Diemert A, et al. Severely decreased activity of placental dimethylarginine dimethylaminohydrolase in pre-eclampsia. *Eur J Obstet Gynecol Reprod Biol* 2012;161:152-6.
207. Ruiz-del-Arbol L, Urman J, Fernandez J, et al. Systemic, renal, and hepatic hemodynamic derangement in cirrhotic patients with spontaneous bacterial peritonitis. *Hepatology* 2003;38:1210-8.
208. Bellot P, Garcia-Pagan JC, Frances R, et al. Bacterial DNA translocation is associated with systemic circulatory abnormalities and intrahepatic endothelial dysfunction in patients with cirrhosis. *Hepatology* 2010;52:2044-52.
209. Buck MG, G; Groszmann, R.J.; et al. Novel inflammatory biomarkers of portal pressure in compensated cirrhosis patients. *Hepatology* 2014;59:1052-9.
210. Mookerjee RP, Sen S, Davies NA, et al. Tumour necrosis factor alpha is an important mediator of portal and systemic haemodynamic derangements in alcoholic hepatitis. *Gut* 2003;52:1182-7.
211. Verbeke L, Farre R, Trebicka J, et al. Obeticholic acid, a farnesoid X receptor agonist, improves portal hypertension by two distinct pathways in cirrhotic rats. *Hepatology* 2014;59:2286-98.
212. Mookerjee RP, Mehta G, Balasubramanian V, et al. Hepatic Dimethylarginine-Dimethylaminohydrolase1 is Reduced in Cirrhosis and is a Target for Therapy in Portal Hypertension. *J Hepatol* 2014.
213. Janssen HL, Reesink HW, Lawitz EJ, et al. Treatment of HCV infection by targeting microRNA. *N Engl J Med* 2013;368:1685-94.
214. Hindorff LA, Sethupathy P, Junkins HA, et al. Potential etiologic and functional implications of genome-wide association loci for human diseases and traits. *Proc Natl Acad Sci U S A* 2009;106:9362-7.
215. Consortium EP. An integrated encyclopedia of DNA elements in the human genome. *Nature* 2012;489:57-74.
216. Emerson BM, Lewis CD, Felsenfeld G. Interaction of specific nuclear factors with the nuclease-hypersensitive region of the chicken adult beta-globin gene: nature of the binding domain. *Cell* 1985;41:21-30.

217. Gilmour DS, Lis JT. Detecting protein-DNA interactions in vivo: distribution of RNA polymerase on specific bacterial genes. *Proc Natl Acad Sci U S A* 1984;81:4275-9.
218. Wu C, Wong YC, Elgin SC. The chromatin structure of specific genes: II. Disruption of chromatin structure during gene activity. *Cell* 1979;16:807-14.
219. Lee DY, Hayes JJ, Pruss D, et al. A positive role for histone acetylation in transcription factor access to nucleosomal DNA. *Cell* 1993;72:73-84.
220. Djebali S, Davis CA, Merkel A, et al. Landscape of transcription in human cells. *Nature*;489:101-8.

8.0 Supplemental methods

Chapter 3: Recombinant AAV vector production

S3.1 Triple transfection of rAAV plasmid, helper Ad plasmid and packaging plasmid into HEK293T cells

In this study, the three-plasmid system was used which involved the triple transfection of 293-T cells with a helper Ad plasmid (HGTI) a pAAV-based plasmid (a vector flanked by the AAV-serotype 2 ITRs and harbouring the cDNA of interest), and a packaging plasmid containing the AAV Rep and Cap genes, at a molar ratio of 3:1:1 respectively (Figure S3.1). Since the generation of pseudotyped AAV vectors was required, the packaging construct contained AAV serotype 2 Rep proteins, but Cap proteins from serotype 9.

The day before transfection, 293-T cells were seeded into 40 (15cm diameter) dishes at a cell density of between $8-9.5 \times 10^6$ cells/dish, so that the cultures were about 70% confluent the following day. On the day of transfection, a transfection mixture was prepared for 10 dishes in a 50 ml Falcon tube, containing 300 μ g HGTI, 100 μ g pAAV_DDAH1, 100 μ g pAAV_9, 0.25M CaCl₂ and ddH₂O made up to 12.5ml volume.

While aspirating the above mix with a 1ml pipette to create bubbles, 12.5ml 2 \times HEPES- buffered saline (HBS; 280mM NaCl, 10mM KCl, 1.5mM Na₂HPO₄, 12mM dextrose and 50mM HEPES; pH 7.05) was added at a steady slow rate. The transfection mix was incubated at room temperature for 2min and then the entire 25ml was transferred to 200ml of pre-warmed growth medium and mixed gently by inversion. The culture medium was removed from the 10 (15cm diameter) dishes containing the 293-T cells and 22ml of the transfection mix was carefully added without disruption of the cell monolayer. After an incubation period of 2 to 3 days, the culture medium was removed from the transfected cells leaving 2-3ml in each dish into which the cells were scraped. The scraped cells from each dish were then pooled and pelleted by centrifugation at 1000g for 10min and the cell pellet was re-suspended in 15ml cell lysis buffer (150mM NaCl, 50mM Tris-HCL; pH 8.5). The cells were then lysed by four cycles of freeze/thaw by alternately placing in ethanol/dry ice and then a 37C water bath. Lysis of the cells results in the release of the AAV particles into the supernatant. The lysate was then treated with 3 μ l (100 Units) of benzonase, which is an enzyme used to dissociate aggregated rAAV

particles by digesting any extraneous nucleic acid, before purification. An aggregate of virus particles would behave as a single transducing unit, therefore, it is important that these are separated to maximise the infectious virus titer. The benzonase-treated lysate was vortexed, followed by incubation at 37C for 1h and then centrifugation at 6,500 rpm for 20min to clarify the cell lysate.

S3.2 Purification of the clarified lysate by iodixanol step gradient ultracentrifugation

To isolate the rAAV particles from the clarified lysate, the latter was loaded onto a step- gradient of iodixanol. Upon ultracentrifugation the virus particles sediment into the 40% iodixanol gradient fraction. The most concentrated iodixanol fraction (60%) is the lower layer and functions as a cushion to prevent the particles pelleting at the bottom of the tube. The iodixanol fractions were prepared as shown in Table S3.1.

% Iodixanol	Iodixanol (ml)	5M NaCl (ml)	*5× PBS-MK (ml)	ddH2O (ml)	Phenol Red (µl)
15%	12.5	10	10	17.5	-
25%	20.8	-	10	19.2	100
40%	33.3	-	10	6.7	-
60%	50	-	-	-	100

Table S3.1: Preparation of iodixanol fractions

*5x PBS-MK (5x PBS, 5mM MgCl₂, 12.5mM KCL)

The clarified lysate was transferred to a Quick-Seal Ultra-Clear Ultracentrifuge tube using a Pasteur pipette and then carefully underlayered with the iodixanol fractions in the following order: 5ml 60% iodixanol, 5ml 40% iodixanol, 6ml 25% iodixanol, 9ml 15% iodixanol.

The remaining space in the tube was filled with cell lysis buffer before heat-sealing the ultracentrifuge tube. Ultracentrifugation of the iodixanol step-gradient was performed in a Beckman Ultracentrifuge using a Type 60Ti rotor at 60,000 xg for 90min. The 40% fraction is easily distinguished owing to the presence of phenol red in the 25% and 60% iodixanol fractions. Using a 19-gauge needle and 10ml syringe, the 40% fraction was removed by carefully puncturing the tube at the 60%/40% interface and withdrawing no more than 4.5ml of the fraction. The purified virus was then loaded onto a single Biomax 100 ultrafiltration device and the volume brought up to 15ml with 1× PBS-MK. The filter device was centrifuged at 2000g at room temperature until approximately 1ml remained. The virus stock was re-diluted and re-concentrated a second time, ending with a final volume of 500µl, which could then be stored at -80°C.

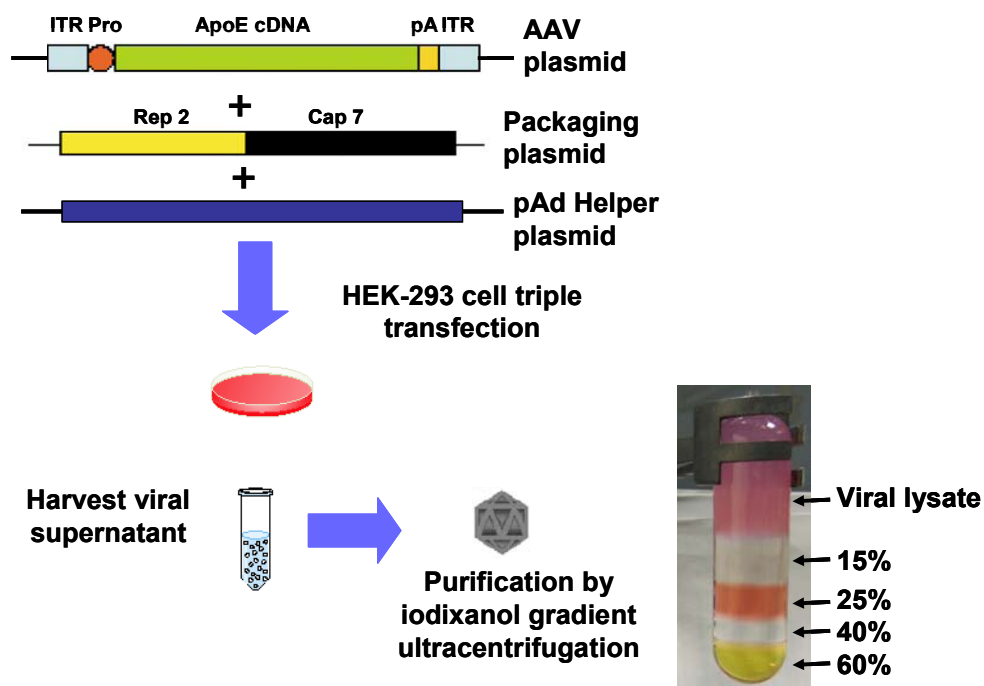


Figure S3.1 – Purification of rAAV using an iodixanol gradient

3.6.3 Determination of virus particle titer by DNA dot-blot hybridisation analysis

To estimate the virus particle titer, rAAV vector genomes were isolated from 1µl and 5µl portions of the virus stock and transferred to a nitrocellulose membrane, together with a serial dilution of known quantities of the corresponding pAAV vector. To extract vector genomes, the virus was treated with DNase I (1U/µl) to digest any extraneous DNA. To the 1µl and 5µl virus portions, 5µl of DNase I and 20µl of 10× DNase I reaction buffer was added and brought to 200µl with serum-free DMEM. Following incubation at 37°C for 1h, the virus was treated with 200µl of 2× proteinase K buffer (20mM Tris-HCl, 20mM EDTA and 1% (^{w/v}) SDS) containing 100µg of proteinase K and incubated a second time at 37°C for 1.5h. The proteinase K digests the virus capsid proteins releasing the vector genome. The vector DNA was then isolated by the addition of 400µl of phenol:chloroform:isoamyl alcohol (25:24:1) and vortexed to form an emulsion, which was centrifuged at 10,000 g for 10min. The upper aqueous phase was transferred to a 1.5ml microfuge tube and 40µl 3M sodium acetate (pH 5.2) and 2µl of glycogen (20µg/µl) was added. This was vortexed and then 1ml ethanol (2.5 vol) was added, mixed and incubated at -80°C for 30min to precipitate vector genome DNA. The preparations were centrifuged at 10,000 g for 20min at room temperature to pellet the DNA, which was clearly visible due to the presence of glycogen. The supernatant was removed and the pellets washed with 800µl 70% ethanol and centrifuged at 10,000 g for 5min at 4°C. Once the supernatant had been removed, the DNA pellets were air-dried and dissolved in 400µl of 0.4M NaOH/10mM EDTA (pH 8).

For dot blot analysis, a two-fold serial dilution of the corresponding pAAV vector was prepared, ranging from 80ng to 0.3125ng. To each 5µl pAAV dilution, 400µl of 0.4M NaOH/10mM EDTA was added. While heating the viral and plasmid samples at 100°C for 5min a piece of Hybond-N+ nitrocellulose membrane and three pieces of 3MM Whatman blotting paper were cut to the size of the dot-blot manifold and pre-wetted in ddH₂O. The manifold was set up with the membrane overlaying the three sheets of blotting paper and attached to a vacuum pump. Each well to be used in the analysis was washed with 400µl of ddH₂O and the vacuum was applied to dry. The two denatured vector genome samples and the pAAV DNAs were then added to the appropriate wells of the apparatus and the vacuum applied. Once the samples had passed through, each well was rinsed with 400µl 0.4M NaOH/10mM EDTA and the membrane was removed and air-dried for 15min.

The ECL direct nucleic acid labelling and detection system was used for labelling the DNA probe and the subsequent hybridisation and detection of the DNA dot-blot. The

membrane was first rinsed in 2× SSC (NaCl and Na₃Citrate·2H₂O) and transferred to a hybridisation cylinder with 34ml ECL gold hybridisation buffer containing 1g NaCl and 1.7g ECL blocking agent pre-dissolved at 42°C for 2h. The membrane was pre-hybridised by incubation with rotation at 42°C for a minimum of 1h. Meanwhile, the DNA probe, which was 100ng of an agarose gel-purified DNA fragment derived from the pAAV vector, was diluted to 10ng/μl in ddH₂O and denatured by incubating at 100°C for 5min. The denatured DNA was cooled on ice and 10μl DNA labelling reagent was added, mixed gently, followed by the addition of 10μl of glutaraldehyde solution. The labelling mix was vortexed and incubated at 37°C for 10min. The labelled DNA probe could then be added to the cylinder containing the pre-hybridised membrane and incubated at 42°C with rotation overnight. The next day the hybridisation mix was replaced with 100ml pre-warmed primary wash buffer (1L = 2× SSC, 360g urea, 4g SDS) and incubated at 42°C with rotation for 30min. The wash procedure was repeated once more and then the membrane was removed and washed twice with 400ml of 2× SSC at room temperature for 6min with gentle agitation. Detection was carried out by chemiluminescence, with the use of an ECL system (described in section 2.6.5 western blot).

The intensity of the signals produced by the 1μl and 5μl portions of virus stock was compared with those of the quantified pAAV serial dilution and densitometric analyses was used to estimate the number of vector genomes in ng in each dot.

Chapter 4: *In situ* hybridisation

S4.1 Synthesis and labeling of riboprobes

PCR primers were designed to amplify a 220bp amplicon from Hs DDAH-1 cDNA, as in section 2.2.1. The PCR product was subsequently cloned into the pGEMTE vector (Promega UK), as in sections 2.2.3-2.2.6. The construct was subsequently sequenced from the T7 forward sequencing primer.

In vitro transcription of the riboprobe was performed by linearising the construct by digesting with Spe1 for transcription from T7 polymerase promoter, and Nco1 for transcription from SP6 polymerase promoter. In vitro transcription was performed using the Roche SP/T7 RNA polymerases, and the riboprobes were labeled with the Roche DIG RNA Labelling kit according to manufacturers instructions.

Subsequently a dot-blot was performed of each probe to determine the degree of labeling. Detection of DIG labeling was performed using the Roche DIG Detection kit according to manufacturers instructions.

S4.2 *In situ* hybridisation

Paraffin embedded sections were dewaxed and rehydrated using serial alcohol and water immersion according to standard techniques. Sections were subsequently permeabilised using Tris-EDTA buffer containing 10ug/ml Proteinase K. Subsequently sections were incubated with prehybridisation solution (1.5ml 4x DEPC treated SSc + 1.5ml Formamide) for 2 hours at 37°, followed by hybridisation with 5ul of riboprobe in 1ml of hybridization buffer (1M Tris pH7.5 200uL, 100x Denharts 2.5mL, 20x SSc 1.95mL, Formamide 10mL, 40%Dextran sulfate 4mL, Salmon sperm DNA (10mg/ml) 500uL, DEPC H2O 350uL) overnight at 37°C.

Subsequently, sections were incubated with 100uL of 20ug/mL RNase A at 37 degrees for 30 minutes, and washed in RNase buffer and 2xSSC/Formamide for 10 minutes each. Antibody detection was performed by incubation with 150uL anti-Dig Ab (1:500) in for 4 hours. Signal was developed with NBT/BCIP stock solution (Roche, UK). A negative control section was treated with RNase A for 30 minutes at 37°C prior to incubation with riboprobe.

A further set of experiments were performed on paraffin embedded sections using the Affymetrix ViewRNA kit for mRNA and miRNA in situ hybridization. Dewaxing and rehydration was performed as above. Subsequently protease digestion and probe hybridisation was performed according to manufacturers instructions. Subsequently signal amplification and detection was performed according to manufacturers instructions.